A study of collagen structure in canine myxomatous mitral valve disease

Mojtaba Hadian

Submitted in satisfaction of the requirements for the degree of

Doctor of Philosophy

Division of Veterinary Biomedical Sciences
College of Medicine and Veterinary Medicine
The University of Edinburgh
2009

Declaration

I declare that this thesis has been composed by me and work described here is my own unless stated otherwise. I have not been registered for a degree at any other institution throughout the period of registration at the University of Edinburgh.

This thesis is dedicated to:

My Father Ali-Akbar,

My Mother Zahra,

My Brother Ali,

&

My Beautiful Sisters Jila and Zhaleh

My heartfelt and special thanks to:

Ahmed Durrani and his family, and Idalja Walendziak

Table of contents

TABLE OF CONTENTS **1**

Acknowledgment 6

Abstract 8

Abbreviations 10

CHAPTER ONE **14**

INTRODUCTION **14**

Background *15*

Influence of gender, age, body weight and build and breed *16*

Age and breed *16*

Influence of gender *17*

Influence of body shape *18*

Developmental anatomy of the heart *19*

Anatomy and histology of mitral valve *20*

Human mitral valve prolapse: an analogous of MMVD? *25*

Aetiopathogenesis of MMVD (MVP) *28*

Pathology and histopathology *33*

Collagen biosynthesis *37*

Post-translational modification *39*

Glycosylation of hydroxylysine residues *41*

Glycosylation of asparagine residues in propeptide *44*

Procollagen assembly and helix formation *45*

Procollagen trafficking from the ER to the Golgi *52*

From the Golgi apparatus to secretion *54*

Procollagen processing *56*

Collagen suprastructure *58*

Cross-links and lysyl oxidase *62*

Catalytic properties and cofactors of lysyl oxidase *69*

Inhibitors of LOX *71*

Substrate specificity to LOX *72*

Other biological roles of LOX *73*

Collagen turn-over and degradation *74*

Clinical signs and diagnosis *80*

Electrocardiography *81*

Diagnostic imaging *82*

Aim, scope and hypothesis *83*

CHAPTER 2 ..... **85**

X-RAY DIFFRACTION IN THE EVALUATION OF CONNECTIVE TISSUE CHANGES IN MMVD **85**

X-rays studies *86*

X-ray diffraction *87*

X-ray diffraction in biological research *89*

Aim 90

Materials and methods 91

Specimen holder *92*

X-ray diffraction measurements *92*

Data analysis *93*

Results 95

Estimation of total tissue *97*

Collagen fibril orientation *98*

Collagen fibril density *98*

Degree of collagen alignment *99*

d-spacing measurement *102*

Discussion 103

CHAPTER 3 ..... **107**

DIFFRACTION ENHANCING IMAGING (DEI) IN THE ASSESSMENT OF STRUCTURAL CHANGES IN MMVD **107**

Diffraction enhancing imaging (DEI) *108*

Aim 109

Materials and methods 110

Results 112

Discussion 113

CHAPTER 4 ..... **116**

HYDROXYPROLINE ASSAY AS A MEASURE OF COLLAGEN CONTENT IN CANINE MITRAL VALVES **116**

Introduction *117*

Proline and hydroxyproline metabolism *118*

Aim 121

Materials and methods 122

Results 124

Discussion 125

CHAPTER 5 ..... **130**

DIFFERENTIAL SCANNING CALORIMETRY (DSC) AND THERMAL STABILITY OF COLLAGEN IN MMVD **130**

Differential scanning calorimetry *131*

Aim 134

Materials and methods 134

Results 136

Discussion 138

CHAPTER 6 ..... **143**

NEUTRON SCATTERING AND COLLAGEN CROSS-LINKS IN MMVD **143**

Neutron scattering *144*

Aim 147

Instrumentation and methods *148*

Results 152

Discussion 153

CHAPTER 7 157

HIGH PERFORMANCE LIQUID CHROMATOGRAPHY (HPLC) FOR THE MEASUREMENT OF MATURE COLLAGEN CROSS-LINKS IN MMVD 157

High performance liquid chromatography 158

Aim 161

Materials and methods 162

Sample injection 164

Pre-column derivatisation 165

Collagen extraction 168

Results 169

Discussion 173

CHAPTER 8 178

COHERENT ANTI-STOKES RAMAN SCATTERING SPECTROSCOPY (CARS) STUDY OF CANINE MITRAL VALVE 178

History of spectroscopy 179

Raman spectroscopy 179

CARS imaging 182

Aim 183

Materials and methods 183

Results and discussion 186

CHAPTER 9 193

CONCLUSIONS 193

Conclusions 194

CHAPTER 10 200

REFERENCES 200

APPENDIX 233

PUBLICATIONS ARISING FROM THIS THESIS DURING COURSE OF MY PHD 233

Original papers.....*234*

Papers presented in congresses.....*239*

Acknowledgment

I owe an immense debt of gratitude to my supervisor Professor Jeremy Bradshaw without whose patience, understanding and guidance during last 4 years, this project could not have been fulfilled. Throughout my years in his laboratory, he provided sound advice, good teaching and wonderful company. I would have been lost without him! I would also like to thank my other supervisor Professor Brendan Corcoran for trusting and supporting me unconditionally. I warmly thank Dr Geoff T. Pearson for his contribution in presiding over my thesis committee.

I am deeply grateful to Professor Graham Pettigrew whom without his great help and advice, HPLC work would have not been completed. I am very indebted to Dr J. Gunter Grossman and Kalotina (Tina) Geraki for their never-ending support during my regular visits to Daresbury Synchrotron Radiation Source. Bruno Demé's technical support at the Institute Laue Langevin (Grenoble, France) is appreciated. The following people were particularly helpful at Elettra Synchrotron Light Source (Italy): Dr Giuliana Tromba, Dr Ralf H. Menk, Dr Fulvia Arfelli and Dr Lucia Mancini. I would also like to extend my thanks to Dr Andy Downs for his invaluable assistance of CARS facility and his ongoing co-operation.

Dr Alastair Macdonald was a constant source of encouragement. He was always available to chat with me and cheer me up. He deserves a big thank you!

I am also sincerely grateful to Dr Ann Haley for her kindness and confidence in my abilities as part of the teaching staff at the Biology Teaching Organisation (BTO).

Special thanks also go to all staff in Iran's Academic Representative in the UK, especially Professor Salehi, Mrs Emami and Mrs Tadayon (Afzalan).

The project itself was supported by Council for the Central Laboratory of the Research Councils (CCLRC), the Kennel Club Charitable Trust and the cavalier King Charles spaniel club of England.

I would also like to express my deep appreciation to Iran Ministry of Science for all-out sponsoring and supporting me throughout of my course at the University of Edinburgh.

Finally, I wish to thank my former and current lab-mates and friends, Dr Kia Balali-Mood, Richard Han, Farid Sa'Adedin, Yan C.S.M. Laurenson, Daniel Baptista-Hon Lijing Ke, Theo Kiosses and Louise Gillam for their help, care and comradeship.

Abstract

Myxomatous mitral valve disease (MMVD) is the single most common acquired cardiac disease of dogs, and is a disease of significant veterinary importance. It also bears close similarities to mitral valve prolapse in humans and therefore is a disease of emerging comparative interest. Realising the importance of collagen fibres in mitral heart valves and considering the paramount significance of myxomatous mitral valve disease, a better understanding of the pathogenesis of MMVD is essential. Thus, this study was designed to investigate the changes in collagen molecules, including fibril structure, fibril orientation, d-spacing, collagen density, collagen content, thermal stability, and the status of mature and immature cross-links. A combination of biophysical and biochemical tools such as x-ray diffraction, neutron diffraction, HPLC were utilised in order to fulfil the objectives. Biochemical assay of hydroxyproline revealed a 10% depletion of collagen in mildly affacted (grade I and II) leaflets, while a 20% depletion of fibrillar collagen was revealed by mapping the collagen fibrils onto the anatomy of cardiac leaflets using x-ray data. Differential scanning calorimetry showed that there were no significant differences in the onset temperature of denaturation of collagen between the healthy and affected leaflets. However, in affected areas of leaflets, the enthalpy of denaturation significantly dropped by 20%. In the affected regions, neutron diffraction results showed an increase in the immature reducible cross-links though the low number of the samples can be considered a limiting factor in this regard. However, the HPLC results showed a 25% decrease in the number of mature cross-links. Additionally, the recently introduced imaging technologies to biology and medicine such as

differential enhancing imaging (DEI) and coherent anti-Stokes Raman scattering spectroscopy (CARS) were, to the author's best knowledge, applied for the first time to this disease. In doing so, this thesis furthers our understanding of the pathogenesis of MMVD, especially in relation to the collagen. The thesis provides new findings about MMVD and demonstrates the potential of biophysical tools for studying similar conditions.

Abbreviations

Å .....Angstrom

AG .....aminoguanidine

AGEs .....advanced glycation end products

amu.....atomic mass units

bFGF .....basic fibroblast growth factor

BiP .....binding protein

BMP-1 .....bone morphogeneic protein-1

CARS .....coherent anti-Stokes Raman scattering spectroscopy

CGRP.....calcitonin gene-related peptide

CHF.....congestive heart failure

CKCS .....cavalier King Charles spaniel

CML.....carboxymethyllysine

COP.....coat protein complex

DAG .....diacylglycerol

DEI .....differential enhancing imaging

DPD .....deoxypyridinoline

D-Pyr.....deoxypyridinoline

DS .....dermatan sulphate

DSC .....differential scanning calorimetry

DTA.....differential thermal analysis

ECM.....extracellular matrix

EDM.....electric dipole moment

EP1-EP4.....prostanoid receptors

ER.....endoplasmic reticulum

ERGIC .....ER-Golgi intermediate compartment

ET-1.....endothelin-1

FMN ..... flavin adenine mononucleotide

FWHM .....full with half maximum

GAGs.....glycosaminoglycans

Ge .....germanium

GGT .....glucosyltransferase

GPCs .....Golgi plasma membrane carriers

Grp78 .....glucose regulated protein

GT.....galactosyltransferase

HP..... hydroxylysyl pyridinoline

HPLC .....high performance liquid chromatography

HSP47.....heat shock protein 47

IL-1β..... Interleukin-1β

IP3 .....inositol triphosphate

LO.....lysyl oxidase

LP .....lysyl pyridinoline

LTQ.....lysine tyrosylquinone

MG .....methylglyoxal

MMP .....matrix metalloproteinase

MMVD .....myxomatous mitral valve disease

MR.....mitral regurgitation

mTLD.....mammalian tolloid

MVP .....mitral valve prolapse

NAD^+ ..... nicotinamide adenine dinucleotide

NE.....norepinephrine

NF-kB.....nuclear factor-kappa B

NO .....nitric oxide

NOS ..... nitric oxide synthase

NPY .....neuropeptide Y

OAT.....ornithine- γ -aminotransferase

OI..... osteogenesis imperfecta

OPA..... *o*-phthalaldehyde

OPO.....optical parametric oscillator

P5C..... pyrroline-5-carboxylate

PAC.....plasma aldosterone concentration

PBS.....phosphate buffered saline

PDGF ..... platelet-derived growth factor

PDI .....protein disulphide isomerase

PG.....proteoglycans

PM .....plasma membrane

POX.....proline oxidase

PPI.....peptidyl prolyl *cis-trans* isomerase

PRA .....plasma rennin activity

PYD .....pyridinoline

Pyr .....pyridinoline

SHI .....second harmonic imaging

SLRPs.....leucine-rich repeat proteoglycans

SRS.....synchrotron radiation source

SRP.....signal recognition particle

TGF-β1.....transforming growth factor-β1

TGF-β1.....tumour growth factor-β1

TIMP-1.....tissue inhibitor of matrix metalloproteinase-1

TLD .....thermally labile domains

TLH.....telopeptide lysyl hydroxylase

TLL-1.....tolloid-like protease-1

TNF-α.....tumour necrosis factor-α

TPEF .....two-photon excitation fluorescence

UDP .....uridine diphosphate

VCAM-1.....vascular cell adhesion molecule-1

VTC.....vesicular tubular cluster

β-APN.....β-aminopropionitrile

Chapter One

Introduction

Background

Myxomatous mitral valve disease (MMVD) is the most common heart disease in dogs, and accounts for 75% of their cardiovascular problems. MMVD in dogs describes myxomatous degeneration of leaflets and it seems that the diseases is sex, age, body weight and build and breed dependent. It is also recognised by different names in veterinary literature, including endocardiosis, chronic valvular disease, chronic valvular fibrosis, mitral regurgitation (MR), acquired mitral insufficiency and mitral valve prolapse. However, none of these terms gives a complete description. Chronic valvular disease is a non-specific term and can embrace a vast array of abnormalities and diseases. Acquired mitral insufficiency implies that the condition does not have a congenital aspect, but the role of mitral valve dysplasia in the condition is unknown. Mitral valve prolapse focuses on only one feature of the disease: protrusion of one or both mitral leaflets towards the left atrium during systole (Kittleson, 1998; Pedersen, 2000; Olsen *et al.,* 2003a; Hyun, 2005).

In general, MMVD is a benign condition, which takes several years to progress from a clinically silent condition to severe heart failure. Some dogs may not develop clinical signs at all, while others may need a range of medical treatment and/or in the end die or are euthanized. Moreover, MMVD may further complicate other medical and surgical conditions (Pedersen, 2000; Häggstrom *et al.,* 2005). Despite the fact that a considerable amount of advances have occurred in the understanding of the disease, the true nature of the disease especially in terms of aetiopathogenesis,

remains widely unknown. I will review several aspect of MMVD in detail in subsequent sections.

Influence of gender, age, body weight and build and breed

Age and breed

Although in most cases the major changes associated with MMVD occur in middle age, as the dogs get older the severity of the condition also worsens. The severe forms of MMVD in dogs are rarely seen before middle age. Besides, compared to human mitral valve prolapse, it seems that the severity of the disease in human increases with much more intensity to dogs. However, this may only be related to the longer life span of human, longer follow-up periods and the difference in the underlying cause of the two diseases. In the study by Kittleson (1998) on dogs aged between 5 and 8 years and dogs aged between 9 and 12 years, clinical evidence of MMVD was demonstrated in 10% and 25% of dogs, respectively. Echocardiographic screening in the cavalier King Charles spaniel (CKCS) has shown early signs of the disease at an early age and that the severity of the disease progresses as the dogs approach its senescence. However, this finding may be strongly breed-dependent. Häggstrom *et al.* (1992) have shown that 7-10 year old CKCSs had a higher risk of mortality or euthanasia due to heart failure than those of the same age group of dachshunds. In fact, 10% of CKCS developed a grade 3 or 4 murmur, while a much smaller number of dachshunds was found to have murmurs.

The breed predisposition to MMVD is well recognised and commonly quoted breeds, include the poodle (miniature and toy), miniature schnauzer, cocker spaniel, chihuahua, cavalier King Charles spaniel, fox terrier, beagle, Pekinese, dachshund and Boston terrier. Of these, the CKCS is of greater importance since it has a unique susceptibility and is a very popular breed. The prevalence of MMVD in this breed is 50% at 4 years and 100% at the age of 10 (Häggstrom et al., 1992; Beardow and Buchanan, 1993; Van Vleet and Ferrans, 2001). However, only 10 – 15% of affected CKCS develop severe MR leading to death or euthanasia before the age of 10 (Häggstrom, 1996).

Influence of gender

The exact influence of gender on MMVD incidence is not obvious and is a contentious matter. Echocardiographic data from dachshunds and CKCSs has shown that the gender does not have any significant difference in the incidence of MMVD among the young dogs. A study based on necropsy findings of 550 dogs has revealed the same degree of prevalence between two sexes (Das and Tashjian, 1965). However, other studies suggest that males are up to twice as likely as females to developing MMVD. Nevertheless, whether there is a difference in the gender prevalence of the MMVD at the early stages, male dogs often display more severe complications, and are more likely to develop heart failure than female dogs (Pederson, 2000). A study has found that the development of congestive heart failure due to myxomatous mitral valve in male cocker spaniels was 4.5 times greater than in females (Detweiler and Patterson, 1965). The latter is in good agreement with the

study byOlson *et al*. (1999) in which they showed that the severity of MMVD in male dachshunds above the age of two increased at a faster rate compared to females.

Influence of body shape

As MMVD has a propensity to occur in small breeds, it is interesting to speculate on the relationship between body size, weight and disease incidence. A study of 153 cocker spaniels showed that there was a negative correlation between the severity of the disease and body weight (Buchanan, 1977; Pederson *et al*., 1999). Similar studies in different small breeds substantiate the concept of negative correlation between body weight and disease severity (Olsen *et al*., 1999). Furthermore, a negative correlation has also been found between the circumference of the thoracic cage and severity of disease. However, it seems that narrow-chested breeds (i.e. cocker spaniel and chihuahua) are more inclined to being affected than breeds with a more rounded and broad chest, such as beagle and Cairn terrier.In comparable studies in humans, it has been shown that there is a negative correlation between weight and the severity of mitral valve prolapse and that this is not a function of height. Additionally, which might be comparable to dogs, the low anteroposterior chest diameter has been related to mitral valve prolapse in human patients. The suggested explanation for this relationship is that the heart is trapped in the chest cavity, small for the surrounding architecture and so making its anatomical structure distorted (Raggi *et al*., 2000).

Developmental anatomy of the heart

Development of a mammal embryo can be divided into 5 stages including, gametogenesis, fertilization, cleavage, gastrulation and organogenesis. The heart is the first organ to be formed and differentiated in the embryo, in order to deliver the demands of a highly growing embryo. Initial signs of cardiac development appear in the splanchic mesoderm, leading to the formation of the cardiogenic plate and then the endocardial tube (Figure 1.1). Peristaltic movement in the endocardial tube can be observed as early as 18-19 days of gestation (Noden and de Lahunta, 1985).

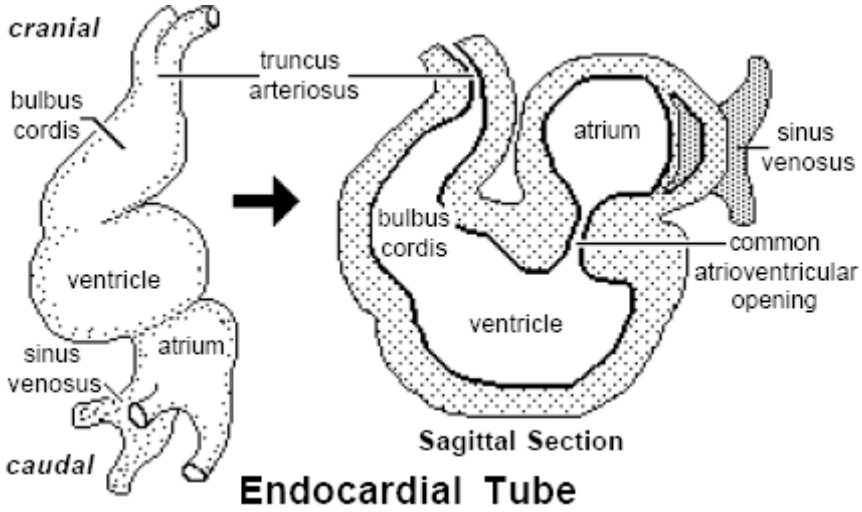

Figure 1.1: Five primitive regions in the endocardial tube, namely truncus arteriosus (presumptive aorta and pulmonary trunk), bulbus cordis (presumptive right ventricle), ventricle (presumptive left ventricle), atrium (presumptive right and left auricles) and sinus venosus (presumptive coronary sinus and wall of right atrium) (Fletcher and Weber, 2004).

As the embryo grows the region between bulboventricle and atrium become more constricted and the proliferation of mesoderm in the canal results in a crest-like tissue protruding into the tube. These protrusions join together, forming the atrioventricular endocardial cushion, which is responsible for creating two separate atrioventricular orifices. Subsequently, dilation, hypertrophy and trabeculation occur in the ventricular walls, which allow the mesenchymal strands of the atrioventricular endocardial cushion to form the cusps of the A-V valves and chordae tendineae (Noden and de Lahunta, 1985).

Anatomy and histology of mitral valve

The mitral valve, like its counterpart in the right heart is a one-way valve that allows blood to flow from the left atrium to the left ventricle during diastole and prevents the backflow of the blood during systole. The mitral valve is located immediately adjacent to the aortic valve; contrary to the tricuspid valve, which is separated from the pulmonic valve by myocardium. The name “mitral” is thought to have been suggested by Andreas Vesalius for its similarity to the plane view of a bishop’s mitre (hat). Mitral valve leaflets along with the annulus of the mitral valve, chordae tendinae and left papillary muscle are the parts of the mitral valve apparatus.

The leaflets and cusps are embraced by a fibrous ring called the mitral annulus that is located between the atrium and the ventricle. The mitral annulus is a D-shaped, cord like and fibrous structure that maintains the attachment of the leaflets. The straight border is a continuation of the aortic root and the anterior leaflet. The fibrous annulus tissue is thickened at both ends, forming the left and right fibrous trigonum. The

annulus provides a firm origin for the leaflets and is involved in a dynamic process called delayed contraction during systole. However, as the fibrous ring cannot contract by itself; it is thought that the atrial musculature present in the proximal part of the posterior leaflet provides the necessary contraction.

The mitral valve of a dog is composed of a large septal or aortic (anterior) leaflet and a medium sized mural (parietal or posterior) leaflet (Figure 1.2).

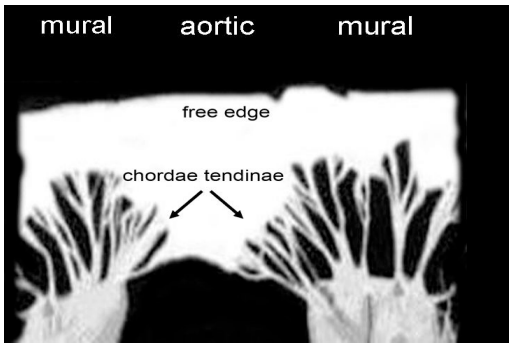

Figure 1.2: A normal canine mitral valve spread open by cutting through the mural leaflet.

The two leaflets receive chordae tendineae from both papillary muscles equally. The spaces between chordae tendineae (interchordal) provide a vital path for blood flow. Furthermore, between leaflets there are small commissural cusps, which only attach to one papillary muscle. Chordae tendineae themselves are divided into marginal (first order) and basal (second order) depending upon whether they attach to the free edge or ventricular aspect of the leaflet, respectively. The atrial surface of the leaflets is smooth. However, the ventricular surface is a combination of rough (where the chordae meet the leaflets) and otherwise smooth areas (Kittleson, 1998; Colville and Bassert, 2002).

There are two papillary muscles, namely the anterolateral and the posteromedial papillary muscle. Half of the anterior and posterior leaflets are supported by one or other of the papillary muscles (Figure 1.3)

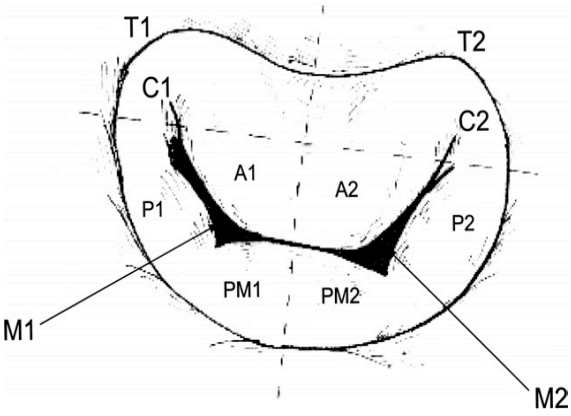

Figure 1.3: Schematic atrial view of mitral valve. The connections for anterolateral and posteromedial papillary muscles are identified with the numerals 1 and 2, respectively. T1= left trigone, T2 = trigone, C1 = anterolateral commissure , C2 = posteromedial commissure , A1 and A2 = anterior leaflet , P1 and P2 = posterior leaflet lateral scallops and PM1 and PM2 = anterolateral and posteromedial segments of posterior leaflet (Degandt *et al*., 2007).

The geometry of the mitral valve complex is also vital to its anatomy. The important criteria in this regard are the left ventricular diameter at the level of papillary muscles, the annular diameter and the annulo-papillary length. Moreover, recent data show that contrary to the long-held belief that the lengths of the two leaflets are equal to the diameter of the annulus, there is a small overlap between the leaflets. It is assumed that this overlap is necessary to prevent of production of a regurgitant jet during systole (Espino *et al*., 2007).

Histologically (Figure 1.4), the atrioventricular valves have 4 layers: atrialis, spongiosa, fibrosa and ventricularis. The atrialis and ventricularis layers are continuous with the endothelial layer of the heart. The fibrosa layer is the main component of the leaflet and is mostly composed of well-structured and packed

collagen fibres which continue with the collagen fibres of tendinous cords where they attach. Between the atrialis and the fibrosa, there is a thin layer of spongiosa, which contains loose collagen fibres, smooth muscle, fibroblasts and elastic fibres in a mucopolysaccharide-rich stroma (Kittleson, 1998; Banks, 1993; Dellmann and Eurell, 1998).

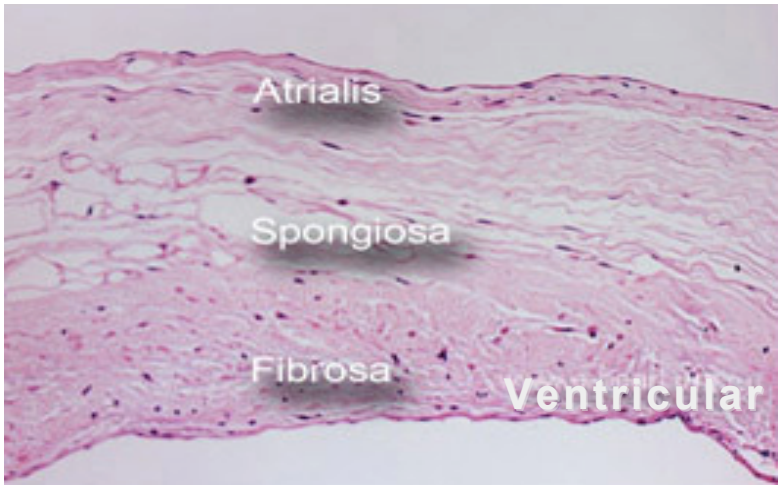

Figure 1.4: four discreet layers of mammalian mitral valve leaflet upon light microscope examination. Atrialis and Ventricularis are lined with the endothelium. Spongiosa is consisted of loosely arranged collagen fibrils, proteoglycans and some elastic fibrils. Fibrosa is mainly composed of well structured collagen fibrils type I and III with proportions of about 70% and 30%, respectively (H&E, 400 X) (photo courtesy of www.e-heart.org).

Human mitral valve prolapse: an analogous of MMVD?

It was about 40 years ago when John Brereton Barlow described the origin of late-systolic murmur and the associated clicks in relation to the mitral valve (Barlow *et al.,* 1963). Later on, Barlow and his colleagues chose the term "billowing mitral leaflet syndrome" and attributed it to leaflet, chordeal or myocardial pathology, although Criley preferred using the term "mitral valve prolapse" to describe the condition (Criley *et al.*, 1966; Pocock and Barlow, 1970). Since then, there have been many developments in the understanding of the disease. Mitral valve prolapse in humans is a heterogeneous disease with different clinical and pathological manifestations. Previously, it was believed that the young females were affected more than the males; in other words 2.1% prevalence in males and 2.7% in females. However, epidemiological studies based on the Framingham Heart Study, and application of the current criteria for long axis 2-dimensinal echocardiography, have shown that the prevalence of disease is around 2-3%, with no disparity between men and women (it is estimated that between 7 and 144 million individuals are affected by MVP worldwide). The age distribution of the patients with MVP is similar in both genders with onset around the third decade of their lives (Freed *et al.,* 1999; Hayek *et al.,* 2005).

The potential causes of mitral valve prolapse make an extensive list, including connective tissue disorders (e.g. Marfan syndrome, Ehlers Danlos syndrome, osteogenesis imperfecta, adult polycystic kidney disease and pseudoxanthoma elasticum), congenital heart disease (e.g. pectus excavatum), genetic abnormality, haematologic disturbances, neuroendocrine disorders (e.g. angiotensin II type 1

receptor involvement), sequel to acute rheumatic fever, ischemic heart disease, metabolic abnormalities (e.g. magnesium deficiency) and other diverse disorders. However, all of theses causes may also be categorised into primary mitral valve prolapse (idiopathic in otherwise healthy people) and secondary mitral valve prolapse (in association with other disorders) (Stefanadis and Toutouzas, 2000; Szombathy *et al*., 2000; Benjamin, 2001; Braunwald, 2001; Pschirrer *et al.,* 2002; Jouan *et al.,* 2004; Kitlinski *et al.*, 2004; Weyman and Scherrer-Crosbie, 2004).

It seems that genetics plays an important role in the development of nonsyndromic MVP. However, the condition is heterogeneous. Primary MVP may be familial or sporadic. An autosomal inheritance mode has been recognised in familial cases with different degree of expressivity and MMVP1 and MMVP2 genes have been mapped to chromosomes 16p11.2-p12.1 and 11p15.4, respectively with age-dependent penetrance. A third chromosomal locus for MVP has also been mapped to chromosome 13q31.3-q32.1. Furthermore, a rare form of X-linked MVP was identified over three decade ago. It is linked to chromosome Xq28. Many experiments have been done on genes encoding collagen in the valve leaflets, but to date, no involvement of these genes has been observed. The existence of marked abnormalities in collagen fibres in the affected leaflets combined with other evidence suggest that the defective collagen fibres might be the result of post-translational changes rather than gene sequences (Braunwald, 2001; Chou *et al*., 2004; Weyman and Scherrer-Crosbie, 2004; Hayek *et al.,* 2005).

The symptoms of MVP include late systolic murmurs, mid-systolic clicks, fatigue, palpitations, atypical chest pain (nonretrosternal), dyspnoea, dizziness, postural

orthostasis, syncope or presyncope, neuropsychiatric symptoms, infective endocarditic, severe mitral regurgitation needing surgical intervention, heart failure, cerebral and coronary embolic events, arrhythmias and even sudden death (Stefanadis and Toutouzas, 2000; Hayek and Griffin, 2002). Another interesting feature of MVP is the established association between MVP and low blood pressure, high heart rate and increased levels of catecholamines. An increased level of catecholamines in normal individuals often leads to increased blood pressure through stimulation of β1 receptors. Stimulation of β2 postsynaptic receptors nevertheless causes an arteriolar vasodilatation and could lower the blood pressure. Additionally, in the patients with MVP it has been shown that while β2 receptors show an exaggerated response to the agonist isoprotrenelol causing more blood pressure drop, treating the patients with a non-selective β blocker such as propranolol results in an increase in blood pressure. It seems that supercoupling and preponderance of β2 receptor are responsible for this phenomenon observed in MVP patients (da Silva *et al.*, 2007). No similar study has so far carried out in affected dogs to see whether there is a corresponding alteration in the receptors.

The large numbers of the studies on mitral valve prolapse have also included the psychiatric studies. The similarities of some of the clinical symptoms of MVP to those of panic disorder, such as palpitation, chest pain and fatigue, have probably been the main driving forces behind this. So far, several studies have been carried out. Nevertheless, they have produced very different results that have failed to establish any strong association between these two conditions. Differences in the methodological approaches and biased sampling might explain the discrepancies in

the results. Moreover, even if there is a association between the panic disorder and MVP, it appears that the connection is weak and non-specific and is comparable to those of seen in generalised anxiety disorder and social phobia (Filho *et al.,* 2008).

However, more than half the people with MVP might be asymptomatic during their life span (Jonkaitiene *et al.,* 2005). In general, when there is no apparent sign, no treatment is suggested. However, symptomatic patients might receive a range of medications, including anxiolytics, antibiotic prophylaxis, beta blockers, calcium channel blockers, and antiarrhythmic agents (Scordo, 2005). Surgical intervention might also be needed in patients with MVP in whom the disease progresses towards severe valve regurgitation. It is estimated that 85,000 heart valve replacement operations are performed annually in the USA, and 275,000 worldwide, of which mitral valve procedures accounts for the majority of them (Schoen, 2005; Schoen and Levy, 2005).

Aetiopathogenesis of MMVD (MVP)

MMVD or mitral valve prolapse in dog is also likely to be the result of a variety of causes, and in that respect bear some similarities with the human condition and allowing careful extrapolation of existing data between these two conditions may prove useful (Pedersen and Häggstrom, 2000). What the exact relationship is between MVP and MMVD in both humans and dogs is not clearly understood, and while the conditions may be one and the same, this might also not be the case. Overall, little is known about the underlying cause of MVP and MMVD. For the

purpose of this thesis MMVD and MVP will be presumed to be part of the same disease process.

The response to injury theory for MMVD is one that suggests changes are due to the effects of continuous impact on the leaflets. During a normal lifespan of a dog the mitral leaflets open and close more than 1 billion times. Every time, they must withstand the pressure of contractions and of the blood itself. However, there must be some other contributory factors explaining why the condition occurs in some breeds more than others. The fact that certain breeds, like the cavalier King Charles spaniel have the propensity to develop the disease suggests that the condition has a hereditary component. In small breeds, MMVD is thought to be a polygenic threshold trait. In due course, with full characterisation of the canine genome, we may be able to identify a series of genes, which are responsible for MMVD (Kittleson, 1998), but one consideration is that differences in cardiac geometry between breeds might also support the response to injury theory, and this question may be answered with the development of 3-D echocardiography.

The endothelium of the leaflets has also been suggested to have a role in initiating the series of events that lead to progression and aggravation of the disease. It has been shown that the damaged endothelium is responsible for the production and secretion of a number of mediators such as endothelin-1 (Mow and Pedersen, 1999). Endothelin-1 (composed of three similar 21 amino acid polypeptides) is known originally to be a pressor and vasoconstrictor in the cardiopulmonary system, but is also a mitogen that promotes the proliferation of smooth muscle cells and fibroblasts. In addition, an increase of collagen production and, conversely, the breakdown of

collagen are triggered by endothelin-1. The biological functions of endothelin-1 are mediated through two cell surface receptors ETA (mainly in vascular smooth muscle) and ETB (mainly in endothelial cells). Following binding to the receptor, the signal is transduced by a series of second messengers, including Ca^{2+}, 1,2-diacylglycerol (DAG), inositol triphosphate (IP3), cyclic adenosine 3′,5′-monophosphate (cAMP) and arachidonic acid. The synthesis of collagen occurs when the protein kinase C becomes active. Apart from these effects of endothelin-1, it has recently been shown that it also reduces the expression of a tissue inhibitor of matrix metalloproteinase-1 (TIMP-1) and induces matrix metalloproteinase-2 (MMP-2). This might lead to degradation of extracellular matrix (ECM) and collagen. Besides, endothelin-1 is capable of modulating the release of cytokines such as tumour growth factor β1 (TGF- β1), tumour necrosis factor α (TNF- α), platelet-derived growth factor (PDGF) and basic fibroblast growth factor (bFGF) (Droge, 2002; Khatib *et al.,* 2002; Horstmeyer *et al.,* 2005; Mishra *et al.,* 2006). Mow and Pedersen have demonstrated that there is a significant correlation between the density of endothelin-1 receptor and the severity of MMVD in dogs (Mow and Pedersen, 1999). Although the endothelin-1 receptor antagonists contradict the effect of endothelin-1, extensive clinical trials are needed to prove their efficacy in preventing or treatment of MMVD

Nitric oxide (NO), its regulatory balance with endothelin and its extracellular matrix functions have been the subject of many recent studies. Nitric oxide is produced from L-arginine in the presence of NADPH and O_2 (Figure 1.5). This reaction is catalyzed by nitric oxide synthase (NOS). Nitric oxide synthase is found in three forms,

neuronal (nNOS, type I), inducible (iNOS, type II) and endothelial (eNOS, type III). While two of these enzymes, namely nNOS and eNOS are constitutively expressed in mammalian cells and the increase of calcium levels is responsible for their activation, iNOS is expressed in immunologically active cells and works independently of the calcium levels (Myers and Tanner, 1998; Droge, 2002). Moreover, eNOS has the unique feature of increasing production of NO in response to sheer stress. This can have a significant importance in MMVD where abnormal closure of mitral valve places an extra strain on the leaflets. Although the synthesis of NO is stimulated by endothelin, NO per se inhibits the synthesis and effects of endothelin (Stricklett *et al.,* 2005). By measuring NADPH diaphorase, it has been shown that there is a strong correlation between NOS expression and mitral leaflets affected with myxomatous degeneration that even corresponds to the severity of the disease (Olsen *et al.,* 2003b). Apart from its interaction with endothelin in extracellular matrix, NO triggers some direct effects on collagen via a paracrine mechanism. Inhibition of NO production in a co-culture system (porcine coronary endothelium + vascular smooth muscle cells) has caused an increase in collagen, especially collagen type I (Myers and Tanner, 1998).

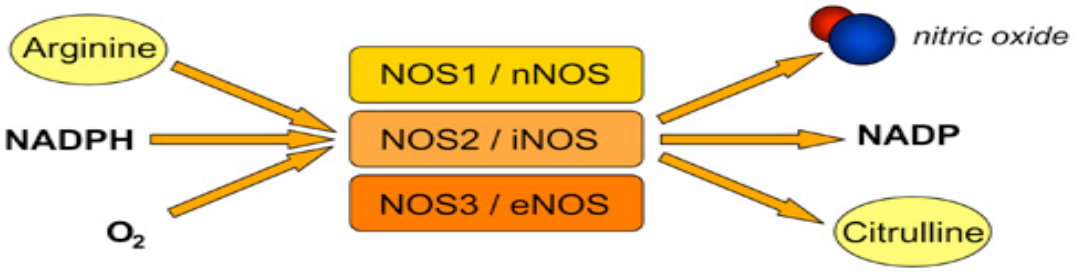

Figure 1.5: Nitric oxide synthase produces NO from L-arginine in the presence of NADPH and O_2 (diagram courtesy of Phil Dash, St George's, University of London).

Neuroendocrine abnormalities also occur in MMVD and may play a role in the aetiopathogenesis of the disease. Of these, norepinephrine and epinephrine system and renin-aldosterone regulation abnormalities have been extensively investigated. In one study, a higher plasma rennin activity (PRA) and a lower plasma aldosterone concentration (PAC) were found in murmur-free cavalier King Charles spaniel dogs, but not in an age and sex-matched control group (Pedersen *et al*., 1995). In another study in men, it was shown that there was a significant increase in PRA in patients with MVP after upright activity, compared to supine, and also compared to controls. However, the concentration of aldosterone was considerably increased in the control group after upright activity while it remained unchanged in patients with MVP (Zdrojewski *et al.,* 1995). In this connection, Pedersen has shown that although there is no strong association between PRA and mitral regurgitation in dogs, a significant correlation exists between increased renin release and the severity of mitral valve prolapse (Pedersen *et al.,* 1998). It should be noted that an increase in renin release largely corresponds with the sympathetic activity in patients with mitral valve prolapse. It is also well recognised that any depletion of blood volume which reduces the ventricular volume can lead to ventricular-valvular disproportion causing more stress on the leaflets. Whatever the cause of activation of the sympathetic system, a sustained sympathetic activity leads to various adverse consequences, including apoptosis and matrix remodelling. These in turn might have a deleterious effect on the diseased mitral valve (Tallaj *et al.,* 2003). In this respect, the impact of the rich innervations of mitral valves is worth taking into account. A recent study shows that

mitral valve action is not merely a mechanical response involving opening and closing in response to the pressure of blood. Rather, there is a profuse network of motor and sensory nerves. Calcitonin gene-related peptide (CGRP), norepinephrine (NE), neuropeptide Y (NPY) and some contributions from postganglionic autonomic nerves are just a part of the dense innervations of mitral valve (Williams and Jew, 2004). However, recent work from our group has shown a decrease in valve innervation with age but no change associated with MMVD (according to Geoff Culshaw, personal communication, November 6, 2008).

Pathology and histopathology

Whatever the underlying cause might be there is a clear pattern of change to the leaflet morphology which by itself contributes to the leaflets mechanical failure. The following section will concentrate mainly on the complexity of collagen synthesis and production (see later) as investigation of changes in the biology of collagen will be the main theme of the thesis.

Microscopically and macroscopically, there are similarities in the pathology of myxomatous mitral valve disease in dogs and primary human mitral valve prolapse. In the dog the disease begins with the appearance of small and discrete nodules at the free margins of the leaflets. As the disease progress these small nodules coalesce, forming bigger nodules. The affected areas, in contrast with other regions, are thick, and opaque, but there is no sign of inflammation of any kind. In 30% of cases the

tricuspid valve is also involved. Some studies suggest that leaflets start to shrink, but the evidence is the leaflets begin to enlarge in size. However, these can easily be overlooked, since they mostly present themselves as interchordal hooding (rolled up edges). The concept of shrunken leaflets may derive from the fact that the compensatory enlargement of the left heart makes the leaflets appears relatively small. Nevertheless, in the very advanced stages of the disease some shrinkage due to secondary fibrosis might occur. In MMVD, when the valves become incompetent, it is not because the so-called shrunken leaflets cannot span the annulus but rather because redundant leaflets cannot coapt properly.

Grossly, on the basis of the Whitney classification (Whitney, 1974), myxomatous valves can be categorized into three grades. In grade I there are very small and separate nodules along the leaflet edges. The presence of larger nodules, accompanied with irregular and more thickened areas on the free edges, is seen in grade II disease. Grade III is recognised as considerable thickening in the entire leaflet, dilatation of the mitral annulus and redundant and flail leaflets. However, it is not possible to judge the extent of the disease solely on the basis of the thickening of the leaflets, since a degree of thickening might be a normal phenomenon both in humans and dogs as they age. A gross pathological assessment is necessary when a heart is dissected and before detachment of the mitral valve from its surrounding tissues. In addition to the mitral valve changes, other changes, including rupture of the chordae , dilation of the left atrium, eccentric hypertrophy of the left ventricle, atrial jet lesions and a full thickness tear of the atrium or ventricle might also be

present (Kittleson, 1998; Schoen, 1999;Van Vleet and Ferrans, 2001; Häggstrom *et al*., 2005).

Histopathological studies of MMVD have shown that changes to the endothelium on the atrial side of the leaflets are one of the first changes that occur. Subsequently, the size of the spongiosa layer increases noticeably. Valve interstitial cells have been shown to trans-differentiate from quiescent fibroblasts to activated myofibroblasts and trans-locate towards the damaged the endothelium (Disatian *et al*., 2008; Han *et al*., 2008,) and production of extracellular matrix intensifies, mainly composed of proteoglycans. Proteoglycans are macromolecules of glycosaminoglycans (GAGs) covalently bound to a core protein. Proteoglycans and hyaluronate tend to associate with water molecules, so occupy large volumes, called domains. Proteoglycans filaments, except in bone, run orthogonal to the collagen fibrils with a separation interval about 60 nm. In bone their orientation is in between or mostly in parallel with collagen fibrils. It has been suggested that they often bind to collagen fibrils through the gap regions of collagen molecules. Therefore, it seems that by the interaction with collagen they could determine the fibrils layout, forming cross-links, and affecting mechanical properties and fibrils diameters. Proteoglycans have also been suggested to down-regulate the collagen fibrillogenesis (Weber *et al*., 1996; Raspanti *et al*., 2008). The type of proteoglycans is also important in determining the extracellular matrix structure. For example, dermatan sulphate (DS) is found in those tissues with a plentiful oxygen supply while keratin sulphate is a substitute for the connective tissues where there is less oxygen supply (Scott, 1991). It is not clear

whether a change in oxygen could actually switch the synthesis of one type PG to another.

While the total elastin content of affected leaflets increases, there are some signs of fragmentation in elastin fibres, which bear some similarities to that of digestion processes mediated by elastase. Nevertheless, no cellular source of elastase has yet been found in leaflets. It has also been suggested that the increased amount of elastin is the result of production by either abnormal or immature elastin (Whittaker *et al.,* 1987; Kittleson, 1998; Tamura *et al.,* 1995; Akhtar *et al.,* 1999; Grande-Allen *et al.,* 2004). What is interesting about elastin is its high tensile strength compared to collagen and so it could contribute more per unit weight to the valves mechanical integrity.

Overall, the changes in the fibrosa (collagen mainly) are characterised by a thinning and degenerative processes. Under the microscope, collagen bundles appear disrupted, swirled, fragmented and attenuated. As the disease progresses and especially when it leads to congestive heart failure (CHF), fibrosis in the leaflets, at least in human, becomes apparent which might be an adaptational response to the growing stress on the leaflets (Grande-Allen *et al.,* 2005).

Although of the pathology the disease in dog and human bear close resemblance to each other, one major difference is the development of bacterial endocarditis in humans. In elderly male patients bacterial endocarditis is a common complication of MVP and is found in surgical intervention for mitral regurgitation in 10% of patients, but is rarely identified in canine patients (Agozzino, 1992).

Collagen biosynthesis

Collagens are a major protein of all vertebrates, accounting for 30% of the proteins in mammals. At least, 30 distinct types of polypeptides are implicated in producing about 27 different types of collagen. However, here only fibrillar collagen (types I, II, III, V and XI) will be discussed. The following is a brief account of fibrillar collagen biosynthesis and a more detailed review can be found elsewhere (Bornstein, 1974; Kivirikko and Myllylä, 1984). All fibrillar collagens are all about 300nm in length. They are formed from three separate polypeptides, called alpha chains, each a left-handed helix. The whole molecule itself, however, is a right-handed superhelix. This triplet structure could be homotrimeric or heterotrimeric depending on the collagen type. The sequence of amino acids in each chain is a regular repeating of a tripeptide, Glycine-X-Y where X is often proline and Y is often 4-hydroxyproline. Proline and hydroxyproline impart rigidity to the molecule whereas glycine, because of its small size, plays an important role at points where three chains are in close contact with each other. Collagen type I is a major component of fibrils in tendon, skin, bone and mitral valve, whereas in cartilage the collagen is mostly made of type II. Collagen fibrils may also be hetrotypic if they contain different types of fibrillar collagen. For example, collagen type III is also found in collagen fibrils in mitral valve alongside collagen type I. This is also true for type II and XI collagen in the cartilage. Collagen fibrils can also differ in length at various stages of their development, ranging from 20 nm to 500 nm, exceeding the size of the fibroblasts from which they have been secreted. Small-diameter collagen fibrils are found in a very highly organised arrangement, such as in the cornea where they ensure optical transparency.

Collagen biosynthesis takes place in several stages, and though it resembles other proteins, some co-translational and post-translational modifications are unique to collagen. As different tissues express different α chains molecules, it appears that they have various genes for these chains. The locations of some of these genes have already been determined. For example, in humans, genes for α1 (I), α2 (I) and α1 (III) are located on chromosome 17, 7 and 2, respectively (Huerre *et al.,* 1982). The size of these genes is ten times bigger than corresponding translated mRNAs, because the coding information is located in more than 50 exons (varying between 51 and 54 in fibril forming collagen), which intermittently are interrupted by introns (non-coding regions). While the exons sizes are homologous in these genes, the sizes of the introns vary widely. The structures of these complex genes have been categorized into 3 groups namely: collagen helix, C-propeptide protein region and N-propeptide protein region. The helical domain of collagen is composed of 44 exons (between exon number 6 and 49) each containing 54 bp (base pairs) coding for 6 Gly-X-Y repeats. However, it is also possible to find exons with 45, 99, 108, and 162 bp. The finding that most of the exons coding for helical regions have 54 bp suggests that current collagen genes are the result of the duplication or multiplication of an original single unit containing 54 bp. Each individual exon in the helical region of a given collagen gene begins with a codon for glycine and ends with a codon Y which would precede glycine residue of the next exon. The N and C terminals of the triple helix are coded by the junctional exons 6 and 49, respectively, which are also responsible for coding of the non-helical region of α chains and part of the propeptide. Possessing three different structural domains in one exon and not interrupted by any exons might be related to a specific functional attribute such as

procollagen protease activity which plays an essential part in collagen biosynthesis. The size of exons coding for the C-propeptide, namely part of exon 49 and (50-52) are much bigger compared to exons destined for triple helix and also very conserved compared to the exons responsible for coding N-propeptide (from exon 1 to part of exon 6).

The mRNA for the pro α chain is produced in the same way as most other proteins in eukaryotes. The primary transcript mRNA is consisted of both exons and introns and is very large. This mRNA undergoes multiple steps of excision and splicing in order to produce a translatable cytoplasmic mRNA. Like other secreted proteins, as collagen products are being synthesized on free ribosomes, the N-terminal signal sequence of the protein is recognized by signal recognition particle (SRP) and the translation is paused until this complex binds to the SRP receptor on the endoplasmic reticulum (ER). This attachment causes the nascent polypeptide chain to cross the membrane, and translation resumes upon this attachment. As preprocollagen emerges into lumen of the RE, the signal peptide is removed enzymatically and the new molecule is called procollagen.

Post-translational modification

Hydroxyproline and hydroxylysine are almost exclusively found in collagen. Their formation is catalyzed in a series of post-translational events by the following three enzymes: peptidyl proline 4-hydroxlyase, peptidyl proline 3-hydroxlyase and peptidyl lysine hydroxlyase. All three enzymes are located in the cisternae of endoplasmic reticulum and hydroxylate proline and lysine on the nascent polypeptide

while it is growing on the ribosomes. However, hydroxylation continues even after the translation has been completed, until the formation of the triple helix prevents any further hydroxylation. These enzymes require Fe^{2+}, 2-oxoglutarate, O_2 and ascorbate for their proper biological activities. The minimum sequence requirements for peptidyl proline 4-hydroxlyase and peptidyl lysine hydroxlyase are -X-Pro-Gly- and -X-Lys-Gly-, respectively. However, there are reports that both of the enzymes are also capable of acting upon some other triplets. Peptidyl proline 3-hydroxlyase would also need its own specific sequence for hydroxylation, which is -Pro-4Hyp-Gly-. The function of 4-hydroxyproline is essential for the stability of the triple helix at physiological temperature and even for the stability of a given collagen molecule at 37ºC, the complete hydroxylation of Y in Gly-X-Y is necessary. However, the exact role of 3-hydroxyproline remains unknown. The extent of methyl hydroxylation varies in terms of different species and it seems the animals that do live at lower temperatures (for example, Arctic fish) show the lower degrees of methyl hydroxylation. Nonetheless, the 50% of proline in fibril forming collagens is 4-hydroxylated. Two functions have been demonstrated so far for hydroxylysine. Firstly, it serves as a site for the attachment of carbohydrate units and, secondly, it is essential for intermolecular cross-links. The extent of hydroxylation of lysine varies between different tissues and types of collagen. The importance of peptidyl lysine hydroxlyase is very well documented in a variant of Ehlers-Danlos syndrome, in which the affected people have a genetic deficiency of the enzyme leading to malfunction of certain connective tissues.

Although the catalytic action of peptidyl proline 4-hydroxlyase and peptidyl lysine hydroxlyase is similar, their primary sequences and subunit structure show considerable differences. Peptidyl proline 4-hydroxlyase is a tetramer comprised of two α and two β subunits, both of which are necessary for the enzyme activity. On the other hand, peptidyl lysine hydroxlyase is a dimer consisting of only one type subunit.

Glycosylation of hydroxylysine residues

The addition of carbohydrates to hydroxylysine residues is catalyzed by two specific enzymes. Peptidyl hydroxylysine galactosyltransferase (GT) is responsible for adding galactose from UDP-galactose to certain hydroxylysine residues. Subsequently, the transfer of glucose from UDP-glucose to galactosylhydroxylsine is catalyzed by peptidyl galactosylhydroxylsine glucosyltransferase (GGT). The free ε-amino group of hydroxylysine has been shown to play a very important role in carbohydrate transfer in both enzymes, as N-acetylation or deamination completely inhibits the reactions. In addition, it seems that the longer the polypeptide chain is, the greater the tendency for the efficient interaction with the enzymes. Furthermore, the two glycosylation events are also affected by the amino acid sequence of the peptide. The number of -X-Hyl-Gly- sequences in the nascent collagen polypeptide has been recognised as a determinant factor in the degree of carbohydrate attachment to hydroxylysine residues, whereas the amino acid sequence in the proximity of hydroxylysine does not seem to have a very important role in this process. As mentioned before the carbohydrate donor for the glycosylation is UDP (uridine diphosphate) and both reactions need a bivalent cation, preferably Mn^{2+} for catalytic

action. Nonetheless, it has been shown that Fe^{2+} and Co^{2+} could also activate GTT in a low concentration, though in higher concentration, they display an inhibitory function (Myllylä *et al*., 1979). Corresponding information for GT is not still available though several other cations are documented to inhibit both transferases. Figure 1.6 shows the proposed mechanism action of GTT.

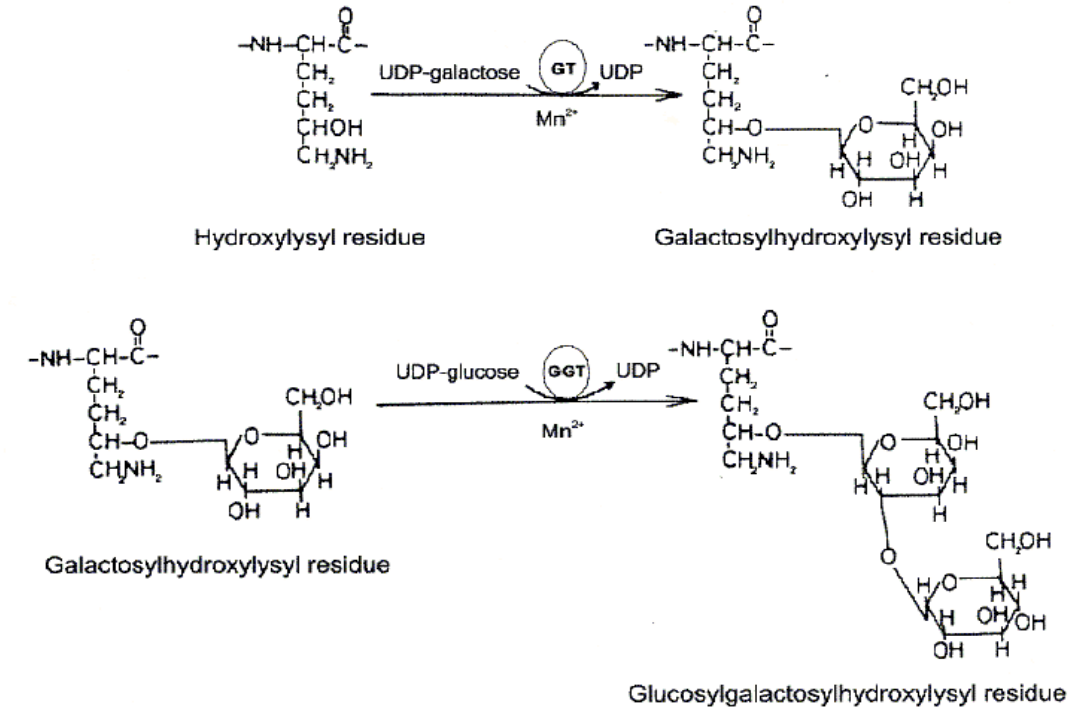

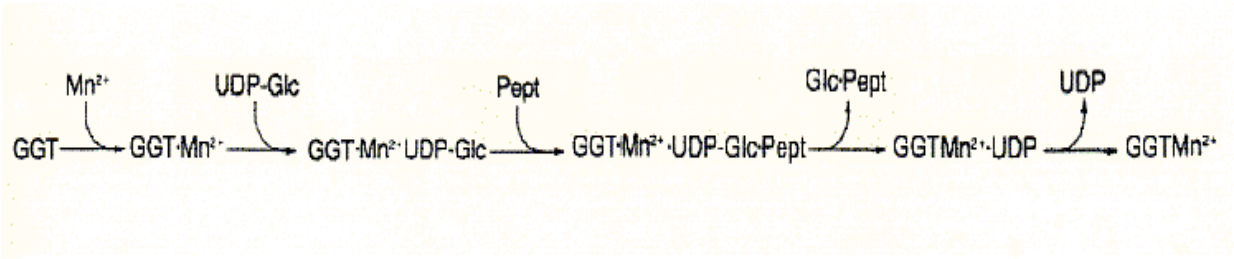

Figure 1.6: Before binding to UDP-glucose, GGT binds successively to two Mn^{2+} and as the dissociation constant for Mn^{2+} for second site in vivo situation is high, it is not firmly bound to the enzyme so has not been shown above. During each catalytic cycle Mn^{2+} often does bind not the enzyme. GGT: galactosylhydroxylysyl glucosyltransferase; UDPglc: UDP-glucose; Glc-pept: glucosylated peptide (Kivirikko and Myllylä, 1984).

Only carbohydrate attachment to mammalian mature collagen exists either as monosaccharide galactose or as disaccharide glucosylgalactose. Like hydroxylation, the glycosylation occurs while the polypeptide chain is being translated and continues after the complete pro α chain is released, until before it is hindered by the formation of triple helix. The precise function of combined hydroxylysine and carbohydrate has not been completely resolved. However, it is thought that they have the following functions:

1. As they constitute quite large molecules on the collagen molecules, they might influence the biological properties of collagen by altering the lateral packing of molecules within fibrils (Grynpas *et al.,* 1980).

2. The sensitivity of collagen molecules to mammalian collagenases might be affected by the extent of glycosylation.

3. In some collagen molecules such as type IV, these hydroxylysine-linked carbohydrates might serve as an attachment site for some cells.

Glycosylation of asparagine residues in propeptide

Unlike collagen molecules, the propeptides of procollagen molecules have asparagine-linked carbohydrates which, in the case of procollagen types I and III, are almost always found in the C-terminal of the propeptide, whereas in procollagen type II both ends of the propeptide, including the N-terminal, is known to contain the same asparagine-linked carbohydrate. As most other proteins, the asparagine linked

carbohydrate is first synthesized on a lipid carrier. Then, the preformed oligosaccharide is transported to a conserved sequence of -Asn-X-Ser/Thr in a nascent polypeptide chain to attach to asparagine residue. In the case of human pro α1(I) and pro α2(I) chains and chick's pro α2(I) and pro α1(III), this sequence is -Asn-Ile-Thr while in chick's pro α1(I) this sequence is -Asn-Val-Thr. The transfer occurs in the lumen of the ER and is catalyzed by an enzyme called oligosaccharyl transferase. Following the transfer, the oligosaccharide undergoes some further changes and additional reactions occur, resulting in the production of mannose-rich complex oligosaccharide structures.

The function of the asparagine-linked carbohydrates remains unknown. There have been suggestions that these mannose oligosaccharides play a role in normal secretion of procollagen from the cell. There are also reports that the clearance of C-propeptide from the circulation by liver endothelial cells is mediated through mannose-receptor endocytosis (Nelson and Cox, 2005; Sellaro, 2003).

Procollagen assembly and helix formation

The propeptides of procollagen contain both interchain and intrachain disulfide bonds. While interchain bonds in type I and type II procollagen are only found between C-terminal propeptides, in type III procollagen, both N- and C-terminals of the propeptides are attached by disulphide bonds. In a complete type III collagen molecule, two interchain disulfide bonds are also found in the C-terminal of the triple helix. Regarding the interchain disulphide bonds, it seems that they are not formed until the translation completes or in other words the polypeptide is released from

ribosomes. Formation of these bonds starts while procollagen molecules approach together in a process called “registration” which plays a role in proper alignment of the molecule (Murray *et al.,* 2000; Diegelmann, 2001). It has been shown that preventing formation of triple helix does not have any effect on the formation of interchain C-terminal disulphide bonds in the propeptide. However, the inhibition of formation of triple helix would prevent the formation of interchain N-terminal disulphide bonds. This clearly indicates that interchain disulphide bonds in the C-terminal of the propeptide are synthesized earlier than those of N-terminal bonds. Additionally, the formation of a triple helix is a requirement for the latter. Protein Disulphide Isomerase (PDI) is an enzyme responsible for catalyzing disulphide bonds in vivo. Interestingly, PDI itself is the β subunit of peptidyl proline 4-hydroxlyase enzyme. However, the role of PDI in peptidyl proline 4-hydroxlyase is not related to its isomerase activity. It seems that PDI functions to keep the insoluble α subunits in proline 4-hydroxylase in the catalytical and non-aggregated state. Two conditions are required for in vivo triple helix formation, namely the complete 4-hydroxylation of the Y position in the Gly-X-Y sequence and the formation of interchain disulphide bonds in the C-terminal of the propeptide. However, *cis-trans* isomerisation of the prolyl peptide bond poses an important rate-limiting step in triple helix formation. It has been documented that this isomerisation process is facilitated by enzymes with peptidyl prolyl *cis-trans* isomerase (PPI) activity. In vitro studies have shown that the drug cyclosporine A, by inhibiting PPI, slows down the folding of procollagen I and III in cultured human fibroblasts. The triple helix of procollagen of fibrillar collagen folds from C-terminal to N-terminal at a rate which is consistent with *cis-trans* isomerisation of prolyl peptide bonds. The main task for

interchain disulphide bonds in terms of procollagen folding has been demonstrated by virtue of fast formation of triple helix in type I and II procollagen, compared to the lengthy process in type IV procollagen which lacks these interchain disulphide binding) and type V procollagen (which only some chains are connected by disulfide bonds) formation. The presence of these disulphide bonds might account for up to one hour difference in folding time in different types of procollagens.

Another quality control mechanism which ensures that only the properly folded procollagen molecules are secreted is the peptidyl proline 4-hydroxlyase enzyme. It has been shown that the peptidyl proline 4-hydroxlyase enzyme interacts continuously with collagen chains in the presence of enzyme inhibitors. In one study, peptidyl proline 4-hydroxlyase was inhibited by α, α′-dipyridyl, and it was observed that peptidyl proline 4-hydroxlyase formed a stable bond with un-hydroxylated and non-helical pro α1 (III) chains. Additionally, upon the removing of the inhibition (by the addition of excess iron) hydroxylation and helix formation resumed. Interestingly, a low affinity of peptidyl proline 4-hydroxlyase for substrate is seen when collagen is fully hydroxylated or helix structure is achieved. This characteristic of peptidyl proline 4-hydroxlyase enables it to retain malformed or immature collagen. For example, in an osteogenesis imperfecta (OI) patient with a 180 deleted amino acids in triple helix, complete intracellular retention of mutant molecules has been reported. These molecules then could be digested by a mixture of enzymes such as trypsin and chymotrypsin.

BiP (Binding Protein) is a 78 kD-ER resident enzyme, which was originally identified as the immunoglobulin heavy chain binding protein or glucose regulated

protein (Grp 78). It is constitutively synthesised inside cells and is presumed to have a general role in the assembly of newly synthesised polypeptides, including collagen. It often recognizes the unfolded polypeptides and by preventing them from inter- and intra-chain aggregation, prepares them for proper folding. However, it has been shown that its production is increased in the presence of mis-folded and under-glycosylated polypeptide. Moreover, it is further induced under stress conditions, which often leads to the accumulation of intracellular incorrectly folded proteins. As some studies have shown, BiP could only act on the C-terminal propeptide of procollagen and in normal conditions, transiently binds to it. Nonetheless, in the case of some abnormalities in the C-terminal propeptide of procollagen, BiP binds stably to this part of polypeptide and subsequent assembly of procollagen is slowed or completely blocked (Gething, 1999; Koide and Nagata, 2005)

HSP47 (or colligin) is a collagen specific binding molecule with 47 kDa molecular weight, which is classified as a heat shock protein. It has been shown that, following exposure of chicken embryo fibroblasts to 45° C, there is a 10 fold increase of the HSP47 transcription. Nevertheless, normal transcription is resumed very quickly if the temperature returns to 37°C. The protein is primary a resident of the ER of vertebrates. The cDNAs for HSP47 have been cloned for human, rat, mouse and chicken. HSP47 bears some resemblance to the serpin family of serine proteinase inhibitors though in *in vitro* assays it does not show any proteinase activity. The expression of HSP47 is closely linked to that of collagen and some in vitro studies have shown that HSP47 cannot display any binding distinction between unfolded chains and mature folded collagen molecules. However, the binding is pH dependent

and stops below pH 6.3, due to conformational changes. The specific sequence, which is recognised by HSP47, has not been fully identified. Some researchers have suggested that HSP47 recognises the amino acid sequence of -Arg-Gly-Asp- (RGDs). However, it seems that other determinants must be involved as HSP47 only recognises collagen RGDs motifs and does not recognise RGDs sequences found in other molecules such as fibronectin (Nagata, 2003; Koide and Nagata, 2005).

HSP47 binds to the polypeptide chain as translation starts and this binding continues through the chain association and triple helix folding. It disassociates itself from the triple helix only when the triple helix enters the Golgi. There are some possible roles for HSP47. Firstly, after triple helix formation occurs in the ER, it might still need some more modification, but at this stage other chaperones are no longer able to recognise the polypeptide. Thus, continuous binding to HSP47 would ensure that this modification will happen. Secondly, binding of HSP47 to the polypeptide protects the newly synthesised triple helix from intracellular degradation that might otherwise take place as a result of prolonged retention in the ER, resulting in a haphazard aggregation of polypeptide. Ishida *et al.* (2006) recently demonstrated that Hsp47-/- fibroblasts produced low levels of type I collagen, which was very thin and frequently branched. They also showed that this low production was due to the accumulation of indiscriminate aggregate of new synthesized polypeptide in ER in the absence HSP47. Thirdly, by covering the reactive groups that are responsible for assembling higher order structures of collagen, HSP47 could guarantee that this does not happen inside the ER. A final suggested role for HSP47 is that this protein provides thermal stability for helical region of procollagen. Thus, by binding to the

helix, HSP47 ensures that thermal disturbances such as heat shocks do not micro-unfold the helix. After the successful formation of fully hydroxylated triple helix, the procollagen-HSP47 complex is transported to the cis-Golgi or the ER-Golgi intermediate compartment (ERGIC) via vesicle transport.

The disassociation of HSP47 from procollagen might be caused through a pH change. *In vitro* disassociation occurs below pH 6.3 and the low pH of in the Golgi apparatus (estimated 5.7) may therefore result in disassociation. However, to validate this mechanism, the exact pH inside of Golgi apparatus should be confirmed. The procollagen triple helices then form some lateral bundles through a mechanism called "cisternae maturation" (Bonfanti *et al*., 1998). Interestingly, the lateral bundling of type one procollagen is inhibited in the presence HSP47, suggesting the contrary function of HSP47 and necessity of its absence inside Golgi apparatus. Figure 1.7 briefly depicts the suggested roles of HSP47.

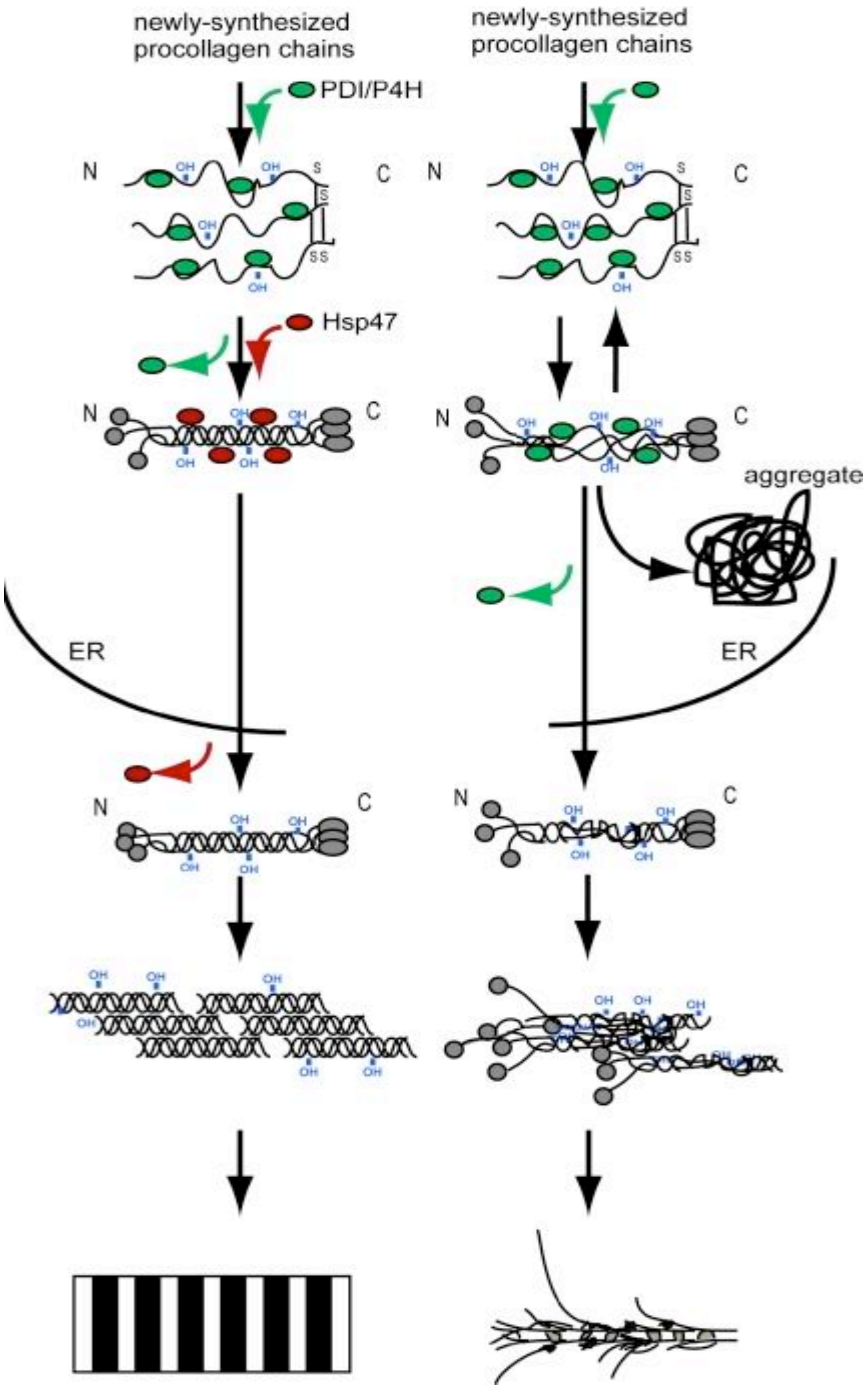

Figure 1.7: HSP47 of action in vivo: Normal cell (left) and HSP47-knockout cell (right). In the knockout cell the secreted collagen would be fragile, disorganised and branched (Ishida *et al.*, 2006).

Procollagen trafficking from the ER to the Golgi

The newly synthesized proteins destined for secretion are transported from the ER to the *cis* face of Golgi. They exit fully processed from the *trans* face of Golgi and then are carried towards plasma membrane (PM). However, the mechanism involved in this transportation has been the centre of heated debate for about 40 years. It is generally accepted that the route from the ER towards the Golgi involves budding of vesicles 60-80 nm of diameter from the ER membrane. The vesicles are coated with a special molecule called COPII (coat protein complex II). COPII is made of 5 different proteins and is thought to play an important role in the structure of the vesicles. Moreover, it has been shown that different populations of COPII provide specific determinants for different protein cargos. COPI is another protein which facilitates the retrograde transport of ER-resident proteins back to the ER. In addition, it also plays a role in later stages of protein transportation (see below). Newly synthesized procollagen proteins are about 300 nm long and are rather rigid, so the conventional 60-80 nm vesicles are unable to contain these molecules. Further research has demonstrated that procollagen molecules exit the ER in a saccular structure called VTC (vesicular tubular cluster) which, interestingly, lacks COPII. However, the process of exit is yet again COPII dependent and COPII is found in the proximity of procollagen exit site. It is thought that COPII might be necessary for increasing the concentration of procollagen or other unknown factors near to the exit site. VTCs move along microtubules towards Golgi apparatus and in later stages might be also called the ERGIC (the ER-Golgi intermediate compartment). In addition, it has been shown that in the same later stages there is a close association between ERGIC and COPI.

Upon reaching the Golgi, procollagen molecules start to undergo some post-translational modification. For example, the processing of N-linked oligosaccharides in the Golgi is very well recognised. Nonetheless, the process of traversing of molecules from *cis* to *trans* cisternae while they are being modified is rather controversial. The conventional approach considers the Golgi as a structure with different cisternae layers and the proteins are transported between these layers via the "vesicle shuttle model", which involves budding off from one layer and merging with another layer. The second approach, which is also called the "cisternae maturation model" and is favoured for procollagen transport, suggests that proteins move across the layers of the Golgi layers without even leaving the lumen of the Golgi apparatus (Bonfanti *et al.,* 1998). In this model, after receiving of the given protein, *cis*-cisternae transform into medial-cisternae and subsequently into *trans*-cisternae (Figure 1.8). The role of COPI vesicles lies at the heart of the controversy. The former model suggests that these type of vesicles are in involved both in anterograde (forward) and retrograde movement of proteins and Golgi-resident enzymes, respectively. In the latter model, COPI is not necessary for anterograde trafficking of proteins and it has been shown in yeast that some protein could be secreted in the absence of COPI function (Malhotra and Mayor, 2006).

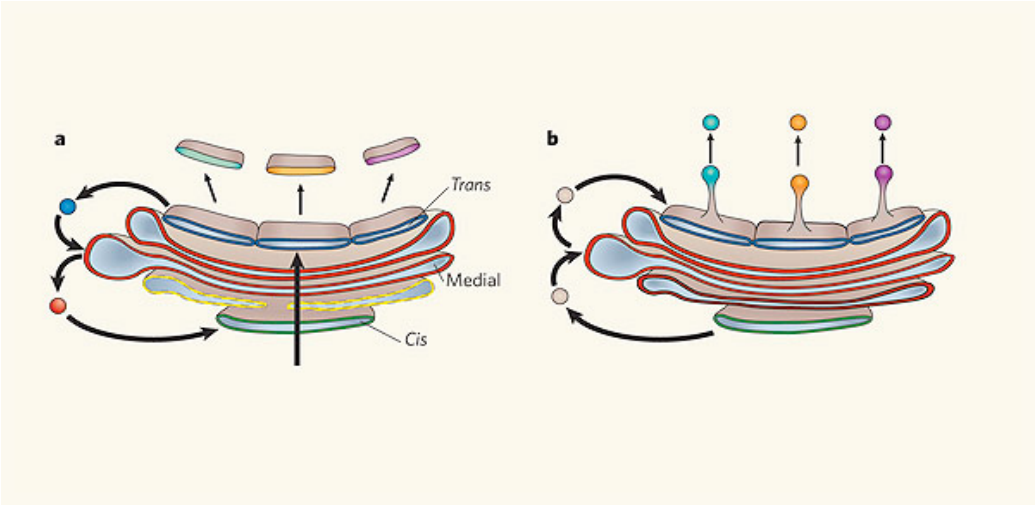

Figure 1.8: Two suggested routes of protein transport in the Golgi: (a) “cisternae maturation model”, in which destined proteins never leave the lumen of the Golgi and (b) “vesicle shuttle”, in which anterograde movement happens via vesicles. It seems that collagen traverses using the cisternae maturation model (Malhotra and Mayor, 2006).

Furthermore, two other intermediate models have also been proposed. The first one, the “hybrid model” suggests a possible combination of vesicular transport and cisternae maturation and the second one, the “intersectional connection model”, proposes a theory of tubules which connect cisternae in the Golgi making it possible for forward and backward movement of cargo proteins and Golgi-resident enzyme. At the present time, a single working model, which is in agreement with all studies and explains the exact role for COPI coated vesicles, seems elusive.

From the Golgi apparatus to secretion

Proteins are finally committed to their different destinations in the *trans* Golgi, as a result of different carriers in various cells. Using confocal and internal reflection

microscopy with fluorescently tagged proteins has proved that these carriers are heterogeneous in terms of their size and shape. Their transport is microtubule dependent. As with collagen, an electron microscopy study of fibroblasts has revealed some electron-dense vacuoles separating from *trans* Golgi. These vacuoles contain bundles of procollagen, and may be as large as 500 nm. At the early stage of deposition of connective tissue, the PM of fibroblasts become very convoluted and studies have shown that collagen fibrils are present in the recesses of convoluted PM and secreted through this structures (Birk and Trelstad, 1984; Ploetz *et al.*, 1991). Producing a solution of collagen molecules using cold or weak acidic buffers, and subsequently warming and neutralizing the solutions, leads to the spontaneous self-assembly of collagen molecules into fibrils with the characteristic 67 nm axial D-periodicity. However, these reconstituted fibrils show no preferred orientation. Canty *et al.* (2004) describe a novel protrusion in embryonic tendon as a fibril depositor or "fibripositors". They further suggest that the conversion of procollagen to collagen molecules, and some degree of fibril formation, occur in vacuoles or GPCs (Golgi Plasma Membrane Carriers), while procollagen molecules are being transported for secretion. They have shown collagen fibrils as large as 28 nm in diameter inside GPCs. Moreover, the fibripositors always orient in along the tendon axis. This finding might establish a link between intracellular transport of collagen and the orientation of fibrils in the ECM. An interesting finding in this study was that they failed to see any fibripositors in the later stages of the life. It seems that they are only found for a narrow span of embryonic life and act as nucleolus for proper orientation of collagen fibrils when tissues start to form their final shape.

Procollagen processing

An important step in the biosynthesis of collagen is the removal of N- and C-propeptides from procollagen molecules by procollagen N- and C-proteinases, giving rise to a collagen molecule 3000 Å long and 15 Å thick that is able to self-assemble into a fibril (Nelson and Cox, 2005). This cleavage does not just happen outside of the cell, but as Canty *et al.* (2004) showed, it can also happen inside GPCs. This proves the theory that production and transport of these proteinases is concomitant with procollagen molecules. Perhaps the Lapiere *et al.* work (1971) is a vivid example of the importance of these enzymes, they showed that cattle fragile skin associated with dermatosparaxis was the result of a defect in the cleavage of N-propeptide in the pro α chain of type I procollagen. Although Lapiere *et al*. (1971) proved the existence of this enzyme, they were unable to isolate it. However, later research led to the isolation and preparation of N-proteinase and showed that various types of the enzyme only act on certain types of intact procollagen molecules and cannot cleave the N-propeptide of heat-denatured procollagen. Furthermore, it has been shown that recognition of the native conformation of procollagen by this enzyme is a function of temperature, and is related to the thermal transition of the helix. For example, a difference of 2 or 3°C between the unfolding temperatures of human type I and chick embryo procollagen seems to play an important role in the activity of the N-proteinase. It could also be said that this sensitivity to the substrate conformation acts as a checkpoint ensuring that all N-terminals have the correct conformation, therefore guaranteeing their later packing (Prockop *et al.,* 1998). The members of the ADAMTS (a disintegrin and metalloproteinase with thrombospondin

motifs) family, namely ADAMTS-2, ADAMTS-3 and ADAMTS-14, are responsible for N-proteinase activity.

In terms of C-proteinase, the members of the tolloid family of zinc metalloproteinases including BMP-1 (bone morphogeneic protein 1), mammalian tolloid (mTLD) and tolloid like 1(TLL-1) are involved in cleaving of the C-propeptides. Although it was said that the N-proteinase activity is important for proper packing of collagen, the C-proteinase activity is significant as a form of rate-limiting step for fibrillogenesis, as it has been shown that the retained C-propeptides are never incorporated in fibril formation (Canty and Kadler, 2005; Ge *et al*., 2006). Furthermore, the cleavage of these propeptides from soluble procollagens (which is essential for intracellular trafficking) produces insoluble collagen molecules. Figure 1.9 shows a rapid snapshot of collagen production.

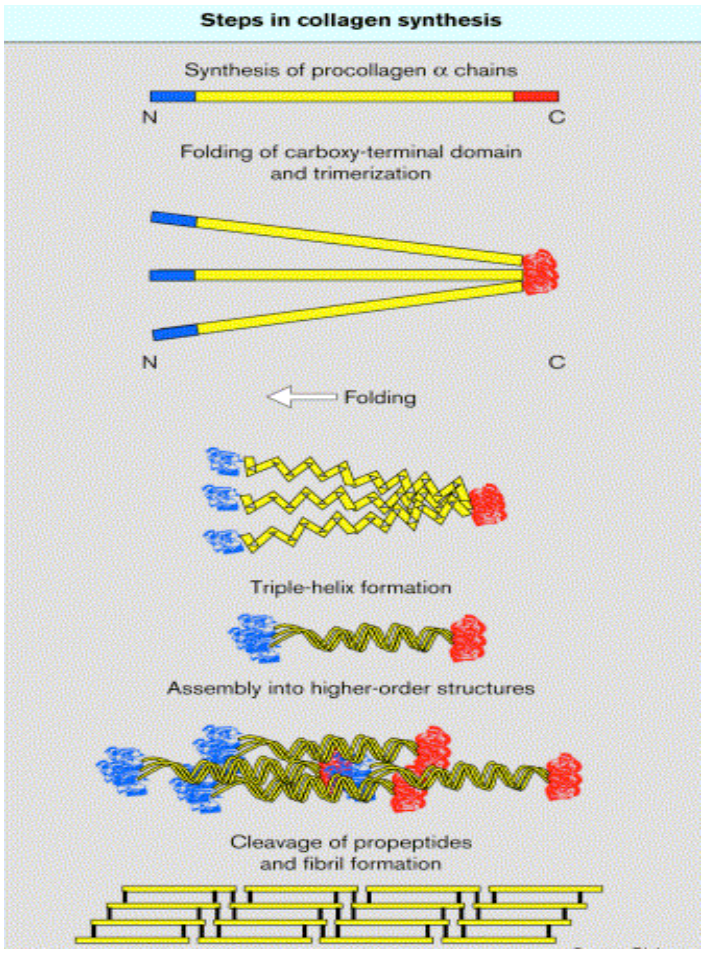

Figure 1.9: A simplified overview of production of collagen. Three procollagen α chains approach together from their carboxy-terminal ends to form a trimer. The folding of these three chains continues towards the amino terminus before the formation of the triple helix. The cleavage of carboxy and amino-termini happens after the procollagen has been transported across the Golgi apparatus, thereby allowing their self-assembly into collagen fibrils (see the text for more detail) (Hendershot and Bulleid, 2000).

Collagen suprastructure

The self-assembly of collagen molecules into fibrils is an entropy driven phenomenon which also occurs in other proteins like microtubules and actin

filaments in order to reach a stable situation. During the assembly, solvent molecules are lost from the surface of the molecules minimizing the surface area/volume ratio of the final assembly and decreasing its free energy. The molecules of collagen align parallel to each other, in quarter stagger pattern. If every molecule is considered to be 4.4D long, then the stagger between adjacent molecules is 1D. The gap between the head of one and the tail of the next molecule is 0.6D. This structure makes a rope-like pattern possessing repeats of gap and overlapping in which each repeat is 1D (between 64 and 67nm depending on the tissue) (Figure 1.10). Additionally this structure is responsible for the characteristic striation pattern observed under electron microscopy.

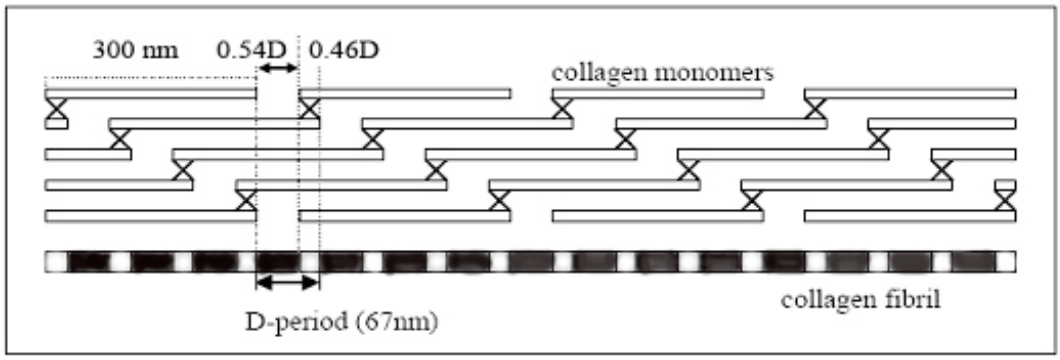

Figure 1.10: Total length the collagen molecules is 300 nM or 4.4 D, where D is the length of striation. In the negative stained methods, dark and light patterns of the fibrils are representing the gap and overlapping areas (Modified from Millard, 2007).

Another study (Holmes *et al.,* 1992) has shown that the primary fibrils have a near paraboloidal pointed tip and a blunt end. The growth of the fibril occurs exclusively from the pointed end. However, as growth continues the blunt end becomes pointed

and growth then continues in the other direction as well. The final result is a fibril having two pointed tips with collagen molecules orientated with their N-termini towards either end of the fibril. Thus, these fibrils are N-N bipolar and it seems that a switch in molecular orientation occurs somewhere along the fibril (Figure 1.11)

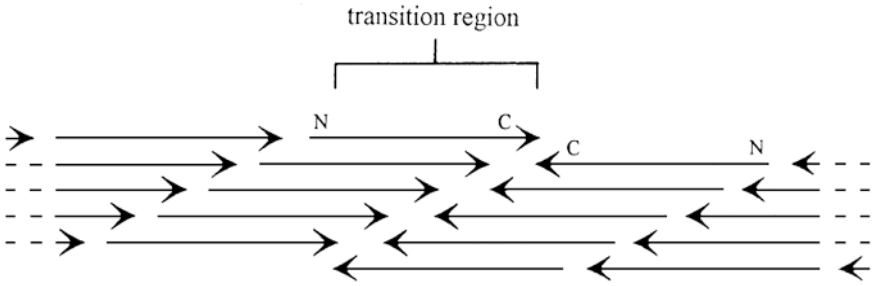

Figure 1.11: Collagen molecules are forming fibrils in N-N bipolar manner where the both end of the fibrils end in N-termini. Although the growth of the fibrils only happens from N-termini end. It seems that there is a switch area in the middle of the fibrils (Kadler *et al*., 1996).

However, this type of orientation seems not to be the case in all fibrils. For example, in 18-day chicken embryo about half of the early fibrils are bipolar and half are unipolar (polarity of the molecules is unchanged throughout the fibril) so the fibril posses both N- and C- termini. Fusion of these bipolar and unipolar fibrils is also matter of the scientific interest. Unipolar fibrils could fuse in a different way that is inconsistent with in-vivo and in-vitro studies. Two unipolar fibrils both possess the

orientation of N- to C- from left to right could fuse side-by-side or end-on-end in order to elongate or thicken the size of fibrils, respectively. Two oppositely orientated unipolar fibrils could also fuse end-on-end giving rise to a long bipolar fibril. However, the following scenarios are disallowed: The side-by-side fusion of two oppositely orientated unipolar fibrils and side-by-side or end-on-end fusion of two bipolar fibrils. The question remains, however, what would be the function for bipolar fibrils. One might suggest that they could play a role in controlling of diameter of collagen fibrils in certain tissues (Kadler *et al*., 1996).

The collagen fibril formation in cell culture is dependent on the integration of fibronectin into the emerging fibrils. Fibronectin is a ubiquitous extracellular matrix protein secreted as a soluble dimer and then assembled into multimeric fibrils at the cell surface. An in vitro study has shown that directing an antibody to the collagen binding fragment of fibronectin would inhibit both the assembly of fibronectin and collagen. It has also been shown that certain integrin molecules do not just potentiate the action of fibronectin, but they also directly interact with collagen molecules. These studies demonstrate that fibril formation begins from the cell surface and in interaction with other molecules such as integrin and fibronectin in a way that assembly of collagen is almost downstream to that of fibronectin. Further investigation is needed to examine whether these events would exactly occur in-vivo.

There are other molecules, which could bind to the collagen molecules and modulate the fibril diameter. In vitro studies have revealed that small leucine-rich repeat proteoglycans (SLRPs) such as decorin, fibromodulin and lumican have an effect on the diameter of collagen fibrils. Keene *et al*. (2000) have demonstrated that decorin

binds to the C-terminus of procollagen type I inducing a delayed fibril assembly and a subsequent reduction in the average fibril diameter, which is essential in some connective tissue, such as cornea to maintain its transparency. Unpublished proteome data have shown differential expression of several of these SLRPs in canine MMVD (according to Richard Han, personal communication, November 6, 2008).

Cross-links and lysyl oxidase

Both collagens and elastin proteins contain lysine or hydroxylysine-derived covalent cross-links. An enzyme that belongs to the family of lysyl oxidase enzymes is responsible for catalyzing these cross-links. The locations of these cross-links depend on the amino acid sequence and the quaternary structures, but they may also be quite flexible. Lysyl oxidase oxidatively de-aminates certain lysine and hydroxylysine residues leading to the corresponding α-aminoadipic-δ-semialdehydes, usually referred to by allysine and hydroxyallysine (Figure 1.12). Thus, there could be two pathways in fibrillar collagen, namely allysine (lysine-derived aldehyde) and hydroxyallysine (hydroxylysine–derived aldehyde). The allysine pathway predominates in skin while hydroxyallysine is the dominant pathway in internal connective tissues like bone, cartilage, ligaments, and tendons, but much less frequent in the skin. However, this is not always true as rat–tail tendon, for example, contains allysine derived cross-links. Generally, hydroxyallysine pathway is abundant in the tissues that bear mechanical loads.

When lysine- and hydroxylysine-derived aldehydes react with corresponding aldehydes on adjacent polypeptide chains or with intact lysine and hydroxylysine

residues initial condensation products form leading to bifunctional cross-links (cross-links that connect two molecules of collagen together). As these bifunctional cross-links posses Schiff base double bonds (-N=CH-), they can be reduced by reagents like sodium borohydride (NaBH4). Furthermore, as these reducible collagen syntheses occur transiently in connective tissues, they are also called intermediate or immature cross-links. Of these, dehydrolysinonorleucine (reduced form: lysinonor-leucine,LN), dehydrohydroxylysinonorleucine (reduced form: hydroxy-lysinonorleucine, HLN), dehydrohydroxylysinohydroxynor-leucine (reduced form: dihydroxylysinonorleucine, DHLN) have been identified and studied extensively (Figure 1.13) (Saito *et al.*, 1997).

During the maturation of the tissue, the intermediate reducible divalent cross-links transform into tri-functional and even tetra-functional cross-links namely, hydroxylysyl pyridinoline (HP or pyridinoline Pyr), lysyl pyridinoline (LP or Deoxypyridinoline- D-Pyr) and histidine adducts.

In the fibrillar collagens (types I and III), four cross-linking sites have been identified. Two sites occur toward the amino terminus, one in the telopeptide region, the other in the helical region. A second pair of sites occurs toward the carboxyl terminus, one in the helical region, and the other in the telopeptide region. However, the hydroxylation of lysine in telopeptide seems to be a very crucial step in determining which cross-links pathway the collagen molecules would follow. It appears the hydroxylation is regulated by an enzymatic system. The enzyme is known to be telopeptide lysyl hydroxylase (TLH). A direct involvement of this enzyme has been recently confirmed in a type of osteogenesis imperfecta called

Bruck syndrome. In this condition, a lack of hydroxyallysine-derived cross-links leads to the fragility of bone despite the presence of allysine-derived cross-links. This shows the different properties of mature cross-links in terms of rendering strength, flexibility and loading-bearing to various tissues. Different variants of TLH have been recognised and it seems that they are tissue-specific. Further investigation of the TLH may reveal different spectrum of cross-link patterns in various tissues.

Lysyl oxidase (LO) belongs to a multi-gene family consisting of five members, namely LOX, LOXL, LOXL2, LOXL3 and LOXL4. However, in this family, lysyl oxidase is the enzyme that has been studied most intensively. Lysyl oxidase was initially detected in embryonic chick epiphyseal cartilage with elastin substrates prepared from 16-day chick embryo aortas labelled with [6-5H] lysine in organ culture in the presence of the lathyrogen, β-aminopropionitrile (β-APN) to inhibit aldehyde formation. From the time of its discovery in 1968 by Pinnel and Martin, plenty of work has been carried out in relation to specificity, purification, physical-chemical properties, expression under different condition and catalytic mechanism. Originally, the investigation of this enzyme was hampered due to the enzyme insolubility and rapid aggregation of the enzyme. A major advance occurred when the enzyme was solubilised using buffers containing 4-6M urea. Full activity was recovered when the urea was removed. Lysyl oxidase has been now isolated from a range of different sources including, human, pig, avian, rodent and bovine. The approximate molecular weight of isolated enzymes is 32 kDa. *In vitro* studies of the translational product of lysyl oxidase have shown that the enzyme is synthesized as a pro-proenzyme product with a molecular weight of 46 kDa. Subsequent signal

peptide cleavage and N-glycosylation result in a 50 kDa proenzyme. The 50kDa proenzyme has been detected both in the cell medium and intracellular fraction. Procollagen C-proteinase, which can be inhibited by EDTA, then cleaves this proenzyme between Gly-168 and Asp-169 (human sequence) to produce a mature and non-glycosylated 32 kDa enzyme, ready to operate (Kagan, 1986; Mäki, 2002; Kagan and Li, 2003). It has also been found that other extra-cellular enzymes including talloid and talloid-like protease are able to cleave the 50kDa proenzyme to its active form at a lower efficiency. It is worth noting that procollagen C-proteinase and procollagen N-proteinase are also responsible for the removal of N- and C-procollagen peptide, respectively. This removal is essential for spontaneous aggregation of collagen molecules into mature microfibrils. Thus, procollagen C-proteinase plays a dual role in collagen cross-links by producing a suitable collagen substrate for lysyl oxidase and also by converting lysyl oxidase proenzyme into a fully functional enzyme.

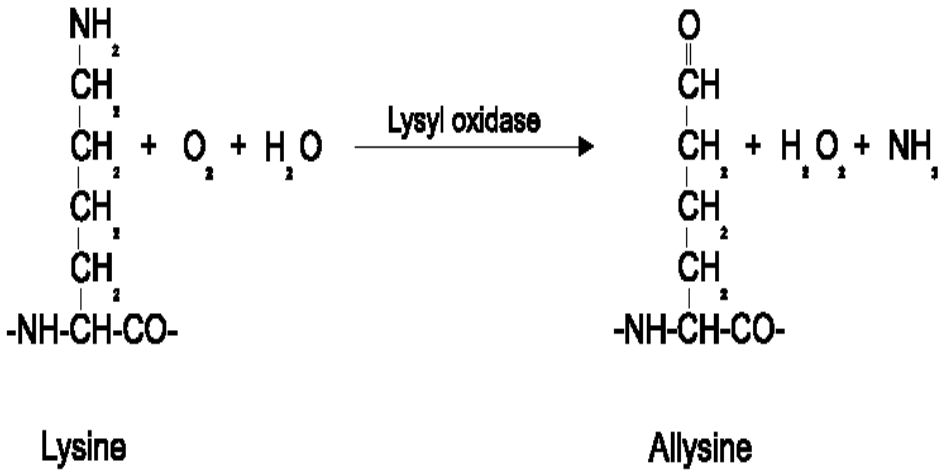

Figure 1.12: Lysyl oxidase oxidatively deaminates a peptidyl lysine to generate a peptidyl α-aminoadipic-δ-semialdehyde (allysine), which spontaneously reacts with corresponding aldehydes to form cross-links (Kagan, 1986).

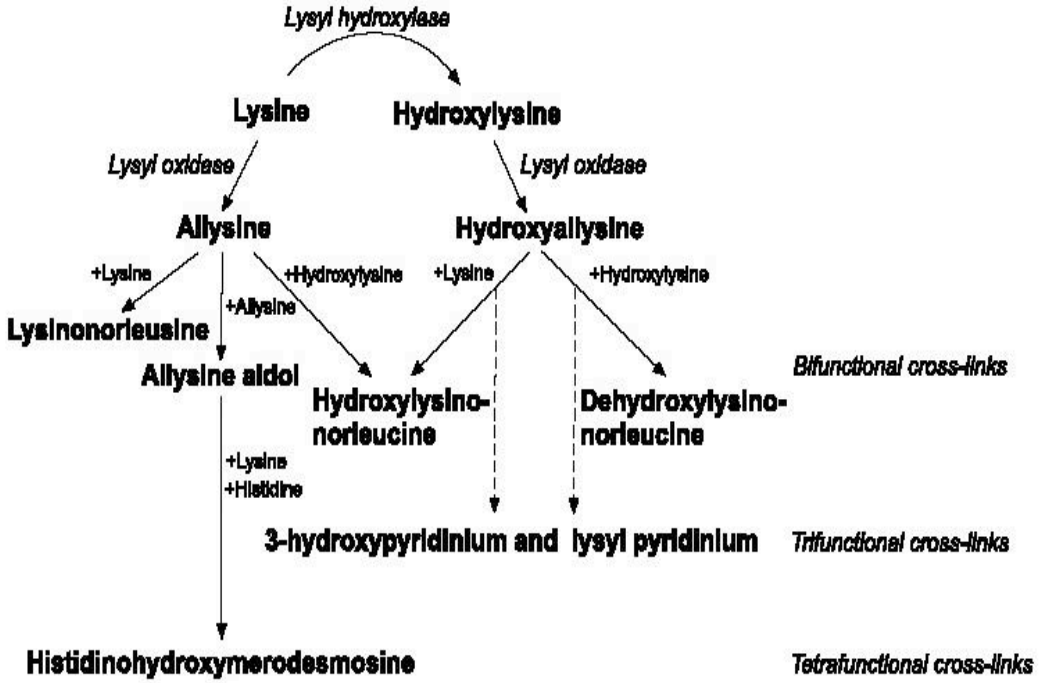

Figure 1.13: A schematic overview of two major pathways in collagen cross-links, allysine and hydroxyallysine and their relevant subsequent reactions leading to bifunctional, trifuctional and tetrafunctional cross-links (Mäki, 2002).

The previous section covered enzymatic cross-links. However, there is another type of cross-links called non-enzymatic glycation cross-links. Generally, non-enzymatic glycation or Maillard reaction occurs between reducing sugars and proteins. In this reaction the reducing sugars react with the free amino groups of proteins, leading to the production of unstable Schiff bases, which themselves then undergo an Amadori rearrangement producing stable fluorophore or chromophore compounds known collectively as advanced glycation end products (AGEs) (Figure 1.14). The formation of AGEs depends on the reactivity of specific amino groups, sugar concentration (glucose, fructose or dicarbonyl compounds) and the half-life of the

given protein. Over the time the concentration of AGEs increases not only because of the persistent glycation but also because of the reduced turn-over of protein associated with the aging. Thus, it seems that proteins with rather long half-life such as collagen and elastin are more vulnerable than others. The accumulation of the AGEs, over the time, has also been attributed to their resistant to proteolytic digestion (Wautier and Schmidt, 2004; Atanasova *et al.*,2008) Increased production of these AGEs has also been studied in a variety of pathological conditions such as diabetes, atherosclerosis and neurodegenerative diseases (Monnier, 1989; Grillo and Colombatto, 2008; Monnier *et al.,* 2008) . In the case of collagen, advanced glycation products derived from glycated lysine and hydroxylysine. *In vitro* studies show that fructose and pentose react much more rapidly with collagen than glucose (Reiser, 1998). These non-enzymatic cross-links lack the proper qualities of enzymatic cross-links and lead to functional impairment of the given tissue. Besides, glycated lysine and hydroxylysine themselves cannot serve a substrate for lysyl oxidase.

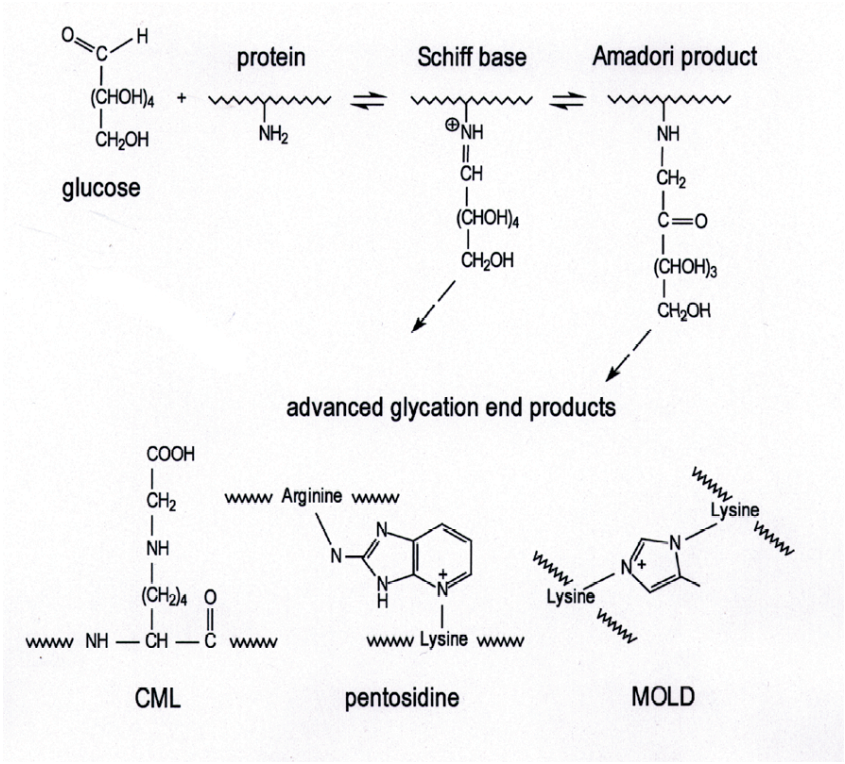

Figure 1.14: Mechanism of formation of the advanced glycation end products (AGEs); pentosidine, carboxymethyllysine (CML) and methyl glyoxal-lysine (MOLD) (Schmid *et al.*, 2002).

Catalytic properties and cofactors of lysyl oxidase

LOX enzyme is categorized as an oxidation-reduction enzyme. Redox enzymes possess the capacity to remove electrons from atomic targets within the substrate (oxidation) and render it to a final acceptor of electrons (reduction) in order to restore the activity of the enzyme. Many enzymes use cofactors like nicotinamide adenine dinucleotide (NAD^+) and flavin adenine mononucleotide (FMN) or dinucleotides (FADs) as electron sinks accepting the electrons that have been removed from the

substrates. However, some enzymes including LOX seem to have chosen another path. LOX possesses two almost unique cofactors: a tightly bound copper Cu (II) and a unique covalently-bound distinct cofactor known as lysine tyrosylquinone (LTQ) (Lucero and Kagan, 2006). The copper cofactor is bound in a tetragonally distorted, octahedrally coordinated ligand field (Gacheru *et al*. 1990). LTQ is catalysed in a newly synthesised LOX by firstly oxidation of a tyrosine residue (Tyr 349 in rat enzyme) by the help of a copper bound enzyme. This produces an intermediate product called peptidyl dihydroxypheyalanine quinone. This is followed by covalent addition of the quinone ring to the ε-amino group of the lysine residue (Lys 314 in rat enzyme). The first stage in catalytic activity of the enzyme takes place when an ε-amino group of substrate lysine residue binds to one of the carbonyl groups of LTQ. The resulting Schiff base formation then undergoes rate-limiting general base-facilitated abstraction, permitting the transfer of two electrons into LTO. This flow of electrons has now produced the reduced form of cofactor known as lysine tyrosyl aminoquinol. Hydrolysis of this intermediate imine leads to the formation of reactive aldehydes ready to form cross-links. After releasing the aldehydes, the molecular oxygen re-oxidizes the cofactor by the help of Cu (II), producing hydrogen peroxide and ammonia. Now the catalytic activity of the enzyme is complete and it is ready for another cycle of reaction (Figure 1.15).

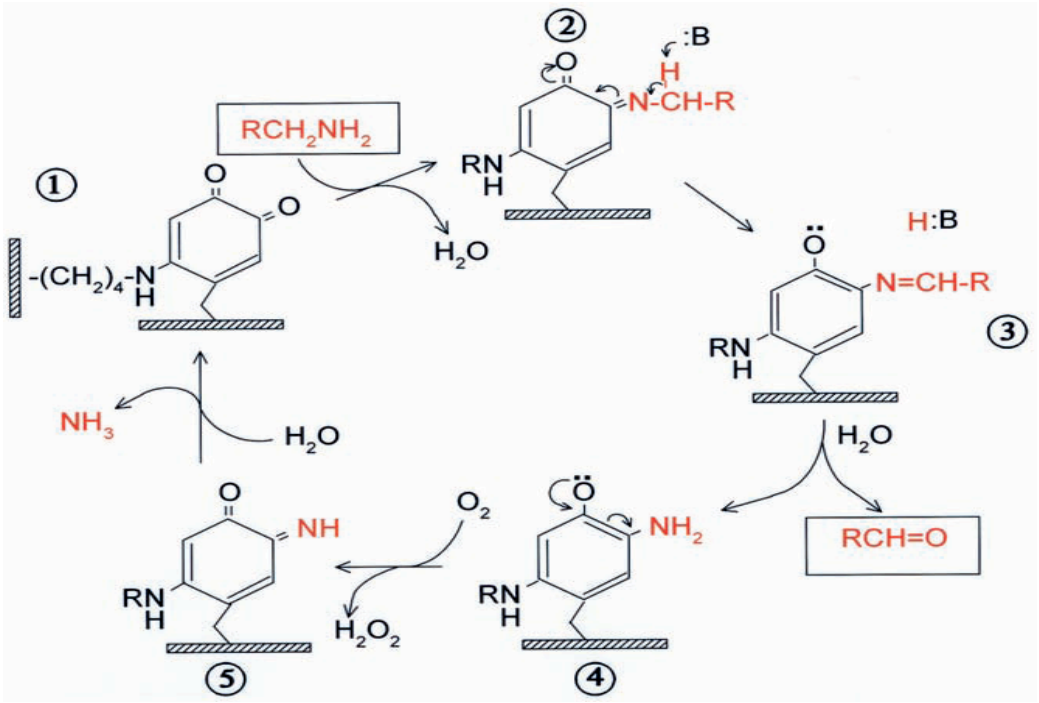

Figure 1.15: An overview of lysyl oxidase (LOX) catalytic activity (Lucero and Kagan, 2006).

Inhibitors of LOX

β-aminopropionitrile (β-APN) is a potent irreversible inhibitor of LOX. Its ability to inhibit formation of cross-links in collagen was recognized before the recognition of *in-vitro* activity of LOX enzyme itself. A disease called lathyrism can be induced experimentally if β-aminopropionitrile is administered to a growing animal. The disease is characterised by fragility of different connective tissues and an increased solubility of collagen fibrils, all due to failed cross-links. Other irreversible inhibitors of LOX are vicinal diamines like *cis*-1, 2-diaminocyclohexane and ethylenediamine. Furthermore, heparin, N-aziridine, trans-2-phenylcyclopropyamine and homocysteine thiolacetone can act as LOX inhibitors.

D-pencillamine can also inhibit lysyl-oxidase activity in standard doses (0.5 g/daily). It binds to aldehydes, especially in soft tissues, where most of the aldehydes come from lysine. It has also been shown that at higher doses, it makes copper unavailable to the enzyme, further interfering with the production of cross-links. It also worth mentioning here that copper deficiency in animals and humans results in several abnormalities including impaired cross-links and although it diminishes the activity of the enzyme, it does not have any significant effect on the level of LOX mRNA indicating that biosynthesis of the enzyme is not markedly affected by copper availability of copper, which may happen in the copper deficient diet. The detail of copper role in catalytic activity of lysyl oxidase can also be found elsewhere (Gacheru *et al.,* 1990)

Substrate specificity to LOX

The dramatic difference in primary and three-dimensional structure of the substrate lysine in collagen and tropoelastin suggests that there must be some kind of flexibility for LOX in terms of its substrate specificity. Moreover, the sequence region in LTQ where the tyrosine progenitor is found, and where the Lys314 forms part of LTQ, is abundant with anionic residues. Thus, in a functional LOX, LTQ provides a rich, negatively-charged active site making the enzyme well-suited to cationic protein substrates. In case of tropoelastin, the susceptible lysine is a cationic molecule and suitably matched for LOX. However, the substrate lysines in collagen are found in a hydrophilic region containing anionic residues and seemingly not suitable for the active site of LOX. Interestingly, the lysine residue within Asp-Glu-Lys-Ser, which is normally the sequence of the N-terminal of the α1(I) chain of

mature type I collagen, is a perfect *in vivo* substrate for LOX. On the contrary, LOX is unable to react *in vitro* with the same sequence in a synthetic collagen-like peptide. However, replacing the Asp residue with Gly makes the reaction possible. The question is, how can the unfavourable negative charges contributed by Asp residues in a naturally occurring collagen be overcome? It is hypothesised that the condensation of collagen molecules and cationic sites in neighbouring collagen molecules within the quarter-staggered microfibril permits the oxidation by LOX. This proposal is supported by molecular modelling studies of the microfibrillar array. In addition, collagen and tropoelastin molecules are not the only biological targets of this enzyme. Evidence has shown that several other basic globular proteins with pI ≥ 8 such as H1 histone can be oxidised by LOX (Smith-Mungo and Kagan, 1998; Lucero and Kagan, 2006)

Other biological roles of LOX

It has already been shown that decrease expression of LOX is implicated in a number of in extra-cellular matrix diseases, including cutis laxa, Menkes' syndrome and spontaneous coronary artery dissection, scleroderma, atherosclerosis, liver cirrhosis and senile plaque formation in Alzheimer and non-Alzheimer dementia. However, recent evidence suggests that more functions may be attributed to LOX, including induction of motility and migration in monocytes, vascular smooth muscle cells and fibroblasts. Moreover, the observance of LOX activity in the cytoplasm and nucleolus has lead to discovery of its involvement in cell signalling and transcriptional gene regulation, probably through binding to histone substrates as noted above. Even more recent studies have shown that non-catalytic domains of

LOX can bind to various proteins such as fibronectin and placental lactogen. Considering the paramount importance of LOX in gene regulation and signal transduction, it is expected that aberrant expression of the enzyme might lead to some types of malignancies. Paradoxically, in some cancers the up-regulation of LOX has been shown to act as a tumour suppressor, whereas in other cancers the up-regulation of LOX has been considered to be a metastasis-promoting factor. The full details of versatile biological functions of LOX are beyond the scope of this dissertation and can be found elsewhere (Smith-Mungo and Kagan, 1998; Szauter *et al*., 2005; Erler *et al*., 2006).

Collagen turn-over and degradation

The traditional view of collagen turn-over favours a fast turnover during the growing period of an animal and very slow rate in adult animals, except in the uterus during pregnancy, wound healing area and some pathological conditions (Sodek, 1976). However, recent studies have shown that collagen turnover in the adult can indeed be fast (Humphrey, 2002). Prior to formation of covalent cross-links, collagen molecules are highly susceptible to degradation, but the degradation susceptibility of mature molecules seems to be independent of the time of their synthesis. Generally, there are two main degradation pathways for collagen, namely intracellular (or degradation of procollagen molecules) and extracellular pathways. Bienkowski *et al.* (1978) studied intracellular degradation and showed that, in some cases, as much as one third of newly synthesised collagen (procollagen) was degraded even before its secretion. The study of the kinetics of this process in different tissues in rats has revealed a very wide range of discrepancy. For example, the amount of degradation

through this process in the skin and heart is about 10% and 60%, respectively. However, whether this degradation occurs inside the cisternae of Golgi or lysosomes is not clear. However, the suggestion is in the case of over-load by faulty procollagens the cisternae of Golgi are that the primary site of degradation (Laurent, 1987).

In the extracellular pathway, collagen is broken down, either before or after formation of the fibrils, mostly by the means of a group of collagenases belonging to a family of enzymes called matrix metalloproteinases or MMPs (Grande-Allen *et al.,* 2005; Diegelmann, 2001). These MMPs are tissue specific. For example, in mitral valves of adult humans and pigs, it seems that MMP-13 and MMP-1 play an important role in collagen degradation. These enzymes are produced by fibroblast-like cells, which constitute the major cell population of connective tissues. Furthermore, there is a population of smooth muscle cells and myofibroblasts that have ability to secret collagenases. It should be borne in mind that these cells are also capable of producing collagen, elastin and proteoglycans. The MMPs cleave covalent bonds in collagen at quite unique and specific positions, namely between a glycine residue and a leucine or an isoleucine residue. It is interesting to note that the catalytic site of MMPs is 8 Å long, while the diameter of a collagen molecule is 1.5 Å . Apart from the size incompatibility, the scissile bond for collagen degradation is buried inside the molecule and is practically inaccessible for the enzyme. Thus, the exact mechanism of the enzyme is still unknown, though some theories have been suggested. The “molecular tectonic” theory states that the MMPs undergo some conformational changes and actively unwind collagen molecules just before acting

upon them. The problem with this theory is that the conformational changes in MMPs would need an energy input while the degradation of collagen molecules require any energy input. There is evidence that collagen in physiological conditions *in vivo* is not as rigid and inflexible as originally thought. It seems that they experience very subtle conformational fluctuations that are also necessary if they are to perform their function. This idea has been confirmed by molecular dynamic simulations that suggest that the MMPs recognise and subsequently bind to cleavage sites that are already partially unfolded. The implications arising from this study are that some surface molecules that bind to the native collagen triple-helix could increase its stability, thereby rending the collagen more resistant to conformational fluctuation and subsequently to MMPs (Salsas-Escat and Stultz, 2007).

Another group of enzymes that could act on collagen, both in extracellular matrix and inside the cell, are cathepsins. They belong to papain-cyctein proteinase family, the members of which have collagenolytic and elastinolytic activities. Several cathepsins have been identified; including cathepsin K, S, B, L and G. Cathepsin K is probably the most widely studied, with a number of studies focussing on its role in osteoclast-mediated bone resorption and joint diseases. The collagenolytic activity of cathepsin K is unique in that type I and type III collagen are cleaved at the end and at the multiple sites, irrespective of its conformation within native triple helix, whereas other cathepsins cleave the collagen molecules only in telopeptide regions, generating monomers of the collagen molecules. Cathepsin K is produced in fibroblasts or osteoclasts in an inactive form of a proenzyme. After autoproteolysis happens, it stays inside lysosomes or is secreted into the extracellular matrix.

Extracellular matrix is an acidic microenvironment and the enzyme is fully functional at the acidic pH of 5.5. In bone, this milieu is provided by osteoclasts in the bone resorption lacunae. The weak expression of cathepsin K in the steady state of other tissues like lungs and skin in the normal tissues has also been demonstrated. However, the over-expression of cathepsin K in diseased conditions suggests that the enzyme plays an important role in remodelling, homeostasis and matrix re-deposition. Nonetheless, the necessary acidic micro-environment for the activity of the enzyme has not been seen in these tissues. It has been suggested that in these tissues collagen binds to specific cell surface proteins such as β1 integrins and urokinase plasminogen activator receptor associated protein (uPARAP), followed by uptake by the cells and delivery to lysosomes where cathepsin K could act effectively in acidic conditions (Garnero *et al.*, 1998; Rünger *et al.,* 2006).

Although these enzymes are produced mainly by transformed fibroblasts of any given tissue, they could also be produced by other inflammatory cells such as neutrophils. Additionally, it has been shown that a range of cytokines could affect collagen turnover. The involvement of Interleukin-1beta (IL-1 β) and tumour necrosis factor (TNF) in myxomatous mitral valves, in the tissue of periodontitis patients and in synovial fluid has been demonstrated, and it was shown that these cytokines can stimulate and increase the activity of both matrix metalloproteinases (MMPs) and cathepsins (Hou *et al.,* 2001; Rabkin *et al*, 2001; Cox *et al.,* 2006).

In addition, these cytokines are not only involved in degradation of collagen molecules, but they also affect the collagen synthesis. A study has compared the ability of human dermal fibroblasts to synthesise types I and III collagen, using

recombinant IL-1 and TNFα. The study showed that there was a decrease in the synthesis of collagen type I in both cases. However, while TNFα acts through the reduction of the amount of procollagen mRNA level, the level of procollagen mRNA in the presence of IL-1 was surprisingly high (Mauviel *et al.,* 1991). This result for IL-1 is in disagreement with some studies which showed that IL-1 could increase collagen synthesis. It suggests that some post-transcriptional interventions might be the cause of the reduction of collagen synthesis. Although differences in the experimental conditions used might explain the observed discrepancy, it could also be related to the status of fibroblasts in terms of whether they are already activated or not. The author also envisages another explanation whether or not it is definitely proved that IL-1 reduces collagen synthesis *in vivo*. The excessive synthesis of procollagen might put a real burden on the collagen biosynthesis pathways leading to the production of many faulty molecules destined for intracellular digestion before secretion.

Prostaglandins also seem to play a key role in metabolism and turnover of collagen. Prostaglandins are synthesised from arachidonic acid via the cyclooxygense pathway and have capacity to affect a vast majorities of regulatory, differentiative and inflammatory processes. PGE2 is of a particular interest in terms of its regulatory effect on collagen turnover. PGE2 achieves this through four different E prostanoid receptors, namely EP1-EP4. These receptors belong to a family of G protein coupled receptors. EP1 activation causes a raise in the level of Ca^{2+}. EP2 and EP4 lead to an increase of cAMP. EP3 activation, however, decreases the level of cAMP. Although it is generally accepted that PGE2 is able to suppress collagen synthesis, the effect of

PGE2 on differentiation and proliferation of fibroblasts in different cell lines has revealed a discrepancy. This heterogeneity might reflect the expression of different receptors in different tissues. This discrepancy in different cell lines obligated studies on primary cells. A study carried out by Huang *et al.* (2007) using histologically normal fibroblasts from adult human lung parenchyma, has shown that PGE2 both suppresses collagen expression and fibroblast proliferation by increasing the cAMP. This was mediated mostly by EP2 receptors and to a lesser degree by EP4 receptors. Thus, as has also been demonstrated in other studies, agents such as β-adrenergic agonists (e.g. isoproterenol), phenylbutyrate (a weak and non-toxic histone deacetylase inhibitor) and forskolin which can raise the level of cAMP, can affect and suppress collagen expression as well (Saltzman *et al.,*1982; Rishikof *et al.,* 2004). Although there is a simultaneous increase in PGE2 levels in cells treated with IL-1, it seems that IL-1 realises its function independently from PGE2 as treating the cells with indomethacin does not affect the ability of IL-1 to reduce collagen production (Mauviel *et al*., 1991).

Not only can indigenous cells in a given tissue play a role in the turnover and metabolism of collagen, but cells from other sources could also have effects. A study on myxomatous mitral valve in humans has revealed an increase in the population of $CD34^+$ fibrocytes in the affected leaflets. These fibrocytes are presumed to derive from circulatory $CD14^+$ and are different from those of mitral valves. Although $CD34^+$ fibrocytes could synthesis type I and III collagen, they are thought to be the main source of MMP9 which is considered one of the important factors in pathogenesis of myxomatous mitral valve in humans (Barth *et al.,* 2005). The reason

why these circulatory cells migrate, transform and dwell in mitral leaflets remains to be elucidated. In unpublished observations in the dog, there is little evidence of accumulation of CD34+ cells in canine MMVD (according to Richard Han, personal communication, November 6, 2008).

In summary, it can be understood that there are delicate and rather complex mechanisms which influence collagen synthesis and turnover in different tissues. For example, while the fractional turnover of collagen (an amount of collagen equivalent of the total collagen mass in a given tissue) in the heart tissue of an adult rat is about 5% per day, the value for that of lung is about 8% per day (Laurent, 1987). From this, the necessity for further research to clarify the subtlety of collagen homeostasis in various tissues ca be appreciated, both at different stages of development and in disease, not least in the mitral valve.

Clinical signs and diagnosis

Most dogs with mild and moderate disease do not present any obvious clinical signs and the disease is usually detected through auscultation during routine physical examination. However, the course of the events at this stage might vary from an insidious condition taking years to a rapidly progressing heart failure. Although the disease mostly occurs among the small breeds, it seems that the deterioration of clinical signs is much more dramatic in some large dogs. In the severe cases which might be accompanied by mitral regurgitation, there is a wide range of clinical manifestation, which results from the compromised heart function. Coughing is caused by pulmonary oedema, the pressure on the left main stem of bronchus or the

combination of both. The cough becomes exacerbated especially at night when the dog lies laterally. Weakness and decreased stamina due to failed left and right ventricular forward flow might also exist. Right-sided heart failure could also lead to ascites. In addition, syncope and sudden death are seen in some dogs (Pedersen, 2000; Häggstrom *et al.,* 2005).

Diagnosis is made on the basis of criteria that include medical history, physical examination, echocardiography and thoracic radiographs. A murmur may be identified in early stages of the disease. This murmur is associated with early systole. Nevertheless, as the disease progresses it incorporates the whole of the systole (holosystolic) and its intensity also increases. Mid-systolic click may be found in the affected dogs. However, detection of these abnormal sounds depends on the experience of the observer, the state of the mind of the animal and concurrent complications such as pleural effusions and cardiac tamponade (Pedersen, 2000; Pedersen and Häggstrom, 2000).

Electrocardiography

Most abnormalities found in electrocardiographic examination of the myxomatous mitral valve result from the accentuation of a normal ECG. In different cases of MMV, different patterns of ECG ranging from normal to complexities in rhythm, rate and configuration have been noticed. However, it has been documented that both dogs and humans reveal severe sinus arrhythmia in their ECG compared to that of

control groups. Additionally, in cases of compensatory left atrial and left ventricle enlargement, prolongation of P wave and QRS wave would be seen, respectively. The mean electrical axis in the frontal plane often remains unchanged throughout the course of disease (Häggstrom *et al.,* 2005).

Diagnostic imaging

Echocardiography is an extremely useful method for screening, diagnosis and prognosis of myxomatous mitral valve disease. The diagnosis is made when there is at least 2 mm displacement of one or two mitral leaflets above the annulus plan towards to the atrium during the systole, in either right parasternal or apical long axis two dimensional view (Hayek and Griffin, 2002; Hansson, 2004; Häggstrom *et al*., 2005). Measurement of the average protrusion of anterior leaflet, posterior leaflet and coaption points between the two leaflets is another method that is also used by some researchers (Olsen *et al.,* 2003a). As the mitral valve annulus is saddle shaped, in normal hearts a four-chamber view echocardiography may show some signs of prolapse which in fact is not the case. It is also important to realize that there is a correlation between the severity of the disease and the degree of the protrusion. In echocardiograms, the lesions, including thickening, usually appear more prominently in the anterior leaflets. In humans, if the thickening is greater than 5mm the condition is called “classic prolapse”, otherwise it is considered as “non-classic prolapse”. In severe cases, the entire leaflet might protrude into the atrium (flail leaflet) raising the suspicion of chordae rupture. However, the echocardiographic features in MMV can be mistaken for the lesions caused by bacterial endocarditis which bear some similarities to that of myxomatous leaflets although in the case of former condition

the lesions are more or less solitary and echodense. Moreover, the signalment of the disease which is febrile and often seen in large dogs could be a clue to differentiate it from MMV disease (Kittleson, 1998). Three-dimensional echocardiography has recently been used to access the anatomical lesions in the myxomatous valves in humans and is of particular value in timing of surgical intervention in order to repair the affected valve (Macnab *et al*., 2004).

In mild forms of the disease there are no apparent changes in the size of left atrium and right ventricle either in echocardiograms or radiographs. Nevertheless, as the disease progresses, there would generally be signs of left atrium enlargement followed by an increase in diameter of left ventricle. However, the wall thickness of the left ventricle usually remains within the normal range (Kittleson, 1998).

Aim, scope and hypothesis

Realising the importance of collagen fibres in mitral heart valves and considering the paramount significance of myxomatous mitral valve disease, a better understanding of pathogenesis of MMVD is essential. It can be hypothesised that there are differences in various characteristics of collagen when comparing healthy leaflets with MMVD leaflets. The hypothesis of this study is that there are changes in fibril structure, fibril orientation, d-spacing, collagen density, collagen content, thermal stability, and the status of mature and immature cross-links in diseased valves. This study was designed to investigate this hypothesis using a combination of biophysical and biochemical tools, such as x-ray diffraction, neutron scattering, differential scanning calorimetry (DSC) and high performance liquid chromatography (HPLC).

Additionally, the recently introduced imaging technologies to biology and medicine, such as differential enhancing imaging (DEI) and coherent anti-Stokes Raman scattering spectroscopy (CARS) were applied to investigating this disease. The hoped outcome of this study was furtherance of our understanding of the pathogenesis of MMVD. The study provides new findings about MMVD and demonstrates the potential of biophysical tools for studying similar conditions.

Chapter 2

X-ray diffraction in the evaluation of connective tissue changes in MMVD

X-rays studies

Without doubt, the name of Wilhelm Conrad Rontgen and x-ray are inseparable. On November 8, 1895 he realized that a paper plate covered on the one side with barium platinocyanide located as far away as two meters from a sealed and covered discharged tube became fluorescent. Later on, he exposed his wife's hand against the newly discovered rays and first x-ray image in history was recorded, showing shadows of his wife's hand bones and that of the ring she was wearing. For this discovery, Röntgen was awarded the first Nobel Prize in physics in 1901 (Franks, 1996).

X -rays are produced by the stoppage of cathode rays or electrons when they strike a metal target. When they hit the target two phenomena occur simultaneously. First, when electrons approach to the nuclei of the target material all their kinetic energy converts to the rays called "continuous" or "white" x-ray radiation. In the second event, electrons which strike the different orbits of the atoms in the metal target remove the electrons from their original orbits or shells. When other electrons transfer to occupy the vacant positions, x-rays are produced. Taking into account that the latter type of x-rays originate from different orbits with various characteristic energies, they are called "spectrum x-rays". The energy of continuous or white x-rays does not depend on the target material, while spectrum x-rays are specific to the target (Michette, 1993; Franks, 1996).

X-rays are now produced by different methods across the world, but for research purposes, one of the common used sources is the synchrotron radiation source (SRS).

In SRSs, electrons are accelerated up to the speed of light within an evacuated polygonal ring. Their movement is maintained by huge external magnets. The bending movement of the electrons at the corners of the polygon produces radiation ranging from infra-red to short wavelength x-rays. The radiation is emitted tangentially from the orbit and is channelled through side gates to different experimental instruments. The high intensity and wide spectrum of x-rays renders the synchrotron radiation an invaluable tool for a variety of scientific applications (Munro, 1996).

X-ray diffraction

Diffraction is defined as the deviation of a wave from its natural direction of propagation when it encounters an object or a medium. When a wave hits an atom it is scattered in a certain direction. The scattering pattern from a single atom is so weak that it cannot be observed. However, if there is an ordered structure with a regular repeat distance between scattering structure, the scattered rays interact with each other to give rise to a special pattern of constructive and destructive interference. This diffraction pattern can be detected by a suitable detector. As the wavelengths of x-rays (0.01-0.1nm) are so close to the inter-atomic distances, they are capable of producing the best diffraction pattern from molecules. In 1912, Max von Laue for the first time discovered the diffraction of x-rays by crystals and showed that x-rays behaved like waves rather than particles. However, the development of x-ray diffraction into a reproducible and calculable technique is thanks to a unique father and son team, namely Sir William Henry Bragg and his son, William Laurence Bragg, who proposed Bragg's Law:

$$n\lambda = 2d\sin\theta \quad (2.1)$$

Where n is an integer, λ is the wavelength of the rays, d is spacing between layers of atoms and θ is the angle between the incident ray and the scattering or diffracting planes. The following example provides a better explanation of the Law. It can be imagined that two rays strike a regular repeating structure molecule where the distance between the atomic planes is a given d (Figure 2.1). The first ray scatters from the first layer at an angle θ. This phenomenon equally occurs in the case of the second ray at the same angle of θ. However, the distance which the second ray travels is farther than the first ray, namely 2a. If 2a is equal to an integral number of wavelengths (nλ), both rays, while they exit from the molecule, will be in phase. This kind of interaction between different rays where they reinforce each other is also called "constructive interference" (Bullen, 1962; Michette, 1993; Watson, 1996).

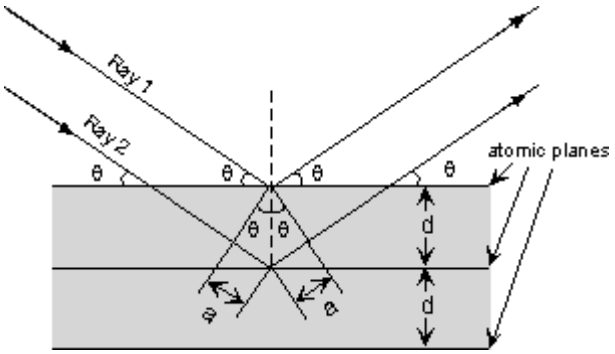

Figure 2.1: The diagram depicting the Bragg's Law. In this drawing the second ray travels 2a farther than the first ray. If this path length is a whole number of wavelength, then the constructive interference will occur. From trigonometry $a = d \sin \theta$ or $2a = 2 d \sin \theta$ thus, $n\lambda = 2d \sin \theta$ (Nelson, 2008).

X-ray diffraction in biological research

X-ray diffraction has played a paramount role in the development of biology. Generally, in terms of its application, it can be categorized into two major various areas: crystallography and non-crystalline diffraction (i.e. mainly fibre diffraction). Many biological molecules including many proteins, viruses and vitamins can be persuaded to form crystals, whereby they are arranged in an ordered lattice (the orderly, regular three-dimensional arrangement of atoms in a crystal). In addition, there are also a number of biological molecules, such as collagen fibres, filamentous viruses, amyloids and DNA molecules, which are not able to form crystals, but which still posses a degree of special spatial ordering. The difference between fibres and crystals is that in fibres the molecules are parallel to each other although

randomly oriented about the fibre axis, so the diffraction pattern is cylindrically averaged. Additionally, compared to crystals, fibres are often more stable and better able to withstand changes in the surrounding environment, including temperature and humidity. Consequently, fibre diffraction is an ideal tool for study of these structures (Lewis, 1997; Miller et al., 1999; Stubbs, 1999).

Aim

Reflecting its importance in MMVD, collagen structure has been the subject of a number of studies using conventional and electron microscopy (Chapter 1). X-ray diffraction has the advantage over electron microscopy that the tissue is maintained in physiological conditions during the x-ray exposure, and prior chemical processing of the tissue is eliminated. Additionally, EM can only examine a localized volume of tissue, so is unable to give information about the whole tissue density. X-rays pass through the entire sample thickness and the results thus represent averages throughout the tissue. X-ray diffraction techniques also have the ability to differentiate the tissue density in terms of collagenous and non-collagenous tissue. They can also distinguish between fibrillous from non-fibrillous collagen while mapping the preferred orientation of the fibrils. So, the purpose of this study was to determine the changes in collagen fibril organization, including tissue density, fibril orientation, fibril density, degree of fibril alignment and d-spacing between diseased and healthy areas of valve leaflets using the technique of small angle x-ray diffraction.

Materials and methods

Mitral valve leaflets were collected from five affected dogs and one healthy control (table 2.1). They were from both sexes and their average age was about 7 years. The pathological status of the samples was confirmed by gross examination at the time of collection. All tissue samples were snap-frozen using dried ice within 10 min of collection and then stored in between -60 and -70 °C freezer until their use. In addition to the control sample, since diseased and normal areas coexist in one leaflet, each valve could also be used as its own control. The Royal (Dick) School of Veterinary Studies School (RDSVS) ethics guidelines on the use of clinical material were satisfied for all samples throughout the study.

Breed	Age	Sex
cross-bred Terrier	11 years old	female
cross-bred Collie	7 years old	male
CKCS	9 years old	male
CKCS	6 years old	male
Beagle	5 years old	female
cross-bred German Shepherd (control)	3 years old	male

Table 2.1: The details of the animals used in the experiment in order to study tissue density, collagen density, the degree of alignment and the fibril orientation.

Specimen holder

The major requirements for a an x-ray specimen holder are a) to keep the sample in a fixed position relative to that of the incident beam, b) to keep the sample humid and prevent it from drying during the course of the runs, and c) exerting a certain amount of pressure in order to maintain the collagen fibres in a stretched condition. The specimen, soaked in normal saline, was sandwiched, flattened and sealed between two sheets of mica. Keeping samples humid maintains the crystallinity of the collagen fibrils and prevents "helicoidal effect" which can produce molecular tilting and changes in the d-spacing (Cameron *et al.*, 2000). The reason for the stretching of the samples by a small amount is that in the relaxed state, collagen fibrils possess a periodic crimp along their length. Thus, it is advised that in order to produce a diffraction pattern free from the splitting of reflections that such a crimp can produce, the fibres should be stretched approximately an additional 10% of their total length (Bradshaw, 1985). Stretching of a sample should be done by clamps evenly pushing the tissue from all directions. In our case, the samples were not treated like this; however, flattening the samples seemed to be enough for the purpose of our experiment.

X-ray diffraction measurements

Collagen molecules lie almost parallel to the fibril axis and diffract x-rays from the 670 Å repeating pattern of gap and overlap regions. The intensity of diffraction is related to the amount of collagen, and the alignment of the diffraction pattern reflects the alignment of the fibres. Therefore, diffraction patterns can be used to probe the

alignment of the collagen fibrils that produced that diffraction. The technique can also be used to determine total tissue content (collagenous and non-collagenous) by quantitative analysis of total x-ray scattering at any point (Miller *et al*., 1985; Meek and Quantock, 2001; Aghamohammadzadeh *et al*., 2004). X-ray diffraction measurements were performed with synchrotron radiation (Experimental Station 2.1, Synchrotron Radiation Source, the Council for the Central Laboratory of the Research Councils (CCLRC), Daresbury, UK) using a method developed from that of Aghamohammadzadeh and co-workers (2004). The specimens were mounted in a specially-designed sample cell, attached to a movable sample stage. The stage was programmed to translate in a raster of 1-mm steps, horizontally and vertically, while a finely focused (0.1 mm vertical × 1 mm horizontal) beam of 1.54 Å wavelength x-rays recorded the fibre diffraction pattern for 45 seconds at each point. Each sample was typically measured at 300 points, in a grid of 20 × 15 pixels. A multiwire two-dimensional area detector, placed 4 m from the sample, collected the diffraction data. The collection of diffraction data and movement of the sample relative to the beam were coordinated by a computer running a Python (www.python.org) script file. Calibration measurements included the detector response, in which the efficiency of each pixel was determined by a long exposure to a randomly decaying radioactive source, and detector calibration, which used the well-characterized diffraction pattern of wet rat tail collagen.

Data analysis

The diffraction pattern of a fibrous material, such as collagen, contains information in the meridional plane, describing structure along the axis of the fibre, and in the

equatorial plane, describing lateral structure. For this study, Bragg reflections of the meridional diffraction pattern were recorded and analyzed to provide information about the collagen content and the degree and prevailing angle of alignment of the fibrils. The level of background scattering was also determined to give an indication of the amount of non-collagen tissue. Data analysis was performed using the program FiberFix (Collaborative Computational Project for Fibre Diffraction and Solution Scattering, CCP13). A ring was defined, centred on the middle of the diffraction pattern and wide enough to encompass the third, fourth, and fifth orders of meridional diffraction (Figure 2.2). This region was chosen because it was sufficiently clear of any x-ray scattering from the backstop but included strongly diffracting Bragg peaks. The third and fifth orders of diffraction are characteristically very bright for type I collagen and have excellent signal/noise ratios, thereby simplifying the tasks of background subtraction and peak shape analysis. PeakFit (Version 4, AISN Software) was used to fit Gaussian peaks to the annular distribution of scattering intensity (Figure 3.3). The Gaussians were then analyzed in terms of peak area (total diffracted intensity of the selected area of the diffraction pattern, related to the amount of collagen), peak centre (angle of preferred fibril orientation), peak width (degree of fibril alignment), and mean background level (related to the amount of non-ordered material). These values were then plotted to produce maps of each parameter across each valve leaflet.

The numerical diffraction values of total the tissue density, collagen fibril density, and degree of collagen alignment were analyzed separately for each leaflet using a two-sample un-paired t-test to compare affected and lesion-free areas. Significant

differences were taken at $P < 0.05$. Analysis of regression was carried out to determine whether there was any relationship between amount of collagen and total tissue density in diseased and lesion-free areas.

Results

A typical small-angle x-ray diffraction pattern from a dog mitral valve leaflet is shown in Figure 2.2. The x-ray beam passed through the sample perpendicular to the plane of the leaflet. Because collagen fibrils can occur in all possible orientations within this plane, the diffraction pattern may appear as a series of concentric circles. The anisotropic distribution of intensity in this example reveals a preferred angle of orientation of the fibrils (Figure 2.3).

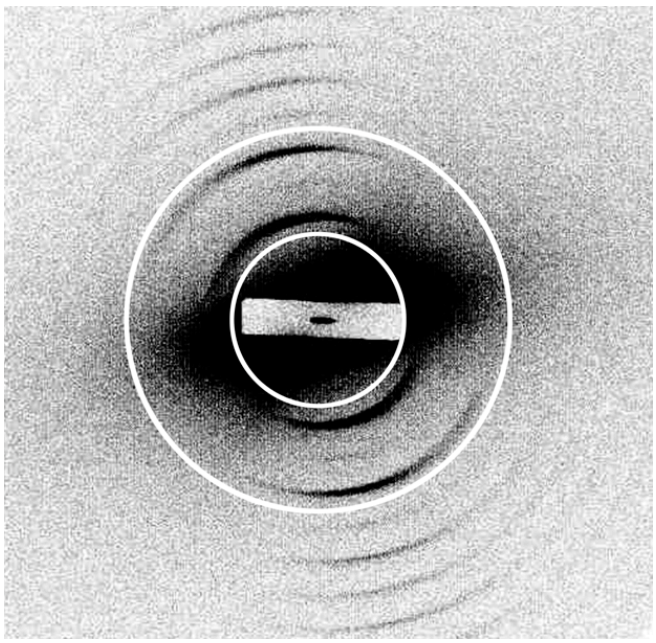

Figure 2.2: X-ray diffraction pattern from canine mitral valve collagen. The pattern is dominated by a series of meridional Bragg reflections, arising from constructive diffraction of X-rays by the regularly repeating 670 Å axial structure of collagen fibrils. The superimposed circles define a ring encompassing the third, fourth and fifth Bragg peaks of meridional diffraction. Circular integration of diffracted intensity in this region was used to provide quantitative information on the amount of collagen fibrils and their orientation.

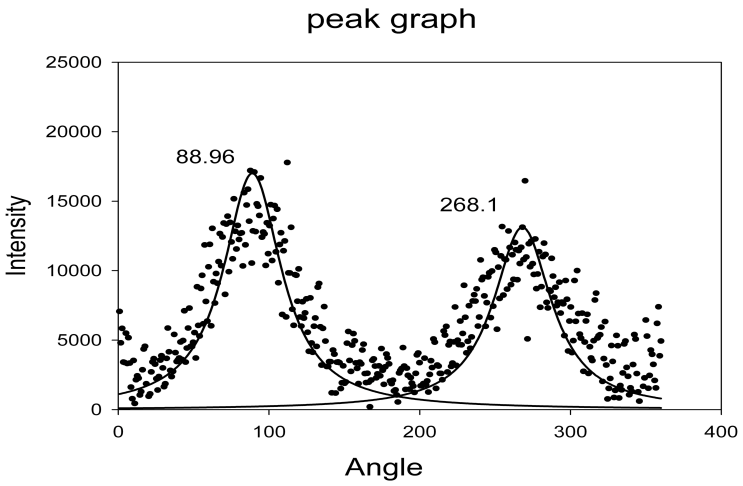

Figure 2.3: The annular distribution of diffracted intensity from canine mitral valve collagen. The data result from circular integration Figure 2.2 (see the text). Horizontal axis, angle; vertical axis, intensity (arbitrary units). Also shown is a pair of fitted Gaussian distributions centred at 88.96° and 268.1°. Note that the peak area, the peak width (full width half maximum) and the peak centre were used to calculate the amount of collagen, the degree of alignment and the orientation of the collagen fibrils, respectively.

Estimation of total tissue

Highly ordered material, such as collagen, produces a well-defined diffraction pattern, which overlays an anisotropic background of x-ray scattering by any disordered material that the x-ray beam strikes. A sensitive measure of the amount of tissue (collagenous and non-collagenous) at any one point on the leaflet is provided by the quantitative analysis of this non-coherent scattering of x-rays. Absorption of the x-ray beam by the sample can also be estimated by comparing the current measured at ion chambers before and behind the sample. A regression analysis of the two methods for one of our samples showed that they are closely related (>95%

significance), thereby validating our approach. Total tissue density differed significantly ($P < 0.05$) between affected and lesion-free areas. The contour maps of the diseased samples also revealed a considerable variation in total tissue content distribution among diseased and unaffected areas that was not consistent with a specific pattern (Figure 2.4 A).

Collagen fibril orientation

Figure 2.4B shows a map of collagen fibril orientation across a single leaflet. In the visibly normal areas of the mid-zone of the leaflets, the collagen fibrils run parallel to the free edge, meaning they take up a transverse course between two commissures. However, when they approach the edge of leaflets close to the annulus, they become oriented more vertically, such that they are orthogonal to the adjacent areas. In diseased areas, which are mostly located on the free margins of the leaflets, the orientations of fibrils are haphazard. This contrasts with healthy regions and healthy valve (Figure 2.4 E), where the direction of fibrils is more or less continuous with the fibrils in neighbouring chordae tendineae and there is an ordered pattern of collagen fibrils across the valve.

Collagen fibril density

Figure 2.4C is a representative plot of collagen fibril density, determined on the basis of the strength of diffraction by the collagen at each point. These plots were derived from two different fibril populations: those with a preferred orientation and those without. This plot therefore shows the total diffraction irrespective of fibril

orientation and so represents directly the relative amount of collagen fibres in the path of the x-ray beam. In all samples, the total diffraction, and therefore the amount of collagen significantly increased ($P < 0.05$) from the diseased free edge of the leaflet to the unaffected base of the valves.

Degree of collagen alignment

Plots were drawn to map the degree of preferred alignment of the collagen fibrils. All the diseased leaflets showed non-uniform distribution of collagen alignment, with clear differences in the degree of preferential alignment between the diseased and healthy areas. These differences were consistent in all samples, and, as illustrated by Figure 2.4 D, it was clear that the maximally aligned collagen is located toward the lesion-free periphery of the leaflets ($P < 0.05$). A comparison of these affected regions with the same areas in apparently healthy leaflets is a clear indication of the effect the disease has on collagen fibril alignment (Figure 2.4 F).

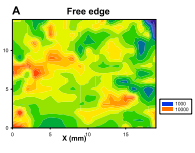
A
Free edge
X (mm)

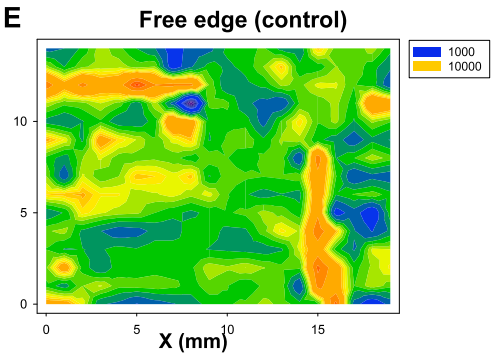
E
Free edge (control)
1000
10000
X (mm)

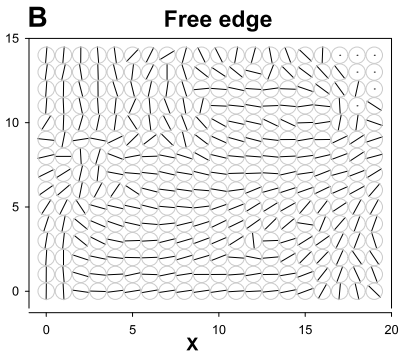
B
Free edge
X

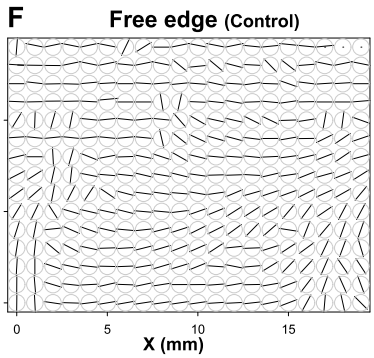
F
Free edge (Control)
X (mm)

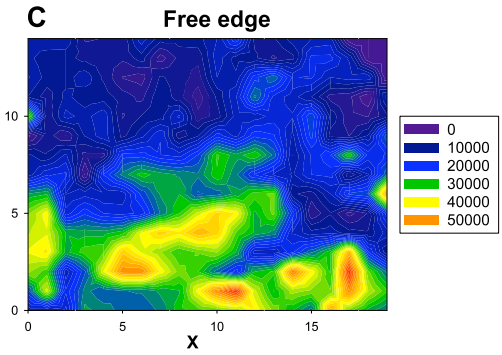
C
Free edge
0
10000
20000
30000
40000
50000
X

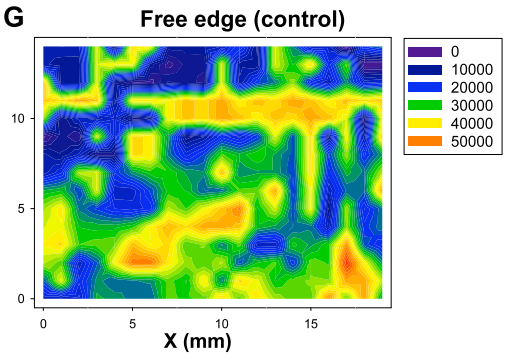
G
Free edge (control)
0
10000
20000
30000
40000
50000
X (mm)

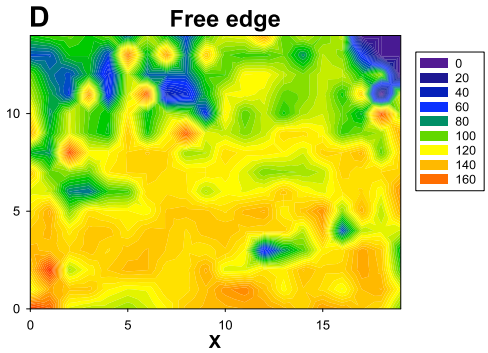
D
Free edge
0
20
40
60
80
100
120
140
160
X

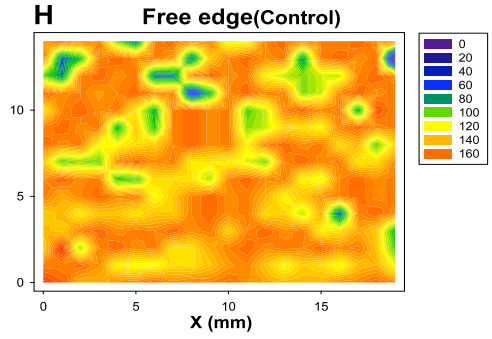
H
Free edge(Control)
0
20
40
60
80
100
120
140
160
X (mm)

Figure 2.4: Contour maps showing an area of 20 × 15 mm of a single canine mitral valve which also contains free edges of leaflets. A and E total (non-collagenous) tissue density of diseased and control sample, determined from the background (incoherent) x-ray scattering in a ring centred on the middle of the diffraction pattern and enclosing the third, fourth, and fifth meridional Bragg peaks. The background was measured in a region of reciprocal space that contained no diffraction features from collagen fibrils. Preferred orientation of collagen fibrils in diseased (B) and apparently healthy (F) mitral valve leaflets, determined by fitting Gaussian distributions to the Bragg peaks and determining the angular position of the peak centre. The major difference between normal and diseased valves is in the free margins of the leaflets, where the disordered collagen fibrils of the diseased valve contrast starkly with the well-aligned fibrils of normal tissue. Collagen fibril density in diseased (C) and apparently healthy valve leaflets (G), determined from the total area under the Bragg peaks (total diffracted intensity). Degree of alignment of collagen fibrils in diseased (D) and apparently healthy (H) valve leaflets, determined from the width of the fitted Gaussian distributions. For ease of comparison with the other plots, the data are expressed as 180° − *W*, where *W* is the full width at half height (in degrees) of the Gaussian distribution. Note that free edges of the leaflets are the locations where lesions are usually found. The figures G and H display a higher amount of collagen density and the degree of alignment towards free margins, respectively compared to the affected leaflet (units are arbitrary).

d-spacing measurement

The x-ray diffraction patterns of connective tissues rich in collagen fibrils possess features that arise from the interaction of x-rays with the molecular spacing. Of these, the most obvious and perhaps most important is the d-spacing. The highly ordered axial arrangement of molecules, in which neighbouring molecules are staggered by about 670 Å, is responsible for this pattern. This repeating periodic function of 670 Å acts as a main diffraction grating and the final image results from Bragg reflections which corresponds to the d-spacing and integral fractions of this spacing such as 670 Å , 670/2 Å ….670/*n* Å where *n* is an integer. These frequencies can also be identified as first-order, second-order etc. The strongest diffraction arises from the axial spacing along the fibril, thus the pattern is referred as the meridional pattern. Using the Bragg equation ($n\lambda = 2d\sin\theta$), it is possible to calculate the d-spacing. The third order of the diffraction was used to calculate the d-spacing, as it was very clear. Data for this calculation was obtained from 4 leaflets obtained from 2 dogs with grade I and II mitral valve invovlment (table 2.2). The results showed that there was no difference between the diseased and healthy areas of the leaflets with a measured d-spacing of 660.0 Å.

Breed	Age	sex
cross-bred Terrier	11 years old	female
cross-bred Collie	7 years old	male

Table 2.2: The details of dogs used for the measuring of the d-spacing

Discussion

The study has shown that small-angle x-ray diffraction may be used to study the different characteristics of the axially projected structure of collagen fibrils in myxomatous mitral valves. This technique has been applied to determine the various attributes of collagen fibrils in the diseased canine mitral valves and develop detailed maps of collagen fibril orientation, collagen density, the degree of alignment of the fibrils, and the relative amount of tissue density. This allows better understanding of the spatial arrangements of collagen within diseased valves. Any changes that affect the quality, quantity, or organization of collagen could lead to the mechanical failure and dysfunction of mitral valves. The identification of collagen fibril orientation is one of the most striking findings of this study and shows that the mass of preferentially aligned collagen runs differently in different regions. In the main lesion-free body of the leaflets, collagen has a transverse course between the commissures. Near the free edge, it is almost a continuation of the collagen fibrils in the chordae tendineae. Because fibre orientation is the most effective way to optimize strength without increasing weight, fibre direction tends to reflect the prevalent tensile forces acting on a tissue (Sellaro, 2003). Therefore, knowledge of pattern of fibril alignment would have important implications for mechanical, bioprosthetic, and tissue-engineered valves and may inform the design of mitral valve substitutes. In contrast, diseased areas showed no distinct preferred orientation, and the collagen fibrils were disorganized with a haphazard and irregular arrangement. This confirmed what was previously suspected from histopathological and transmission electron microscopy studies (Tamura *et al.,* 1995). In other tissue types dynamic changes in collagen alignment can occur in response to continuous

mechanical force, but the short time frame of valve leaflet movement is unlikely to allow collagen fibrils to rearrange in response to changes in force alone. In MMVD, which is an age-related disease, the alignment of fibrils declines, whereas in aged specimens of other tissues, collagen tends to have the best defined patterns, which indicates a greater degree of regularity from increased cross-linking of the collagen molecules. This suggests that the collagen changes that occur with MMVD are not simply an aging process. The quantity of collagen was also greatly reduced in the affected areas compared to non-affected areas. Since the tensile strength of collagen fibrils is directly proportional to the mass of the fibrils, it can be assumed that the affected areas will be less capable of resisting the load and strain imposed by ventricular systole. The free edge of normal leaflets is the thickest part of the leaflet (Ho, 2002), and in healthy valves, collagen content is related to tissue thickness. The plots of baseline scattering in this study showed notable variation across the leaflets, which did not correspond to diseased areas. Regression analysis of the amount of collagen compared to the total tissue content at each pixel ($P \leq 0.01$, n = 120 points) revealed that there was a significant relationship between these two parameters in lesion-free areas. However, this relationship did not hold true in affected areas, where depletion of collagen is not reflected in a parallel decline in total tissue content. One possible explanation is that MMVD involves increased production and deposition of glycosaminoglycans (GAGs). The different types of GAGs have diverse properties for absorbance and for destructive and constructive interference (Kittleson, 1998), and although some of them could produce a clear and ordered diffraction pattern, others would only contribute to tissue density. It is also believed that GAGs in the right proportions do play a role to maintain collagen fibrils in

specific spatial order. Thus, the increasing amount of the GAGs would not only disturb that spatial order but, by reducing the physical space, might also encourage the process of collagen depletion. Determining the exact types of involved GAGs would be useful in furthering understanding of the disease. An additional confounding factor is that the type of collagen present in connective tissues is linked to the type and quantity of related GAGs. Type III collagen tends to be associated with more GAGs, although there are conflicting reports on the changes in Type III collagen content in human myxomatous mitral valve disease (Hammer *et al*., 1979; James *et al.,* 1991), and the exact makeup of collagen types in canine MMVD still needs to be determined.

The d-spacing measurement has also been the focus of several studies. In a study of one kind of muscular dystrophy in mouse it has been shown that there were no differences between the d-spacing of collagen between the affected and healthy mice though there was some abnormality in collagen organization in muscular tissue. On the other hand, the d-spacing of collagen is not a constant value in all the tissues of the same species. For example, in the same study the d-spacing for the muscular collagen and rat tail collagen was 657 Å and 670 Å, respectively (Kurg *et al.,* 1982). Lewis *et al.,* (2000) found differences of the d-spacing comparing malignant, benign and normal human breast tissue. Another study on arterial collagen has also shown that there is a relationship between the fibrillar stretch and the d-spacing and spacing does not remain constant throughout the nonlinear stress-strain of the tissue (Holzapfel, 2008). It seems that in determining the d-spacing not only is the type of collagen an important factor, but the interaction of collagen molecules with different

glycosaminoglycans can also play a role. This variability may also depend upon physiologic conditions. The condition of the sample is also important, whether is wet, dried or fixed. In the current study, no differences were found in the d-spacing between the diseased and healthy leaflets. This corresponds to the result of another study that showed the d-spacing did not change significantly among the myxomatous and healthy leaflets in human patients (James *et al.,* 1991). The same study showed that the there was a slight decrease in the d-spacing with aging. The reason for this decrease has not been fully explained, but it maybe related to the formation of non-reducible rigid cross-links. This finding supports the idea that although MMVD mostly occurs at the middle age or senescence, it is not simply just an aging process.

Chapter 3

Diffraction enhancing imaging (DEI) in the assessment of structural changes in MMVD

Diffraction enhancing imaging (DEI)

Diffraction enhancing imaging (DEI) is a method that produces high-contrast images based on absorption, refraction and scatter rejection in soft tissues. In conventional x-ray photography, the final image results from differential absorption of x-ray energy. This may be sufficient for hard or calcified tissues such as bone, but it has very limited use for the study of soft tissues. In DEI the x-rays which pass through the tissue are more important than those absorbed. These rays are scattered and diffracted in very subtly different ways to each other.

A brief description is presented here and detailed accounts of this method have been provided by others (Chapman *et al*., 1997; Menk *et al.,* 2005). The most important feature of the DEI instrument is the analyzer crystal (Figure 3.1). X-rays from a synchrotron light source pass through a monochromator. The mono-energetic x-rays traverse the sample, undergo diffraction by the analyzer crystal and are finally recorded by the detector. When the x-rays traverse the sample they are refracted by very small angles due to tiny variations in refractive index. The analyzer crystal almost completely eliminates the x-rays which have been scattered to a large angle by the sample. The x-rays emerging from the sample and hitting the analyzer crystal will meet the conditions for Bragg diffraction only for a very narrow range of incident angles. If the x-rays that have been refracted by the sample are within the angular acceptance range of the analyzer, they will be diffracted onto the detector. On the contrary, if the x-rays that have been scattered by the sample fall outside this angular approval range, they will not be diffracted at all. As the angular deviations

due to the refraction are very small, it is necessary to use a perfect crystal, thereby limiting the choice of crystal to silicon (Si), germanium (Ge) and quartz. A variation in the intensity of diffracted x-rays can be observed when the crystal is rotated in an axis parallel to the lattice and perpendicular to the incident beam. This intensity variation is called as the "rocking curve" (Lewis *et al.*, 2003; Li *et al*., 2003; Muehleman *et al.,* 2004).

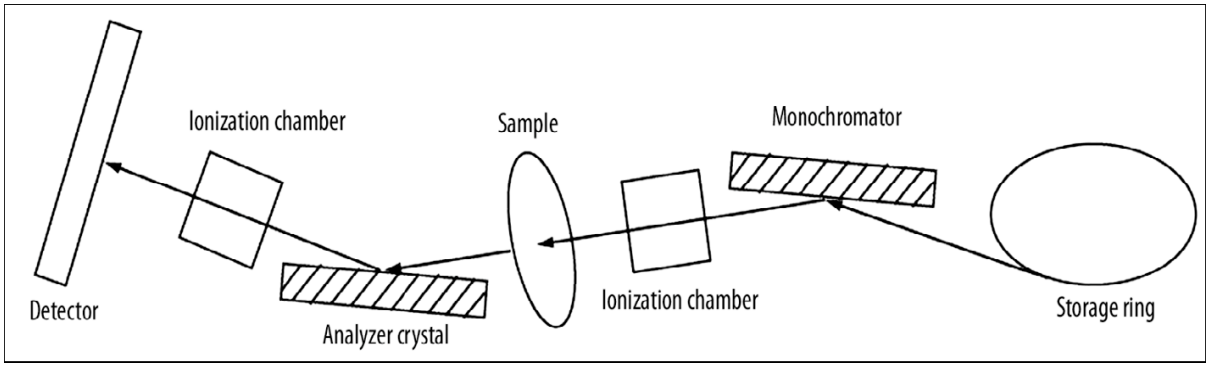

Figure 3.1: a schematic layout of diffraction enhancing imaging (DEI) set-up at the SYRMEP beamline at Elettra.

Aim

MMVD is known to involve structural changes in the matrix of the leaflets (Chapters 1 & 2). In order to characterise these changes further, the following experiment was designed to see what kind of changes (if any) were detectable using the DEI technique, and whether the findings could confirm or enhance the current available information about MMVD.

Materials and methods

The diffraction enhanced images were collected at the 6.1 bending magnet beamline 'SYRMEP' at Elettra, a third generation synchrotron light source operating in Trieste (Italy). The synchrotron can run at 2.0 or 2.4 GeV with a maximum ring current of 320 or 140 mA. In the present work the monochromator consisted of a double flat Si [111] crystal located in the vacuum 18 m away from the bending magnet source. This makes it possible to select energies within the range 8.5 to 35 keV. An aluminium filter, just before the instrument, was used to reduce the beam intensity and the shape of the laminar beam was defined by micrometric tungsten slits. In the experimental hutch, which was about 25 m away from the source, the sample and the detector were placed in vertical micrometric translators. Thus, the acquisition of a 2D image was possible by vertical scanning of the sample by a laminar beam. The analyzer was a single flat perfect crystal of Si [111] with the dimensions 10 mm thick, 130 mm wide and 80 mm long. There were also two ionisation chambers placed upstream and downstream of the sample. The upstream chamber was used as a flux monitor for evaluating the entrance dose in the sample. The downstream chamber was used to calculate the experimental rocking curve. In other words, the ratio between the downstream and upstream signals was assessed for precise positioning of the analyzer crystal. The sample cell was a cuvette-like chamber (made of transparent plastic) with a narrow bottom part to accommodate the leaflet. It was filled with phosphate buffer saline (PBS) in order to prevent the sample from drying. The camera was a 2048 × 2024 pixel CCD detector (Photonic Science Ltd, Roberts-bridge, UK). Each pixel was of 14 × 14 μm^2. The energy of the x-rays was about 20 keV. The distances from the specimen holder to analyzer crystal and from analyzer

crystal to detector were 60 and 32 centimetre respectively. A curve for intensity of transmitted energy (rocking curve) was drawn by rocking the analyzer crystal around the Bragg angle (Chapman *et al.,* 1997). The narrow rocking curve of the analyser crystal makes it possible to record a tiny deviation of the incident beam by a camera as intensity modulations. Each final image from a given point in the sample was interpreted in terms of 3 areas of a related rocking curve. The images acquired at the top of the curve (peak) are not only the result of conventional x-ray absorption but also represent the extinction contrast caused by the rejection of small angle scattering. On the other hand, the images produced by the slope of the rocking (at FWHM) are entirely attributed to the refraction effects. After collection, the images were studied using software ImageJ (Images Processing and Analysis in Java, version 1.40). Four freshly thawed samples (grade I or II) from two dogs were run altogether (Table 3.1)

Breed	Age	Sex
Labrodor	8 years old	Female
Mixed breed Terrier	10 years old	Female

Table 3.1: The details of dogs used in diffraction enhancing imagin (DEI).

Results

At the peak of the rocking curve the samples were hardly visible as there is little information about the refraction. However, images of the leaflets were quite apparent from the slopes of the rocking curve where the refraction was at its maximum Figure 3.2 shows two of the DEI images. The healthy regions of the leaflets showed a smooth pattern with no apparent differences in contrast or refraction indices. On the other hand, the diseased areas revealed a distinct pattern which was distinguishable from the surrounding healthy tissue. The chordae tendineae were also recognisable, especially in their entry point into the leaflets.

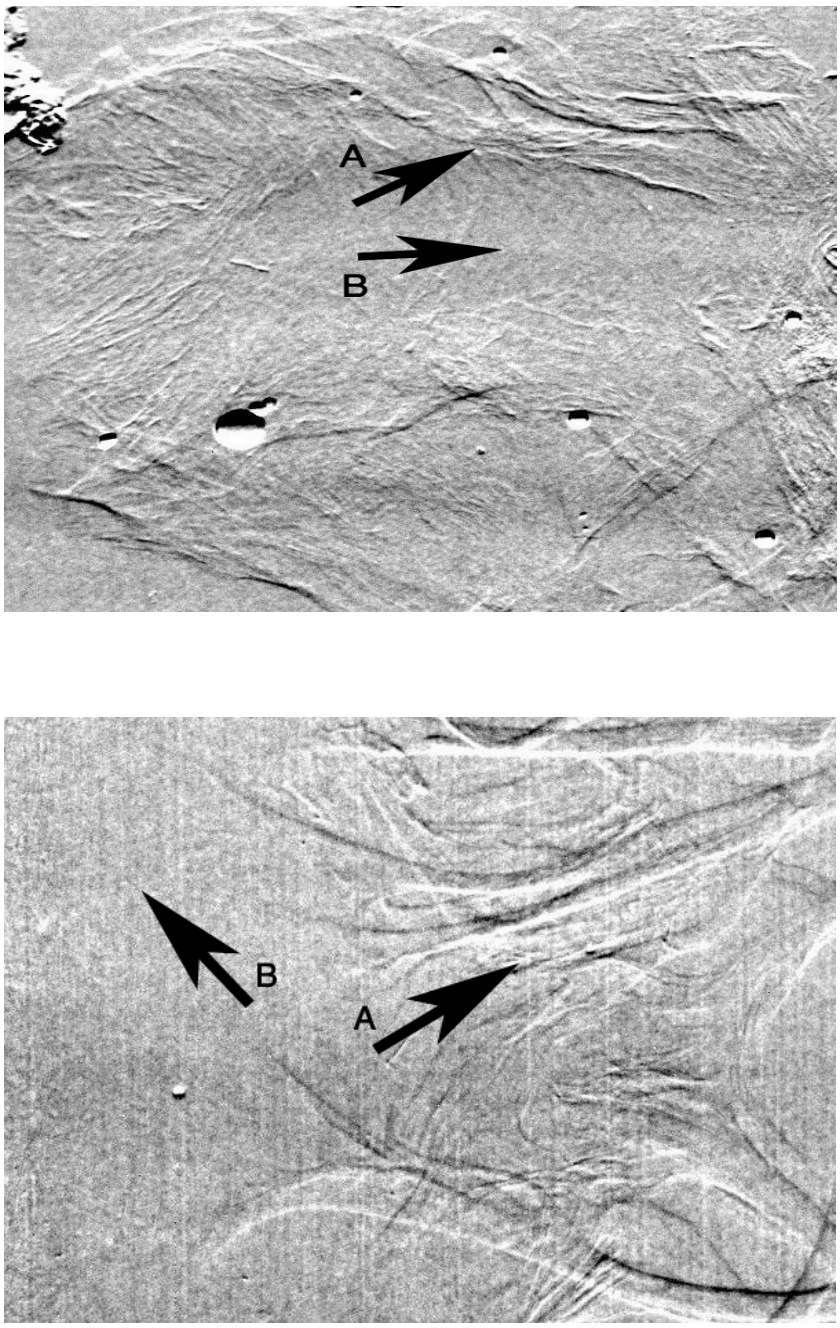

Figure 3.2: Diffraction enhanced image from of the parts (5 mm X 10 mm) of two mitral valve leaflets. Note the increased contrast and number of lines in the diseased areas (arrows A) compared to that of healthy areas (arrows B). Air bubbles can also be seen as an artefact (resolution: 10μM).

Discussion

Synchrotron radiation sources make it possible to produce a high intensity, collimated and tunable x-ray beam for use in the diffraction enhancing imaging technique. In the present study, this method was used to detect architectural distortions in diseased areas of MMVD valve leaflets, compared to healthy zones in the same valve. The detection of collagen fibrils assumes that the material filling the gaps between the collagen bundles has a density that is less than the firm bundles of collagen. In the healthy areas of the leaflets, collagen fibrils run in very close proximity to each other, occupying most extra-cellular spaces. Obviously, this can not give rise to strong DEI signals. However, as other studies and the x-ray data have shown (chapter 2), the collagen in the disease area becomes fragmented, depleted and its orientation becomes disordered. Besides, the increased amount of specific classes of proteoglycans, which is a common finding in MMVD (Gupta *et al*., 2008), can substitute for the depleted collagen fibrils, resulting in increased contrast and material disparity compared to its periphery. These factors may explain the results obtained from the lesion areas of the leaflet compared to the healthy areas. It should be born in mind that, all the differences observed in the leaflet were obtained from a completely soft tissue that otherwise would be invisible with conventional x-ray images.

The DEI result is also consistent with the x-ray diffraction finding (chapter 2) where it was shown that the collagen fibrils were disrupted in the lesion areas. Furthermore, this DEI result is in very good agreement, even in terms of DEI images, with a study performed by Pisano *et al.,* (2000). They studied infiltrating lobular breast carcinoma and confirmed spiculation and architectural distortion in the affected areas compared

to normal ones. Although MMVD and breast carcinoma are totally different pathologies, the architectural distortions appear very similar in the two conditions.

Since the introduction of DEI to biology and medicine in the late 80s, its potential has been tested in different conditions and tissues such as lungs, heart, liver and limbs in mouse; and human articular cartilage (Lewis *et al.* 2003; Muehlemant *et al.* 2004). The high resolution and quality of the images in DEI renders it as an option which can be applied successfully for studying abnormalities in soft tissues. The ability of the technique in depicting strong edge enhancement is another advantage, a property that is lacking in conventional x-ray imaging. This provides strong boundaries, even between soft tissues, and gives them a three dimensional appearances. Further development of the technique will make it possible to obtain images in a fraction of a second, making it easier to image live tissues in humans and animals that would otherwise be blurred because of their motion. One major drawback for DEI is the need for a synchrotron radiation source and its expensive set-up. Additionally, it should be remembered that, DEI is not a useful tool for studying tissues at a molecular level. In summary, the current study demonstrates the successful application of DEI as a useful tool in detecting the structural changes in MMVD. The qualitative DEI results showed structural changes of the matrix in MMVD explainable by the changes observed in x-ray diffraction study.

Chapter 4

Hydroxyproline assay as a measure of collagen content in canine mitral valves

Introduction

Hydroxyproline and proline each have a single hydrogen atom attached to the nitrogen atom of their pyrrolidine ring and are therefore referred to as imino acids (Figure 4.1). Hydroxyproline differs from proline by having a hydroxyl group (OH) attached to the γ-carbon atom. In the extracellular amino acid pool L-proline is one of the major constituents and many features have been attributed to it. Proline acts as an inhibitory neuromodulator and also serves as a precursor for glutamate synthesis in the synapse network of the central nervous system (CNS). Additionally, it has been shown that a gene (PRODH1) involved in encoding of proline oxidase (POX) is inducible by P53, a well-known tumour suppressor. Hydroxy-L-proline is, however, primarily found as an oligopeptide in the body. The major form of hydroxyproline in mammals is 4-hydroxy-L-proline with the origin of endogenous and dietary collagen. 3-hydroxy-L-proline from collagen in basement membrane is found in much smaller quantities (Phang *et al*., 2001; Hu *et al*., 2008).

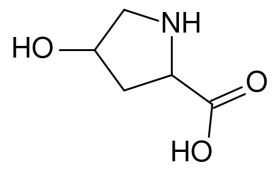

Figure 4.1: The structure of hydroxyproline. Note that in proline and hydroxyproline the side chains are bonded to the backbone nitrogen as well as to the α-carbon. The ring plays an important role in restricting the geometry of any protein where it is present.

Although nonessential amino acids can be synthesized via endogenous pathways, these pathways are not often used when there is a good supply of dietary proteins. However, some endogenous pathways are essential as they provide precursors for other metabolic pathways. Pyrodoxal-5-phosphate coenzyme catalyzed decarboxylation and transamination reactions are necessary for amino acid metabolism. Interestingly, since proline does not have any primary amino group it is excluded from this pathway. The study of proline metabolism is gaining increased interest. A role for proline has been identified in interactions such as defense against osmotic challenge in prokaryotes and plants, as a redox shuttle in insects, and as a mediator of parasite-induced pathophysiology in mammalian hosts (Phang *et al*., 2001)

Proline and hydroxyproline metabolism

Orinithine and glutamate are the main precursors of proline, with pyrroline-5-carboxylate (P5C) or glutamic-γ-semialdehyde as the intermediates. Ornithine-γ-aminotransferase (OAT) is an enzyme responsible for the conversion of orinithine to P5C. The mitochondrial matrix of cells from all tissues accommodates this enzyme. It can also be found in red blood cells. Additionally, P5C synthase, which is an ATP and NADPH-dependent enzyme, can also be found in the mitochondrial inner membrane. P5C synthase catalyzes the production of P5C from glutamate. In mammals, a high activity of P5C synthase has been observed in small intestinal mucosa, colon, pancreas and brain. Conversion of P5C into proline is mediated by P5C reductase with the help of cofactors such as NADH or NADPH. Proline degradation starts by conversion of proline into P5C by an enzyme called proline

oxidase, which is located in the inner membrane of mitochondria. Then, P5C dehydrogenase catalyzes the conversion of P5C into glutamate.

The principle route of biosynthesis of hydroxyproline or 4-hydroxy-L-proline is the post-translational hydroxylation of proline in a newly synthesized collagen. Peptidyl-proline hydroxlyase catalyzes this hydroxylation and requires O_2, ferrous iron and α-ketoglutarate. 3-hydroxyproline, unlike 4-hydroxyproline occurs only in interstitial collagen. The ratio of 3-hydroxlyproline to 4-hydroxlyproline is often used in experiments to determine the amount of basement collagen to that of total collagen. The formation of 3-hydroxyproline occurs in the same manner as 4-hydroxyproline except that it is catalysed by a different prolyl hydroxlyase. The degradation of 4-hydroxy-L-proline starts with steps similar to those of proline degradation, though with the distinct enzyme. However, there is one exception where one single enzyme catalyzes dehydrogenation of both P5C and pyrroline-3-hydroxy-5-carboxylate.This enzyme common to both pathways may be a linking point between the metabolism of proline and hydroxyproline. The degradation of hydroxyproline starts with an oxidation reaction leading to Δ-pyrroline-3-hydroxy-5-carboxylate, similar to that of proline oxidation. Then NAD^+-dependent dehydrogenase catalyzes the conversion of the pyrroline product into 4-erythro-hydroxy-L-glutamte followed by transamination of hydroxyglutamte to form 3-hydroxy-2-oxoglutarate. After this point, however, the similarities between two pathways end. Hydroxyoxoglutarate is sliced into two products, namely glyoxylate and pyruvate. Knowledge about the degradation of 3-hydroxyproline is limited, but its urinary excretion can be used as a marker for

basement membrane turnover. Figure 4.2 shows the main degradation pathways of 4-hydroxyproline in the mammalian tissues.

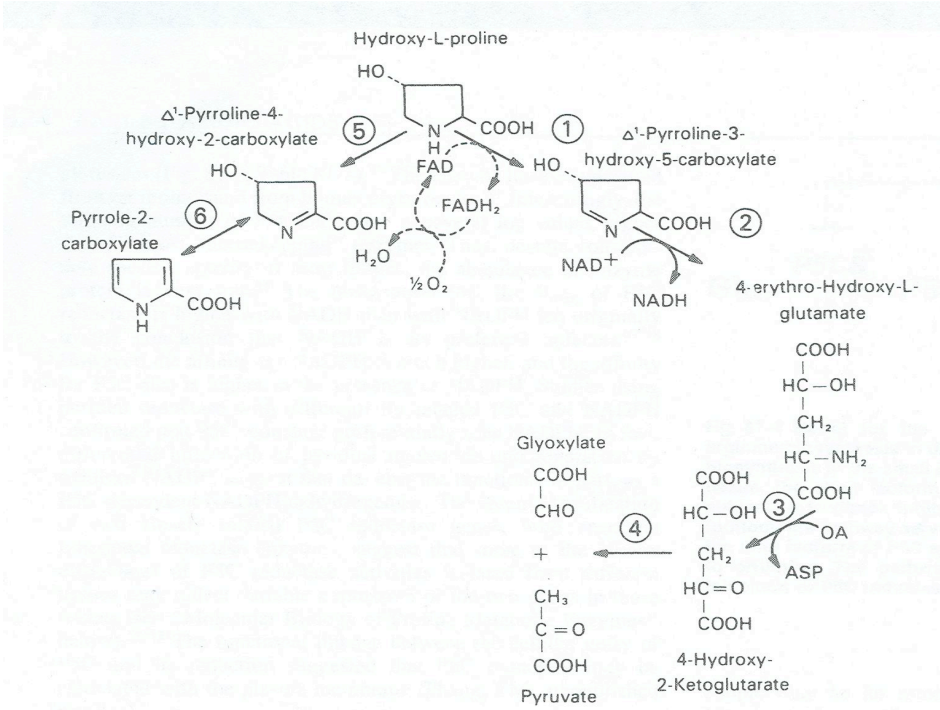

Figure 4.2: The major pathway of 4-hydroxyproline in mammals' tissue. In the major pathway the enzymes are (1) hydroxy-L-proline oxidase (2) Δ-pyrroline-3-hydroxy-5-carboxylate dehydrogenase (3) glutamic-oxaloacetate amino transferase (4) 4-hydroxy-2-oxoglutarate lyase. In the minor pathway, the enzyme is (5) L-amino acid oxidase and the reaction (6) is spontaneous (Phang *et al.*, 2001).

Free hydroxyproline in plasma forms less than 25 percent of the total hydroxyproline of plasma, and this percentage may vary between children and adults. The remainder of the imino acid is incorporated into proteins by peptide bonds. There have been numerous studies performed on urinary excretion of proline and hydroxyproline (Bates, 1977; Hasselbalch, 1987).

The ratio of total proline excretion in urine to that of total hydroxyproline in humans rises from childhood to adulthood. Moreover, excretion of the peptide bound form of hydroxyproline increases from childhood to adolescence, proving a greater turn-over of collagen during the growth period. However at the same time there is no increase in urinary excretion of free hydroxyproline as renal re-absorption of imino acids dramatically increases from infancy and childhood to adulthood.

Hydroxyproline is restricted to collagen and therefore it can be used for measuring collagen turn-over or determining the collagen content of a given tissue. It may also provide useful information for some physiological and pathological conditions such as growth, aging and malignancies.

Aim

Collagen depletion has long been suspected in MMVD and has been demonstrated by conventional and electron microscopy (Chapter 1). X-ray diffraction studies (Chapter 2) showed depletion of fibrillar collagen in the diseased areas. However, there are no previous reports that have quantified the changes (increase or depletion) of collagen in canine MMVD. Collagen composition in human myxomatous mitral valves is also a matter of controversy (Cole *et al.*, 1984; James *et al.*, 1991). This experiment was designed to determine the amount of collagen (irrespective of spatial arrangement) in the diseased and healthy regions. The results would determine whether there is a consistent relationship between the collagen depletion and severity of disease (MMVD grade I in current study). Furthermore, as non-fibrillous collagen molecules also play a role in the pathophysiology of MMVD, this experiment would

complement the results of the differential scanning calorimetry experiment (Chapter 5) in determining the extent of the relation between the whole collagen content to that of fibrillous collagen in MMVD.

Materials and methods

The samples were obtained from 3 dogs with grades I and II myxomatous mitral valve disease (Table 4.1). They were cut to produce three 3 × 3 mm specimens from affected and healthy regions of the leaflets., Their wet weight was also measured. Additional samples were prepared from dog tail tendon. An adapted form of the Bergman and Loxley method was used to determine the hydroxyproline content of the tissues used (Hurtig *et al.*, 2001). Since hydroxyproline is exclusively found in collagen, where it comprises 13.4% of the protein, the total concentration of collagen can be determined by multiplying the hydroxyproline value by 7.46. The tissues were dehydrated in 1 mL acetone (60 minutes) and degreased in 2 mL petroleum ether (120 minutes). The fragments were dried in an incubator at 100°C for 30 minutes. Drying continued in a freeze-dryer for 6 hours. The samples were re-weighed again (dry weight). 100 µL of 6 N HCl was added to each test tube and they were sealed under vacuum. The sealed tubes were incubated at 110°C for 12 hours. The hydrolysates were then dried, resuspended in 1 mL HCl (1 mM) and transferred into 1.5 mL Eppendorf tubes. They were centrifuged at 10000 rpm for 15 minutes. The supernatants were used for the next step of the protocol. This preparation was carried out in triplicate for each sample. To 100 µL of supernatant in each test tube, the following reagents were added in order: 400 µL HCl (1mM); 1 mL isopropanol; and 500 µL of an oxidant solution. The oxidant solution contained 1 mL of 7%

chloramine-T made in distilled water added to 4 mL of acetate/citrate buffer, pH 6 (14.3 mg sodium acetate trihydrate, 9.4 g trisodium citrate dihydrate and 1.4 g citric acid monohydrate were dissolved in 96 mL isopropanol and made up to 250 mL with distilled water). Standard hydroxyproline solutions of 1.5, 1, 1/2, 1/4, 1/8, 1/16, 1/32, 1/64, 1/128 mg/mL were made from L-4-hydroxyproline (Fluka Biochemika) and treated in the same way. A blank control was made by adding 500 µL 1 mM HCl instead of the supernatant or standard solution. The tubes were vortexed and left at room temperature for 4 minutes. 500 µL freshly prepared Ehrlish's reagent solution, containing 3 mL of Ehrlish's reagent (10 g paradimethylaminobenzaldehyde in 11 mL 70% perchloric acid) mixed with 16 mL isopropanol, was added to all tubes. The tubes were vortexed again and incubated in a water bath at 37°C for 2 hours. The absorbance was read at 550 nm (Varian Cary 50 Scan spectrophotometer) for all the samples and concentration of hydroxyproline was calculated using the standard graph.

Breed	Age	Sex
CKCS	8 years old	Male
Mixed breed CKCS	10 years old	Female
Mixed breed Terrier	14 years old	female

Table 4.1: The details of the dogs used in the hydroxyproline assay.

Results

The assay of collagen based on hydroxyproline measurement is summarised in table 4.1. The mean values for collagen content based on dry tissue were found to be 416.15 μg/mg ± 9.21 (SD) and 370.06 μg/mg ± 12.76 (SD) in healthy and diseased regions, respectively. The mean values for wet tissue were also 37.48 μg/mg and 33.15 μg/mg in healthy and diseased regions respectively. Analysis of all triplicate results for healthy and diseased regions using two sample un-paired t-test showed that the quantity of collagen diminished approximately by 10% in the affected valves compared to that of normal valves ($P \leq 0.05$). Comparing the amount of collagen in mitral valve leaflets (irrespective of their disease status) to that of collagen content in tail tendon, (especially wet tissue measurement) reveals a big difference. This may indicate the difference in hydration state between tail tendon and mitral valve leaflets. As the tissues were degreased during the preparation procedure, it may also reflect the difference in lipid or lipid-related compounds between the leaflets and tail tendon.

	µg/mg dried tissue	µg/mg wet tissue
Normal	416.15 ± 9.21	37.48
Affected	370.06 ± 12.76	33.15
Tail tendon	467.17 ± 8.05	172.15

Table 4.2: Collagen content of dog tail tendon, normal dog mitral valves leaflets and valve leaflets from dogs affected by MMVD, determined by quantitative analysis of hydroxyproline (µg/mg) using an adapted form of Bergman and Loxley method (Hurtig *et al.*, 2001).

Discussion

Hydroxyproline assay is an established method of measuring the collagen content of different tissues and of the body as whole. Many diseases, including cardiac conditions, are associated with the depletion or restructuring of collagen. Determination of changes in the amount of collagen in certain diseases can provide valuable information about the pathogenesis. For example, in one form of mouse model of osteogenesis imperfecta (*oim*) where the pro-α2(I) chain of collagen is faulty, there is about 60% less collagen in tail tendon and a 40% reduction in tensile strength to that of wild type mice (Weis *et al.,* 2000). Electron microscopy studies have also shown areas of depleted and disorganised collagen in the affected leaflets in MMVD (Tamura *et al.,* 1995; Black *et al.*, 2005). However, there has not yet been any study of the amount of this depletion. The current study has shown that there is a depletion of about 10% in the mild and moderately affected leaflets (grade I and II). The amount of collagen in the tendon samples, per dried tissue mass (approximately

50%), according to the hydroxyproline assay, was in close agreement with an earlier study of the collagen content of equine superficial digital flexor tendon (Lin *et al*., 2005) and it validates the measurements in the dog valves. The depletion of collagen would certainly affect the general properties of the leaflets making them weaker and less able to resist blood pressure, thereby contributing to the clinical malfunction of the leaflets. However, it should be mentioned that depletion of collagen alone cannot be the only reason for the leaflet dysfunction, as the previous chapters have shown that the structure of the fibrils and their orientation must be of considerable importance as well.

The reason for the depletion of collagen in MMVD or primary mitral valve prolapse remains unknown. In diseases such as osteogenesis imperfecta, it seems that production of faulty collagen fibrils renders the collagen liable to be removed faster than normal. However, in MMVD, the genes that encode collagen seem to display no abnormalities (Pedersen and Häggstrom, 2000). The question is then, why do these apparently properly encoded collagen molecules start to deplete faster than the normal rate? One possible explanation may lie in extensive post-translational modifications that collagen undergoes after its primary formation. Another possible explanation relates to the context of the micro-milieu of the leaflets. Changes in this micro-milieu, such as excessive deposition of glycosaminoglycans and an increased activity in the pathways that may suppress collagen synthesis or enhance its degradation, can also play a part in this process. In this aspect, the role of cytokines needs to be taken into account. Several studies have shown that transforming growth factor-β1 (TGF-β1) in human patients is responsible for deposition of extracellular

matrix in hypertensive blood vessels or fibrosis in aortic valve disease (Grande *et al*., 1997; Lin *et al*., 2008). However, a study showed that there was not any connection between TGF-β1 and human mitral valve prolapse in a population of Taiwanese patients (Chou *et al*., 2002). Other cytokines, such as tumour necrosis factor-α and interferon-γ can also suppress collagen synthesis. Interleukin-6 also strongly inhibits the growth of the fibroblasts (Ihlberg *et al.,* 1993). Injuries and remodelling processes are often accompanied by an increase of hydroxyproline concentration in the most tissues, but it seems in MMVD this remodelling in response to the disease is somehow different. Rabkin *et al*. (2001) have shown that there is no increase in collagen mRNA in the remodelling of connective tissue in myxomatous mitral valve disease, while at the same time there is strong expression of the matrix metalloproteinases, cathepsins and interleukin-1β.

One potentially important area of investigation is the biology of advanced glycation end products (AGEs) as they might also play a role in collagen depletion. It seems that AGEs can affect the matrix-cell interactions, such as migration, growth, proliferation and also gene expression. It has been shown that the cells grown in matrices with high concentration of AGEs have different characteristics in terms of differentiation, response to cytokines, motility, etc. The relation between AGEs and apoptosis has also been studied. In two recent studies, Takahashi *et al.* (2008) have shown that methylglyoxal (MG) (one of the precursors of AGEs) is responsible for apoptosis in endothelial cells of bovine aorta, while Niu *et al (*2008) have shown that AGEs can induce cell arrest and apoptosis in the cultured dermal fibroblast. It has already been shown that receptors of AGEs accumulate during the course of diseases

such as diabetes, Alzheimer disease and also during aging. In vitro studies have demonstrated that binding the AGE to its receptor triggers the activation of the transcription factor NF-kB (nuclear factor-kappa B) via p21ras/MAP. NF-kB is a transcriptional factor responsible for gene modulation of endothelin-1, VCAM-1 (vascular cell adhesion molecule-1), tissue factor and thrombomodulin. It is also related to the generation of some cytokines, such as IL-1α, IL-6 and TNF-α (Singh *et al.,* 2001). Research projects targeting AGEs, in order to reduce their formation and possible detrimental effects, are many and on-going. Several AGE inhibitors have been studied. Of these, some have attracted more interest than others, including aminoguanidine, aspirin, antioxidants (vitamin C and E), metal ion chelators (desferoxamine and ALT-946,N-(2-acetamidoethyl)hydrazinecarboximidamide hydrochloride), penicillamine, pyridoxamine (vitamin B_6), and enzymes that cause deglycation of Amadori products (amadoriases) (Reddy and Beyaz, 2006; Desai and Wu, 2007). Aminoguanidine (AG) and aspirin are potentially promising agents. AG mainly acts by sequestrating 1,2-dicarbonyl compounds (which arise from oxidation of free sugars or Amadori products) through the formation of their corresponding adducts, 1,2,4-triazines, which are relatively non-toxic compounds. Aminoguanidine is also structurally similar to that of L-arginine, which is the precursor in the formation of nitric oxide (NO). It has been shown that AG is capable of inhibiting NO synthase (NOS) (Singh *et al.*, 2001; Wilkinson-Berka *et al*., 2002; Reddy and Beyaz, 2006). NO and its potential relation to MMVD was discussed in Chapter one. Aspirin acts in a concentration-dependent manner and two mechanisms may be involved: scavenging of oxygen radicals and acetylating lysine residues which then blocks glycation, though some have questioned the importance of the latter

mechanism (Hadley *et al*., 2001; Urios *et al*., 2007). More research is needed to shed light on the role of AGEs in MMVD and the possible amelioratory or therapeutic effects of AGEs-inhibitors.

The exact factors which trigger the primary causes of collagen depletion are still unknown. However, it is now well documented that the depletion of collagen in some tissues, especially those that are under repeated stress such as muscle, can lower the threshold of micro-injury level making them more prone to a form of self-perpetuating damage cascade (Gronemann, *et al.,* 2004).

Chapter 5

Differential scanning calorimetry (DSC) and thermal stability of collagen in MMVD

Differential scanning calorimetry

Differential scanning calorimetry (DSC) is a technique that belongs to a group of techniques called “thermal analysis”. The objective behind any thermal analysis is simply to obtain information about thermal changes in a sample by heating or cooling it. In DSC, this is done in comparison to a reference sample. Depending on the specific heat of a given sample any thermal energy supplied to a sample would increase its enthalpy and temperature. The energy supplied to the sample not only increases the temperature and enthalpy, but it can also change the physical and chemical status of the material, leading to melting, denaturation, decomposition etc. DSC and differential thermal analysis (DTA) are two major thermal analysis methods employed in biology. The term “differential” reveals an important feature of the techniques: two identical sensors are connected to the sample and reference and the output signal from the instrument is directly related to the difference between these two samples. The two techniques are often used for solid materials though using them for suspensions or solutions, such as various lipid solutions is not uncommon (Davies *et al*., 1998). The requirement for a very small amount of the sample and rapidity of the methods, have increased the popularity of these thermal techniques. However, differential scanning calorimetry is fundamentally different from differential thermal analysis. In DTA the temperature difference between a sample and reference material is monitored while they are subjected to the same environment of the heating or cooling. Then the plot of DTA is drawn as ΔT (function of temperature) on the y-axis against the time or temperature on the x-axis. In the case of DSC, on the other hand, while the sample and reference are in exactly

similar environments, using a predetermined programme, the temperature for the sample and reference are maintained equal throughout the experiment even when the thermal events occur in the sample. The energy which has to be supplied or withdrawn from the sample to yield a zero temperature difference between the sample and the reference is recorded. Therefore, the DSC plots record energy (heat) in the y-axis against temperature or time on the x-axis. Any changes in the sample which are associated with absorption or releasing of heat are recorded as a peak whose area is proportional to the enthalpy changes and direction (whether negative or positive) indicates the type of the thermal event, namely endothermic or exothermic.

DSC often falls into two major categories: Power Compensated DSC and Heat Flux DSC. In case of Power Compensated DSC, there are separate micro-heaters and temperature sensors for the sample and sensor. In the event of temperature difference between the sample and reference, energy is supplied or withdrawn in order to keep the difference at zero. The differential energy is the source of the instrument signal. In Heat Flux DSC the sample and reference are heated in the same furnace and the temperature difference (ΔT) is measured by thermocouples. ΔT is then converted into differential energy by the use of instrument software. Additionally, in Heat flux DSC (like DTA), an endothermic event produces a negative peak and exothermic event would give rise to a positive peak, which is the opposite of the thermal plots from Power Compensated DSC. A typical thermal analysis curve for Power Compensated DSC is shown in Figure 5.1. Of particular interest of this curve is the extrapolated peak onset temperature (T_e) which is the intersection of the extrapolated

baseline and the tangent line of linear section of main peak. This is more reliable than the maximum temperature of the peak, as it is less affected by the heating rate. The initial peak temperature and the final peak temperature are difficult to pinpoint so they are seldom used (Höhne *et al*., 1996; Laye, 2002; Ramachandran *et al.*, 2003).

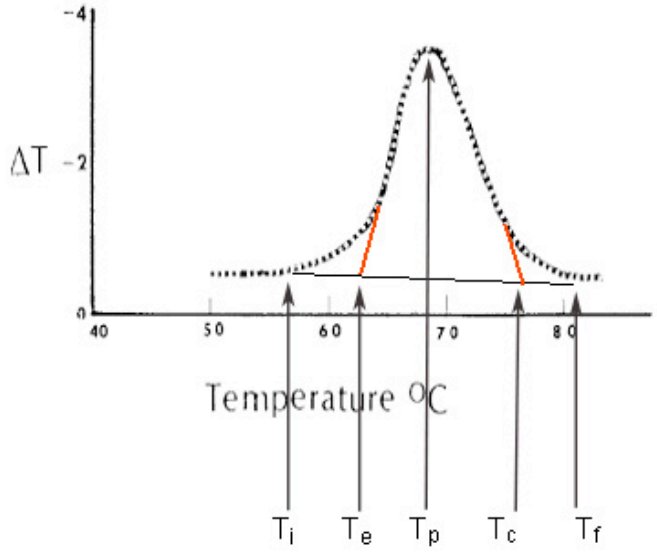

Figure 5.1: Characteristic features of the thermal analysis curve. Initial peak (T_i), extrapolated peak onset temperature (T_e), maximum peak (T_p), extrapolated peak completion (T_c) and final peak temperature (T_f).

Aim

Proteins, including collagen, in their natural tertiary structures are thermally stable compounds with a lower state of energy. The thermal properties of proteins are affected by hydration, hydrogen bonds, environmental conditions (such as pH), cross-links, mechanical loading of proteins etc. An understanding of the physicochemical principles of thermal properties of proteins can help us to understand the functions of proteins. This DSC study was, therefore, designed to investigate changes in the thermal properties of collagen molecules occurring in MMVD. Different aspects of changes which collagen molecules undergo in MMVD have been shown in this thesis and the DSC results are interpreted accordingly in the light of those findings.

Materials and methods

In the current study a Power Compensated Perkin Elmer Pyris I differential scanning calorimeter was used (Norwalk, CT USA). A schematic set up for the experiments can be seen in Figure 5.2.

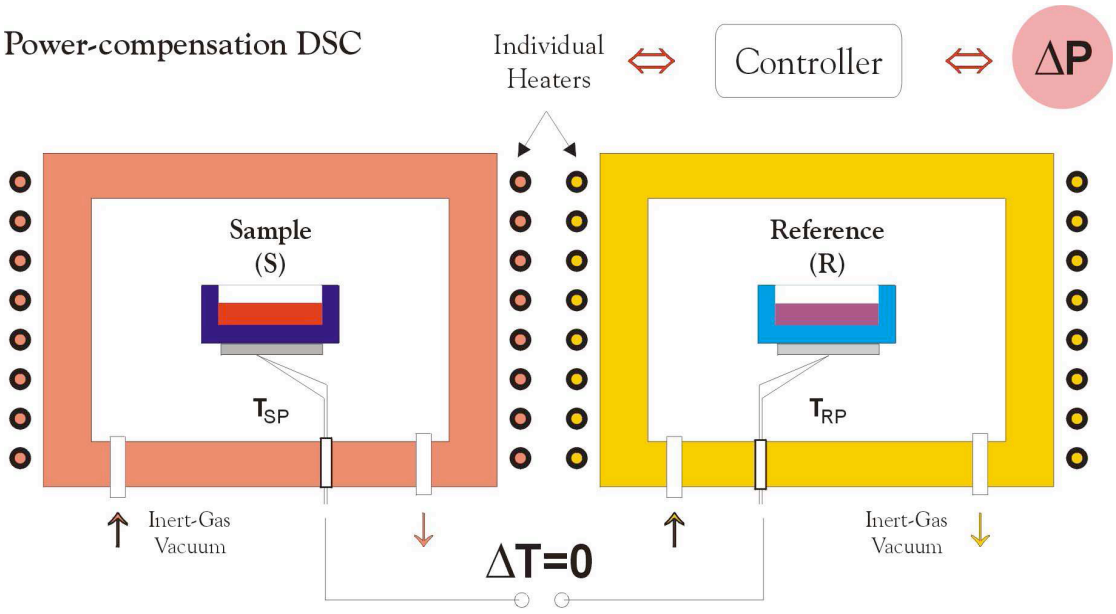

Figure 5.2: A schematic of set up of the Power Compensated DSC used in the current study (Nicula, 2002).

Tissue samples were chosen and excised from the affected grade I MMVD freshly thawed leaflets and also from normal leaflets. Overall, 10 diseased and 7 unaffected samples (from 4 different leaflets of grade I and II) were analysed (Table 5.1). They were cut into small pieces and blotted with a soft tissue and then weighed. They were sealed in aluminium pans (8 mm in diameter) and placed in the DSC instrument. An empty pan was used as a reference. Heating was carried out from 10 to 80°C at a rate of 5°C/min after initially holding at 10°C for 2 minutes. The onset temperature and enthalpy (ΔH) were calculated from thermograms for each process. The enthalpy was determined from the area under the curve between the extrapolated peak onset and the extrapolated peak completion. Rat and dog tail tendons were also run to ensure reproducibility of the data and for comparison, respectively. After completion of the measurements the sample pans were punctured and placed under

vacuum for 3 hours to desiccate the samples before they were re-weighed. The DSC instrument was calibrated with indium and water as standards, prior to the commencement of the measurements. Statistical analysis was performed using a two sample un-paired t-test with significant differences taken at $P \leq 0.05$.

Breed	Age	Sex
German shepherd	14 years old	Male
Beagle	3 years old	Male
Grey hound	9 years old	Male
Collie	10 years old	Male

Table 5.1: The details of the dogs used in DSC experiment. All of them demonstrated grade I and II mitral valve involvement.

Results

Table 5.1 gives the thermometric parameters determined by DSC for samples of myxomatous and healthy leaflets and dog tail tendon. The data reveal a reduction in the enthalpy of denaturation in affected regions of the leaflets compared to that of normal ones ($P \leq 0.05$). The onset temperature of the main endothermic peak was slightly lower in affected areas compared to the normal group, but this was not statistically significant. Comparing the leaflets with dog tail tendon (Figure 5.3) a noticeable difference in the enthalpy of denaturation was found for both normal and diseased tissue. However, the endothermic peak in tail samples was at the same temperature position as those of the leaflets.

	Onset Temp mean	Peak Temp mean	Enthalpy(ΔH) mean
Dog tail tendon	64.56 °C ± 0.23	65.75 °C	8.52 J/g ± 0.19
Healthy sample	65.10 °C ± 0.35	66.37 °C	1.75 J/g ± 0.07
Affected sample	64.60 °C ± 0.30	65.45 °C	1.40 J/g ± 0.05

Table 5.2: Comparison of thermal parameters for collagen denaturation in dog tail tendon (n = 5), healthy sample (n = 7) and affected sample (n = 10). Measurements were performed on a Perkin Elmer Pyris 1 differential scanning calorimeter.

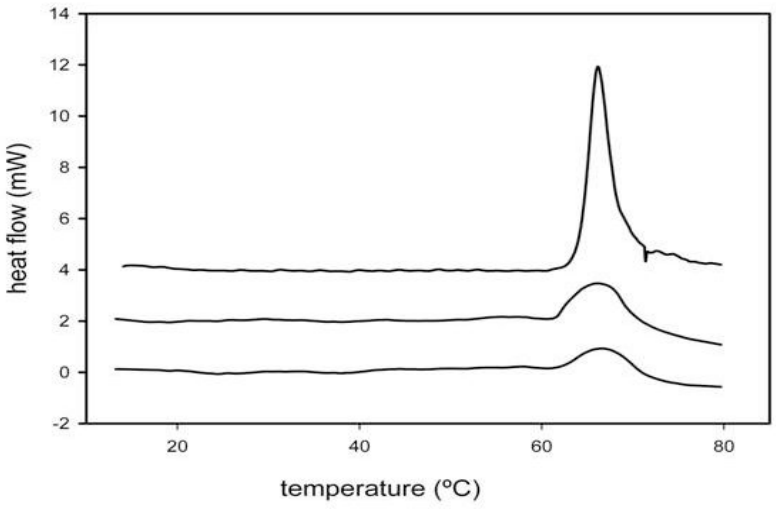

Figure 5.3: A thermogram of differential scanning calorimetry. From top to bottom: dog tail tendon, diseased and normal valve leaflets. The weights of the samples used were: dog tendon 35.2 mg; healthy valve 36.0 mg; diseased valve 36.2 mg. The weights have been mentioned here as the big differences in weight might affect the enthalpy of denaturation.

Discussion

Measurements of the melting process by differential scanning calorimetry give insight into the structural alteration that occurs with myxomatous degeneration of the mitral valve. In general, the thermal stability of collagen depends upon the level of hydration of the collagen, the number of hydrogen bonds and the number and the nature of covalent cross-links (Sionkowska, 2005; Trebacz and Wójtowicz, 2005). The mechanism of denaturation is based on an irreversible process beginning with the rupture of hydrogen bonds coupling the three α-chains followed by breakage of the cross-link bonds (Miles, 1993; Miles *et al.,* 1995). Miles and Ghelashvili proposed that dehydration reduces the free-volume available for denaturation of the α-chains in the presence of thermally stable cross-links in the collagen fibres (Miles and Ghelashvili, 1999). Moreover, this dehydrated collagen could be confined in a spatial arrangement within the lattice of the fibre decreasing the entropy and subsequently raising the thermal stability of collagen (polymer-in-a-box theory). Alternatively, simultaneous with rearrangements in the molecular packing of collagen in the fibre, water molecules that are connected via hydrogen bonds to the triple helix itself would be gradually stripped away, as the fibre is further and further dehydrated. Some of these molecules are involved in water bridge structures that connect one α-chain to another. These hydrogen bonds would need to be broken on denaturation. Thus stripping away of water bridge molecules has several effects, of which the most important one is the reduction of enthalpy of denaturation because fewer hydrogen bonds need to be broken to separate the α-chains and reduce them to random coils. Finally, once the α-chains are uncoupled, the whole molecule becomes unstable, rapidly unzips, and collapses to form random coils.

In the measurements from this study, the enthalpy of denaturation of collagen in both groups of valve leaflets showed distinct differences compared to the tail tendon. Comparison of the affected and normal leaflets also revealed that, in the affected leaflets, the enthalpy of denaturation was decreased by 20% or, in other words, 20% less intact collagen fibrils. To validate the current DSC data experiment, the reanalyses of the x-ray diffraction data was performed on the summed meridional diffraction intensities, normalised using readings taken from ion chambers (in a SRS set-up, ion chambers are often placed after and before the sample. They convert the intensity of beam into number of x-ray photons, providing a useful tool for normalising data and monitoring the incident beam). This produced a value that is proportional to the fibrillar collagen content per unit mass of tissue without taking into account the presence of non-fibrillar collagen. The results also confirmed a 20% decrease of intact collagen fibrils in the diseased areas (two-sample un-paired t-test; $P \leq 0.05$).

This decline in fibrillar collagen cannot simply have been caused by a depletion of collagen in the diseased samples as the hydroxyproline assay has revealed that there was only about 10% depletion of collagen in the affected tissue (Chapter 4).These findings imply qualitative, as well as quantitative, changes in the collagen of affected valve leaflets. However, there was no significant difference in the onset temperature of denaturation between diseased and normal leaflets. The underlying cause must only be affecting the enthalpy of denaturation and not the onset temperature. It is already known that a change in pH or concentration of ions around the collagen molecules only influences the temperature but not enthalpy of denaturation (Miles *et*

al., 1994). Changes in amino acid composition would also impact on both the temperature and the enthalpy. It was Gustavson (1955) who drew the attention of composition of amino acids and collagen thermal stability and highlighted the importance of hydroxyproline residues in forming hydrogen bonds between its hydroxyl group and carbonyl oxygen of adjacent peptide. Although there are long standing reports determining the thermal stability of collagen on the basis of combined content of proline and hydroxyproline, new studies have shown that in the typical collagen motif of Gly-X-Y (which X and Y are proline and hydroxyproline respectively), hydroxyproline stabilises collagen in the Y position independently from the X position, while stabilisation occurs in the X position only if the residue in the Y position can form stabilisation interactions with X (Berisio *et al.,* 2004). It seems that this is the reason why in vertebrates, hydroxylation only happens in the Y residue. Other research into the stabilisation effect of hydroxyproline has been carried out by substituting of hydroxyproline with 4-*trans*-fluoroproline. This has yielded interesting results. 4-*trans*-fluoroproline can form hydrogen bonds but the resultant collagen is very stable. It has been concluded that hydroxyproline is pivotal in the conformational transformation of imino peptide bonds to the "*trans"* mode. As in native collagen triple helix all bonds are in "*trans"* mode, the collective "*trans"* plays a more important role in the thermal stability of collagen than hydrogen bonds (Bann *et al*., 2000). Moreover, glycine's role in determining the thermal stability of the helix needs to be taken into account. It has been shown that in osteogenesis imperfecta, substitution of glycine with another amino acid can affect the thermal stability of the collagen, but not all substitutions of glycine residues are equally important and the effect varies according to the molecular region (Bächinger and

Davis, 1991). However, a change in thermal stability does not necessarily reflect the clinical manifestation of a collagen-relevant disease. In one form of osteogenesis imperfecta, where there was a glycine to tryptophan substitution with associated severe clinical signs, there was only a very slight decrease in the thermal stability of the affected collagens (Nuytinck *et al.,* 2000). All these changes in amino acid sequences can also affect the onset temperature and enthalpy. While the current view is that collagen genes are not affected in MMVD the extensive post-translational modification of collagen during its biosynthesis, especially regarding hydroxylation of proline and its importance in the thermal properties of the tissue, makes amino acid sequence change worth investigating.

The most probable explanation for the observed decrease in enthalpy of denaturation in MMVD collagen is that not all of the collagen molecules are in the form of intact and regularly-structured triple-helix and/or fibrils. This is known by the data from x-ray diffraction study since only the regularly ordered and intact fibrils would contribute to the diffraction pattern (Chapter 2) (Hadian *et al.,* 2007). By comparing affected and normal leaflets, it is clear that there is a 20% decrease in intact collagen fibrils. This non-fibrillous collagen can arise from failure of incorporation of the molecules into fibrils, an uncoupling of the α-chains as a result of enzymatic depolymerisation and subsequent denaturation, or from an alteration in the nature and number of the cross-links responsible for strengthening the collagen helices. Consequently, the onset temperature of denaturation remains unchanged for these molecules, but the enthalpy undergoes some changes. This is consistent with the findings of a study carried out on the superficial digital flexor tendon degeneration in

the horse which showed that the enthalpy of denaturation of degenerated tendon was less than that of normal tendon whereas the temperature characteristics were the same (Miles *et al*., 1994). Interestingly, although the two diseases are very different, both appear in advanced age and the cause has been suggested for both to include a repeated injury mechanism. However, one may question the underlying source for this non-fibrillous collagen. There are reports that the mechanical rupture of tendons makes them more susceptible to denaturation and also proteolysis (Miles *et a*l., 1994). The implication of the "polymer-in- a box" theory is that restriction of the collagen molecules in this way can close or cover thermally labile domains (TLD) where the triple helices lack hydroxyproline. This restriction of freedom of the molecules would prevent molecular gyration and therefore promote thermal stability. This suggests that factors such as mechanical or tensile over-load can disrupt this structure rendering it more susceptible to denaturation and proteolysis. In an experimental model of tendon overload, it has been shown that the enthalpy of denaturation was unchanged while the temperature of denaturation changed (Willett *et al.*, 2008). Although these results are in contrast to Miles *et al.* (1994) and the mitral valve results, where the temperature characteristics remained the same, there is the interesting point of mechanical impact as a possible contributor to MMVD. The leaflets undergo a continuous load during a complete lifespan and this tensile over-load might play a role in disruption of fibrillous collagen from its original ordered structure (especially in older age) resulting in more configurational entropy. However, whether this tensile stress can also change the temperature of denaturation through disruption of the fibrillar lattice needs further investigation.

Chapter 6

Neutron scattering and collagen cross-links in MMVD

Neutron scattering

Neutron scattering has a use in tissue imaging and can elucidate in great detail the structure of biological systems. Neutrons are the subatomic particles first discovered by the English physicist James Chadwick in 1932. The unique property of the neutrons is that they (unlike electrons or protons) do not carrying any electrical charge. Neutrons posses a slightly higher mass than protons i.e. 1.008 amu (atomic mass units) based on the C12 scale or 1.675×10^{-27} Kg. Neutrons also have a large magnetic dipole moment. The overall charge of neutron is a zero but the distribution of the charge is not uniform and, if the electric charge in one end happens to be greater than the other side, then a neutron is said to have an electric dipole moment (EDM). The half life of a neutron (when they are not in a given stable nucleus) is 886 ± 2 seconds, after which it decays to a proton; an electron and an antineutrino. Neutrons display behaviour characteristic of both light and particles. It was Lewis de Broglie who combined the wave-particle duality of neutrons via combining Einstein and Planck equation to a new equation:

$$\lambda=h/mv \qquad (6.1)$$

Where h is Planck's constant, λ is the wavelength, m is the particle mass and v is the velocity. As h and m are fixed, one can see that changing the velocity also changes the wavelengths (Dobrzynski and Blinowski, 1994).

Being forms of electromagnetic radiation, light scattering and x-ray diffraction both are based on their wave properties. Neutron scattering, however, is based on particle

scattering. Neutrons interact with the nucleus of the atoms rather than electron clouds. Consequently, there is a relationship between atomic number and an atom's ability to scatter neutrons, a property called the neutron scattering length (see below). Neutron scattering length can show large variations among the different isotopes of a single element. This makes neutrons a very useful tool for studying isotopes. This effect has wide application, especially for distinguishing between the isotopes of hydrogen. The scattering lengths of hydrogen and deuterium have opposite signs, namely -0.374 and 0.667 m. Furthermore, through their magnetic dipole characteristic they interact with unpaired spins (one electron occupying one orbital) of a molecule.

There are 4 possible outcomes when a neutron interacts with a nucleus, namely: scattering, transmutation, fission and radiative capture. The type of the scattering is mostly depended on the incident wave frequency to that of scattered one. They are the same in coherent neutron scattering. If, however, there is a frequency change during the scattering process, then it is classified as either elastic or inelastic scattering. In elastic scattering, a neutron collides with the nucleus and bounces off without any change in energy. In inelastic scattering, the collided neutron is temporarily absorbed by the nucleus forming a transient compound before emitting another neutron with lower energy together with a gamma particle which accounts for the rest of the energy. Alternatively if there is small change in the amount of energy combined with a frequency shift, the scattering would be quasielastic (Friedli, 1996). Therefore, there are 6 types of neutron scattering: coherently elastic scattering, incoherently elastic scattering, coherently inelastic scattering,

incoherently inelastic scattering, coherently quasielastic scattering and incoherently quasielastic scattering.

There are two important factors which determine the strength of the scattering from an atomic nucleus: scattering length and scattering cross-section. The scattering length (*b*) has the dimension of length and is the ability of a single atom to scatter a neutron. It is a real and constant value for a given atom or an isotope. The neutron scattering cross section of a system is defined by its ability to scatter neutrons, in other words it is an effective area which the target nucleus presents to an incident beam. The neutron scattering cross-section has the dimension of area and is measured in barns (1 barn = 10^{-28} square metre) and mathematically is defined as:

$$\sigma = 1/\Psi \qquad (6.2)$$

where $$\Psi = \frac{number\ \ of\ \ neutrons\ \ impinging\ \ on\ a\ \ surface\ per\ \text{second}}{surface\ \ area\ \ perpendicular\ to\ \ the\ neutron\ beam\ \ direction}$$

Additionally, the relationship between the cross section and scattering length is defined as $\sigma = 4\pi b^2$ (6.3)

Taking into account the above equations results in several important conclusions. By combining the kinetic energy of neutrons (as they have a finite mass) with the Broglie equation, one can deduce that an x-ray photon at the given wavelength has about 200,000 times more the energy than a neutron at the same wavelength. Deposition of this much x-ray energy in sensitive biological samples causes radiation

damage, leading to molecular degradation of the samples. On the other hand, having a small neutron cross-section means that if neutrons hit this area, they would scatter isotropically (equal probability in any directions). This happens as the area of nucleus compared to neutron wavelength is very small and the nucleus acts as a "point of scatter". In case of x-rays, however, they interact with electron clouds which are comparable in size to the incident beam. Consequently, the scattered beam is not isotropic. Furthermore, the interaction and absorption of neutrons by most materials are weak, and this characteristic makes neutron beams much more penetrating than x-rays.

Aim

The cross-links of collagen provide tensile strength and structural stability to collagen molecules and connective tissues. The majority of cross-links in collagen arise from an enzymatic pathway mediated by lysyl oxidase. They are first produced as immature cross-links before transformation into mature cross-links. It has been shown that any abnormality in cross-links can affect functional properties of collagen molecules. The pathways of cross-links production and their significance in disease and health states have been detailed in Chapter 1. The purpose of this neutron scattering study was to investigate whether MMVD could affect immature cross-links. The result could give an insight into the pathogenesis of the disease and could also be interpreted in relation to the integrity of lysyl oxidase pathway and mature cross-links.

Neutrons can be produced in two different ways, namely fission (in research reactors) and spallation (in accelerator-driven spallation neutron sources). In the research reactors, neutrons are produced as the result of chain reactions caused by bombarding heavy atoms such as uranium or plutonium. The heavy atoms then break up into some nuclear fragments, produce energy and emit neutrons. These neutrons are then responsible for self-sustained reactions. Thus, the reactor is a continuous source of neutrons. After moderation (see below) a neutron beam should be converted to a monochromatic beam. This is performed by applying Bragg's Law ($n\lambda = 2d \sin\theta$) to a single crystal which is often made of pyrolytic graphite, germanium or copper. Although the beam has many wave-lengths, spacing between the layers (2d) and scattering angle (2θ) are chosen in a way that only neutrons that satisfy Bragg's Law are directed towards the sample. One example of such reactors is the High Flux Reactor at the Institut Laue-Langevin in Grenoble (France). This reactor was used in the current study. In the spallation method, high energy photons, produced in an accelerator, hit heavy metal targets like uranium or tungsten separating the neutrons. The neutrons from a spallation source are not in continuous flux, but are emitted in pulses. However, spallation produces 20-30 neutrons per photon while in reactors only one neutron is produced per single fission reaction. Primary neutrons produced by either of the two methods are called thermal neutrons and are literally "too hot to handle". If they were used for scattering measurements, they would disturb the atomic positions of the sample materials. Moderation is a process in which the thermal neutrons are directed towards a moderator such as beryllium or graphite. Possessing a large neutron cross-section, these materials cause

thermal neutrons to undergo several inelastic collisions, thereby producing slow and cold neutrons with energy between 0.1 and 10 meV suitable for investigational purposes (Dilip, 2004; Harroun *et al.*, 2006).

The instrument D22 (Figure 6.1), at the Institut Laue-Langevin (Grenoble, France), was used to collect small angle scattering data with 7 Å wavelength neutrons. Using this instrument a well-established technique called isomorphous replacement was applied, which involves replacing hydrogen atoms in the sample molecules with the stronger-scattering deuterium. The ability of sodium borohydride ($NaBH_4$) to react and reduce the keto-amine and Schiff base groups of mostly aldehyde-based cross-links has been reported previously (Robins and Bailey, 1977). The introduction of deuterons into an ordered structure will alter the neutron scattering density profile and therefore its diffraction pattern. Therefore, sodium borodeuteride (NaB^2H_4, 98% atom of deuterium) was used to target the reducible cross-links specifically, using the method of Wess *et al.* (1993). The reducing solution was made by dissolving 70 mg of sodium borodeuteride in 5 ml phosphate buffered saline (PBS) at pH 7.5. Each fresh sample (approx 1 g in weight) was immersed separately for 20 minutes followed by washing with phosphate-buffered saline at pH 7.4 to stop the reaction.

The 96 x 96 cm detector was placed at two positions, 2.5 and 11.2 metres, to collect data spanning the range from the 1^{st} to the 7^{th} order of meridional diffraction. Neutron scattering data were collected from each mitral valve leaflet sample at each detector position, and then the same samples were treated with sodium borodeuteride and re-measured. Due to constraints on the allocated instrument time, it was only possible to run one unaffected and one diseased (grade I and II) sample obtained from two

different mitral valve leaflets and one dog tail tendon (Table 6.1). An empty cell and detector-calibration (water cell) measurements were also performed, for use in correcting and analysing the data.

Breed	Age	Sex
German shepherd	10 years old	Male
Jack Russell	8 years old	Male

Table 6.1: The details of the dogs used for neutron diffraction experiment.

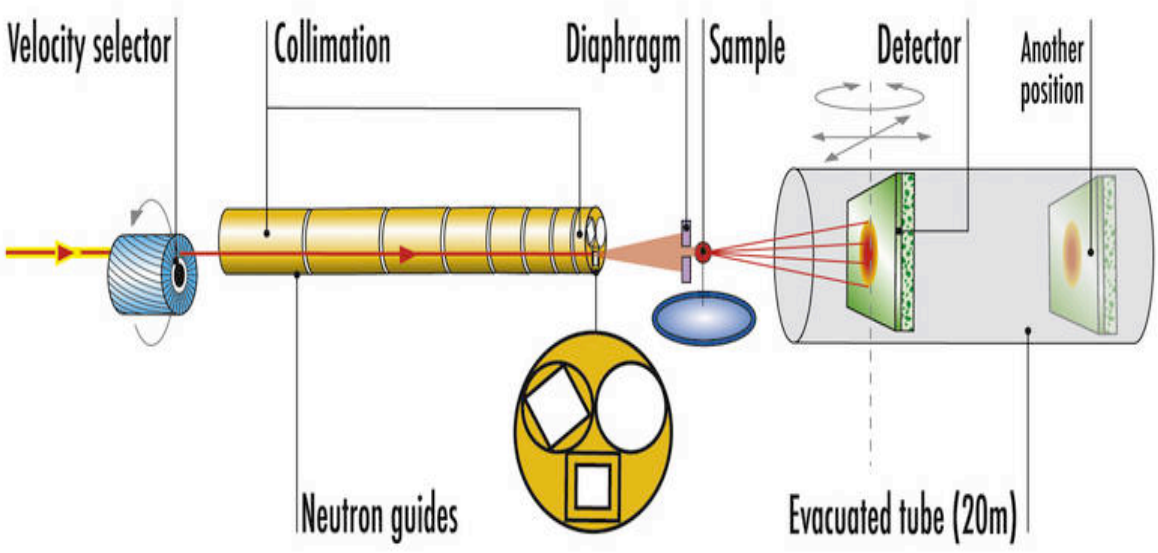

Figure 6.1: The layout of D22 instrument at ILL. The incoming neutrons are monochromized by a mechanical velocity selector and the beam is collimated using collimators and neutron guides before they hit the sample. The detector is inside an evacuated tube and its distance from the sample can be adjusted accordingly (diagram courtesy of ILL official website).

The *LAMP* program (Large Array Manipulation Program, ILL) was used to normalize the data to water with all corrections (transmissions and background) carried out on radially-averaged data. Diffraction spectra were obtained by sector summation and ratios of diffracted intensity were calculated for each of the seven orders of meridional diffraction by dividing the diffracted intensity of treated tissue by the corresponding intensity of untreated tissue. The data sets have been scaled to give a first order ratio of 1.0. For comparison corresponding data from an earlier study of rat tail tendon, by Wess and co-workers (1990), was analysed in the same way.

Results

Table 6.2 shows the effect of NaB^2H_4 treatment on the three different types of tissue. The results are expressed as ratios of Bragg peak intensity, before and after reduction of the cross-links. There were clear differences in the pattern of altered intensities between tail tendon and healthy heart valve. The intensity changes are larger in tail tendon, suggesting that all mitral leaflets, irrespective of their pathological status (healthy or diseased), have only a small number of reducible cross-links. However, there are also clear differences between the systematic changes of healthy and diseased valves, with the pattern of diseased valves lying closer to that of the dog tendon implying an increase in the amount of reducible cross-links in the leaflets affected by MMVD.

Diffraction order	Dog tail tendon	Healthy leaflet	Diseased leaflet	Rat tail tendon
1	1.00	1.00	1.00	1.00
2	1.05	0.94	0.94	0.90
3	0.95	0.91	0.93	0.93
4	1.14	0.96	0.99	0.80
5	1.22	1.01	1.01	1.15
6	1.27	1.01	1.03	1.37

Table 6.2: The effect of sodium borodeuteride treatment on the meridional diffraction pattern of collagen from dog tail tendon, normal dog mitral valves leaflet and valve leaflet from dog affected by MMVD: The data were calculated by dividing the diffracted intensity of treated tissue by the corresponding intensity of untreated tissue. The data sets have been scaled to give a first order ratio of 1.0. Also shown are corresponding ratios from rat tail tendon, calculated from Wess *et al*., (1993).

Discussion

In previous reports, the study of deuterated tendon using neutron diffraction for collagen molecule has provided reliable results (Wess *et al*., 1990; Wess *et al*., 1996). The neutron diffraction data from dog tail shows systematic changes that are comparable to those of reported by Wess *et al.* (1990 & 1993), indicating the presence of a high number of reducible cross-links in the tail tendon. There is a marked difference in the number of reducible cross-links between tail tendon and valve leaflets, irrespective of the pathological status of the valves. However, according to the same sets of neutron data there are more reducible cross-links in the diseased leaflets than in the healthy leaflets. As mentioned before, the cross-links are formed enzymatically through the intermolecular reactions of aldehyde residues catalyzed by lysyl oxidase. Initially, there are two pathways based on the precursor, namely lysine aldehyde and hydroxylysine aldehyde. The latter is the predominant

form in most connective tissues. Both of these pathways lead to the production of cross-links which are primary borohydride-reducible giving the opportunity to investigate them by neutron diffraction, in a non-destructively and highly sensitivity manner. However, as the tissues mature these reducible cross-links tend to transform to mature and non-reducible cross-links.

Although the qualitative state of this approach and low number of sample pose a limiting factor, the observed changes in the qualitative state of reducible cross-links have a number of implications. It is known that MMVD in the dog and human is an age associated condition. Studies of other systems have shown that, with advancing age, the activity of lysyl oxidase decreases. This indicates that collagen from older patients will tend to have fewer cross-links than those found in younger patients (Eyre *et al*., 1988). Other studies have shown that the increased deposition of proteoglycans (PGs), which is a proven histopathological aspect of MMVD, might interfere with the formation of cross-links (Scott and Orford, 1981). Accumulation of advanced glycation end products (AGEs) which are non-enzymatic cross-links, derived from prolonged exposure of proteins to reducing sugars, has been also reported to have detrimental effects on mechanical properties of a tissue and might also interfere with the formation of enzymatic cross-links. Increasing importance is being given to the role of AGEs in the process of aging and has been discussed earlier (Haus *et al.*, 2007; Shiraki *et al.,* 2008). Another interesting finding comes from the studies done by Akeson *et al.* (1977) and Harwood and Amiel (1992) in which they reported increased reducible collagen cross-links in periarticular collagen of rabbits after some weeks of immobilization. They have described it as a secondary

increase due to the lack of stress and motion. Although in some tissues motion and tonic neuronal input is essential for the remodelling of the connective tissue and collagen, which otherwise would result in atrophy, these studies have not explained clearly how the reducible cross-links can increase while a given organ and its surrounding connective tissue is immobilised.

Nevertheless, in the neutron diffraction study, the increase in reducible cross-links can be explained in a different way, namely collagen depletion and an altered population of collagen-secreting cells (Rabkin *et al*., 2001; Black *et al*., 2005, Disatian *et al*., Han *et al*., 2008). Collagen depletion had been observed before and has been quantified by the current study (Chapter 4). In terms of cell population, the transition from quiescent fibroblasts to activated myofibroblasts, and finally to smooth muscle-like cell phonotype, has been documented for myxomatous mitral valves (Rabkin et al., 2001; Black *et al*., 2005). On the other hand, the presence of reducible cross-links is an indicator of collagen synthesis and shows that the integrity of the pathways for formation of the cross-links is almost intact. This suggests that the products of recently-activated myofibroblasts or smooth muscle-like cells are likely to be young and immature collagen molecules. As turn-over increases there would not be enough time for the transformation of immature reducible cross-links into mature ones. Consequently, with more reducible cross-links, the mitral leaflets will be rendered less strong. One of the roles of the cross-links in mitral valve collagen would be to provide enough tensile strength in order to withstand pressure of ventricular systole. It is known that prolapse (bulging) of affected leaflets towards the atrium during the systole, which is one of the manifestations of MMVD in dogs

and MVP in humans (Pederson, 2000; Hayek *et al*., 2005, Hyun, 2005), can be caused by hyper-extensibility of affected leaflets. All in all although reducible immature cross-links lack the properties of mature cross-links, their synthesis is an important step towards the formation of the mature cross-links and as discussed earlier their study can deepen our knowledge regarding collagen fibrils.

Chapter 7

High performance liquid chromatography (HPLC) for the measurement of mature collagen cross-links in MMVD

High performance liquid chromatography

High performance liquid chromatography is a separation technique in which solutes migrate through a column or are held back in a stationary phase at rates that depend upon their distribution ratios. The distribution ratio or D is determined by the relative affinity of solutes for the two phases and is described as the ratio of total solute concentration (C_S) in the stationary phase to that of it in the mobile phase (C_M):

$$D = C_S / C_M \qquad (7.1)$$

Therefore, the larger the D value, the longer the migration time we would expect and vice versa. As the interaction of the solutes with the stationary phase slows down the migration of the solutes, the process is called **retention** or **retardation**. Column separation describes the time that solutes take to pass through the column, while retention time (t_R) and retention factor (K) are directly proportional to D. The equation for this is:

$$t_R = t_M (1+K) \qquad (7.2)$$

In the above equation t_M is known as the dead time and is the time required by non-retained solutes to go through the column. These non-retained solutes migrate at the same velocity as the mobile phase, so their K value is zero, leading to $t_R = t_M$. Solutes with values of K and D are greater than zero are often retarded proportionately in the column. To keep the retention time in an acceptable range in chromatographic conditions, the K values should be less than 20. The elution order is

dependent on the chemical nature of the solutes and the overall polarity of the two phases (Kealey and Haines, 2002). Moreover, size of the particles and pore size of the column, and type of the material in the stationary phase are essential determinants for the efficient elution of the solutes. The solutes eluted from the end of the column pass through a detector (often of ultraviolet light or fluorescence) so that a sequence of peaks, differing in absorption or intensity, can be detected and identified. There are several modes of HPLC which are mostly classified according to the type of stationary phase and the sorption mechanism. Sorption is a process in which solutes are transferred from mobile phases into the stationary phase. Desorption is the reverse process. In this scheme, almost 90% of all HPLC modes can be classified into the following groups:

Adsorption chromatography, in which the stationary phase is adsorbent and separation is based on differing degrees of adsorption and desorption.

Ion-exchange chromatography, the stationary phase is an ionically charged material with a charge that is opposite to that of the sample.

Size-exclusion chromatography, the stationary phase comprises precisely controlled microparticles, and separation is based simply on molecular weights.

Normal phase chromatography, the stationary phase is made of strongly polar material and the mobile phases are non-polar such as n-hexane or tetrahydrofuran.

Reverse phase chromatography, the stationary phase is a non-polar material; and the mobile phase is polar liquid such as methanol, acetonitrile, water or a mixture of them.

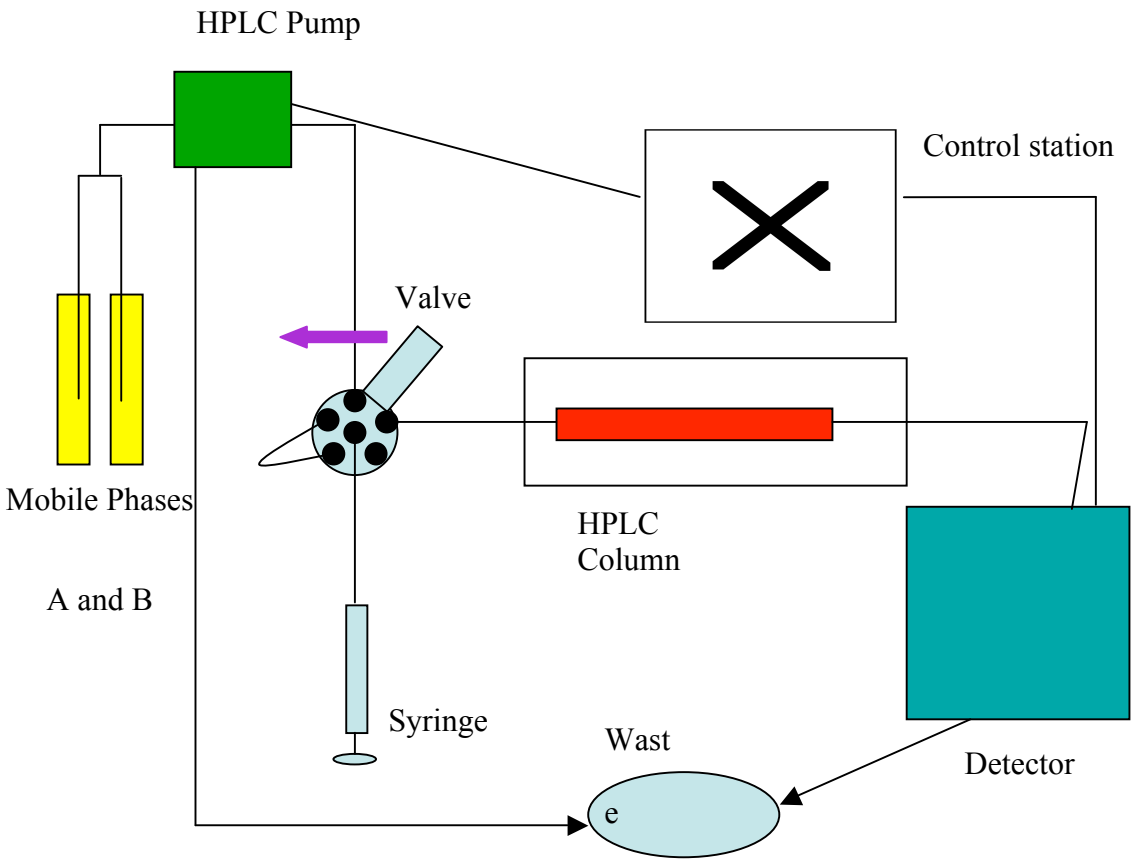

Figure 7.1: A simplified diagram depicting the main parts of a typical HPLC set-up. The pump provides a steady high pressure with no pulsation, and can be programmed to vary the composition of the mobile phase during the course of the separation. While mobile phases are running, sample is injected into the loop and upon turning the valve it will be included in the circuit directed towards the column. The detector will monitor the mobile phases while it emerges from the column and will respond to the physical properties of the solutes which are not exhibited by the pure mobile phase (in this case UV absorbance). After passing through the detector the mobile phase is directed to the waste container.

Aim

In Chapter 6, immature cross-links were studied qualitatively. However, due to the nature of neutron scattering experiment, measurement of the mature cross-links was not feasible. So evaluation of the cross-linked state of collagen in MMVD was not complete because it only studied immature cross-links. In a fully developed tissue, most of the attributes of cross-links results from mature type (see Chapter 1). The following study was designed to investigate quantitatively the state of mature cross-links in MMVD using reverse phase HPLC.

Materials and methods

In the current study, reverse phase chromatography was used, with the following materials and instruments: acetonitrile (HPLC gradient grade), methanol (chromasolve), sodium dihydrogen orthophosphate (NaH_2PO_4), boric acid and *o*-phthalaldehyde (OPA-complete solution) (Sigma-Aldrich, UK). Sample mature cross-links standard, pyridinoline (PYD) and deoxypyridinoline (DPD) were kindly supplied by the Rowett Research Institute (Aberdeen, UK). A standard single amino acids collection was from VWR International (UK). The conditions used for chromatography were generally in accordance with the Bartolomeo and Maisano methods (2006). Chromatography was performed on a Pharmacia LKB.VWM 2141 HPLC system at room temperature using *Phenomenex Luna* 5μm C18 (2), reverse phase column (150 × 4.6 mm) with UV detection at λ=338 nm. Mobile phases were NaH_2PO_4 40 mM adjusted to pH 7.8 with 2 M NaOH (buffer A) and acetonitrile/methanol/water (45/45/10) (buffer B), and the below gradient was followed for the runs at 2 mL/min.

Time (min)	% B
0	0
1.9	0
16.3	100
16.4	100
20	100
21	0
26	0
30	0

Table 7.1: Gradient used in HPLC experiments. Mobile phases were NaH_2PO_4 40 mM adjusted to pH 7.8 with 2 M NaOH (buffer A) and acetonitrile/methanol/water (45/45/10) (buffer B).

Sample injection

The samples were injected via an external sample loop directly into the pressurised flowing mobile phase just ahead of the column, using a round tip Hamilton micro-syringe pipette. The loop was filled with the sample while the mobile phase flowed directly to the column. By turning the handle of the loop's valve, the mobile phase was diverted into the loop, injecting the sample into the column without any flow stoppage (Figure7.2). The valve injection was computer automated, so the chromatogram recording started as soon as the injections had been completed.

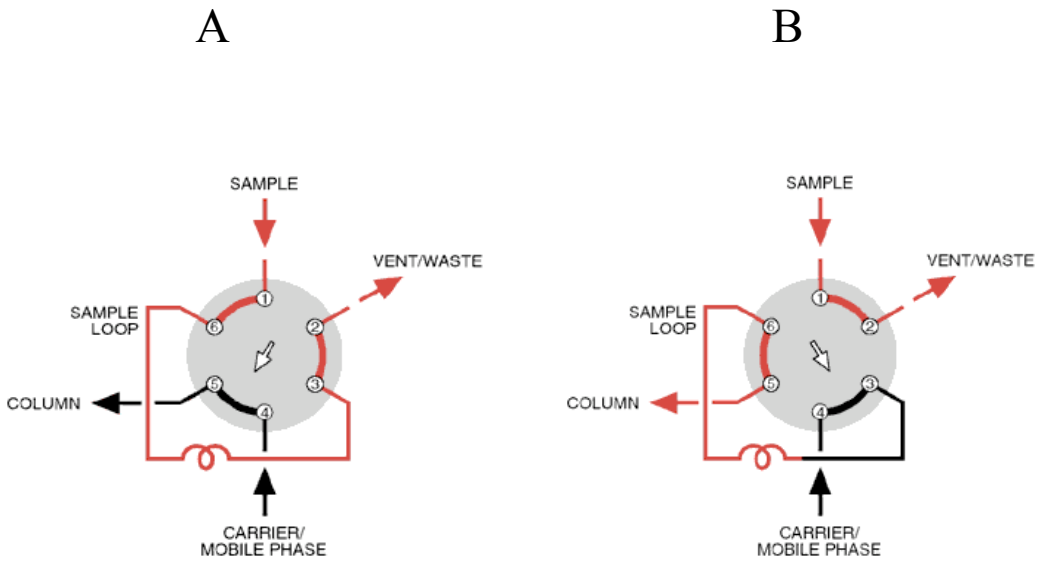

Figure 7.2: Sample injection valve and loop. Sample loading position (a); sample injection position (b) (diagrams courtesy of Valco Instruments Co.).

Pre-column derivatisation

The separation and quantification of amino acids, or their derivatives can provide an invaluable insight into the structure and characteristic of proteins. Often, there is only a very low concentration of the target substance in a given sample. Most amino acids and their derivatives also lack chromophores and fluorophores. These amino acids must therefore be quantified in the presence of other substances which might interfere with their detection. Considering this there has always been a high demand for a chromatography system which possessed high sensitivity and specificity. The introduction of ion-exchange chromatography, followed by the post-column derivatisation seemed to have resolved these problems. However, ion-exchange chromatography is of low resolution and requires a longer run time. Furthermore, post column derivatisation not only increases the time, but the addition of an extra pump in the post column system adds to the complexity of the system. Additionally, reactions of background contaminants contribute to an increase in baseline noise. The development of the pre-column derivatisation offers a technique with better sensitivities and shorter analysis times.

The two major approaches for pre-column derivatisation of amino acids use dansyl chloride and *o*-phthalaldehyde (OPA). Dansyl chloride (1-dimethylaminonaphtalene-5-sulphonyl chloride) is very useful for determining the N-terminal of the residues and the derivative is highly fluorescent and also stable to acid hydrolysis (Jones, 1986).The reaction of OPA with primary amines is the result of the formation of an OPA2/2-mercaptoethanol adduct which then reacts with a primary amine of the amino acid to form a highly fluorescent and UV absorbent thio-substitute isoindole.

However, some amino acids cannot be detected by OPA. Proline possesses a secondary amine group and is unable to react with OPA, and cysteine also has a low response (Jarret *et al*., 1986). Otherwise, the reaction is rapid and proceeds at room temperature as shown in Figure 7.3:

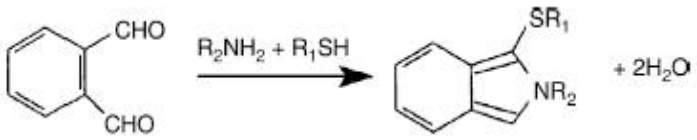

Figure 7.3: The reaction of *o*-phthalaldehyde complete solution (with 2-mercaptoethanol) with a primary amine on a peptide.

To establish the least required and appropriate concentration ratio of OPA with the given sample in terms of standard amino acids and standard mature cross-links, a total of about 100 runs of HPLC were performed. The following approach proved to be optimal. The best results for single primary amino acids required thoroughly mixing 7.5 nM of OPA with 1nM of the amino acid in 0.4 M borate (pH = 10.4) and 0.1 M sodium acetate (pH = 7.2) and incubation for one minute at room temperature before injection.

There are no reports of derivatisation and detection of standard mature cross-links under UV as these compounds are naturally fluorescent and are often detected by HPLC fluorescence. However, their chemical structures contain three primary amine groups and therefore they should be capable of reacting with OPA (Figure 7.4).

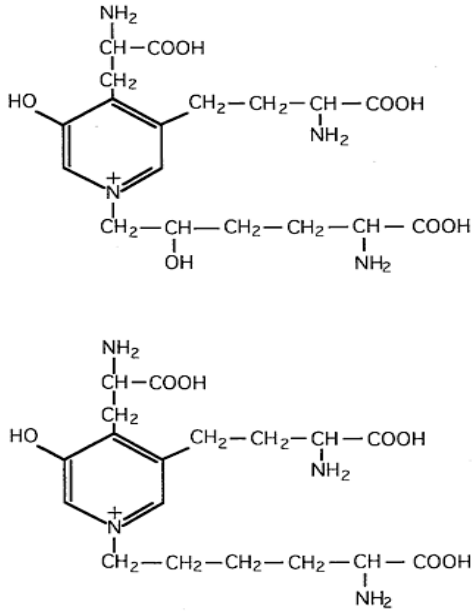

Figure 7.4: Mature cross-links of collagen, top pyridinoline and below deoxypyridinoline with three primary amines.

A series of runs revealed that at the ratio of 37.5 nM of OPA to 1.0 nM of DPD or PYD, there was an optimum reaction. The increased amount of OPA might be explained by the fact that the molecules of the cross-links contain three primary amine groups. Nonetheless, this increase is not proportional when it is compared with molar concentration of OPA used for determining standard profile single amino acids.

Collagen extraction

Rat tails were frozen immediately after removal from donor rats. During the processing, each sample was placed in a Petri dish containing 70% ethanol for 20 minutes. The tip of the tail was cut crosswise with scissors. The skin was pulled back about 0.5 cm to expose the tendons and then each tendon was pulled out with blunt tip forceps. After that, samples were washed with PBS buffer and cut into small pieces (approximately 5 × 5 mm). In the case of the mitral valves, freshly frozen mitral valves were left to thaw at room temperature and then the same procedure was repeated, with the only difference being that, after cutting them into the pieces, they were homogenised. Tissue was selected from visually diseased and normal areas within each valve towards the free edge. Collagen was isolated from the rat tail tendons and mitral leaflet samples according to O'Leary *et al.* (2004), by dissolving in 0.017 M acetic acid at 4 g/L. The solution was gently agitated by stirring for 48 hours at 4°C. In order to purify the collagen solution, they were centrifuged at high speed (10000 × g) at 4°C for one hour in a fixed angle rotor (JA-20; Beckman Coulter) using a Beckman Coulter high-speed centrifuge (Collier *et al*., 2006). Supernatants were separated and dried using lyophilizer at -40 °C for 12 hours. They were weighed into 5mg groups and were hydrolysed in 200 µL of 6 N HCl under vacuum for 12 hours. The hydrolysates were dried and resuspended in 700 µL 1mM HCl and centrifuged at 15000 rpm for 15 minutes. Supernatants were filtered and used for HPLC purposes. In total four diseased and four healthy collagen samples obtained from two dogs with mxomatous mitral valve (grade I-II) were prepared in duplicates. The same number of runs was performed with collagen obtained from rat tail tendon.

Breed	Age	Sex
Yorkshire Terrier	9 years old	Male
Mixed Setter	8 years old	------

Table 7.2: The details of dogs used in HPLC experiment.

Results

A series of different runs was completed using various concentrations of standard mature cross-links in order to characterise the exact appearance of the related peaks in the chromatogram and to produce a standard graph. Figure 7.5 shows a typical chromatogram of mature cross-links. As the figure shows, pyridinoline and deoxypyridinoline appeared at 12 and 12.4 minutes, respectively. Taking into account the pattern of chromatogram of amino acids, another series of HPLC runs was conducted using standard amino acids in order to calibrate the machine and also to see whether there would be any possible peak interference with those of standard mature cross links (Figure 7.6). HPLC was also run for the samples (diseased and healthy leaflets and rat tail) (Figure 7.7). From this figure (7.7) it is apparent that in all sample-runs (in the rat tail and mitral valve collagen samples, irrespective of their disease status) only one type of mature cross-link, namely pyridinoline, was detectable. The analytical areas for the respective peaks were determined and the amount of pyridinoline cross-links was calculated in picomoles (Figure 7.8). Statistical analysis was carried out using Kruskal-Wallis for analysis of variance. It showed a statistically significant difference in pyridinoline content between the three

groups with 25% reduction of pyridinoline content in the affected areas comparing to the healthy ones ($P \leq 0.05$).

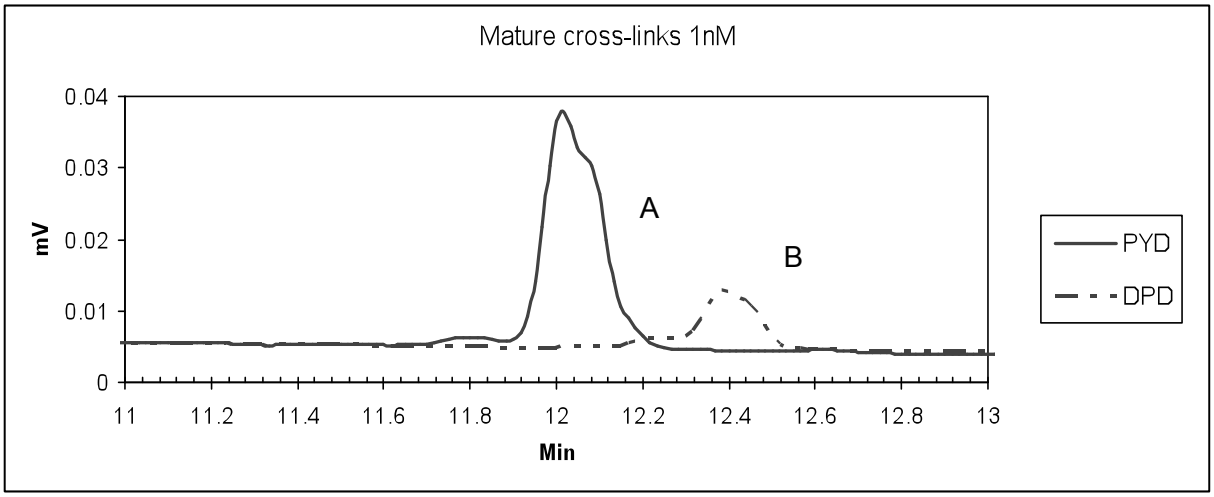

Figure 7:5: Chromatogram of mature standard cross-links at 1 nM concentration each. Pyridinoline (A) and Deoxypyridinoline (B).

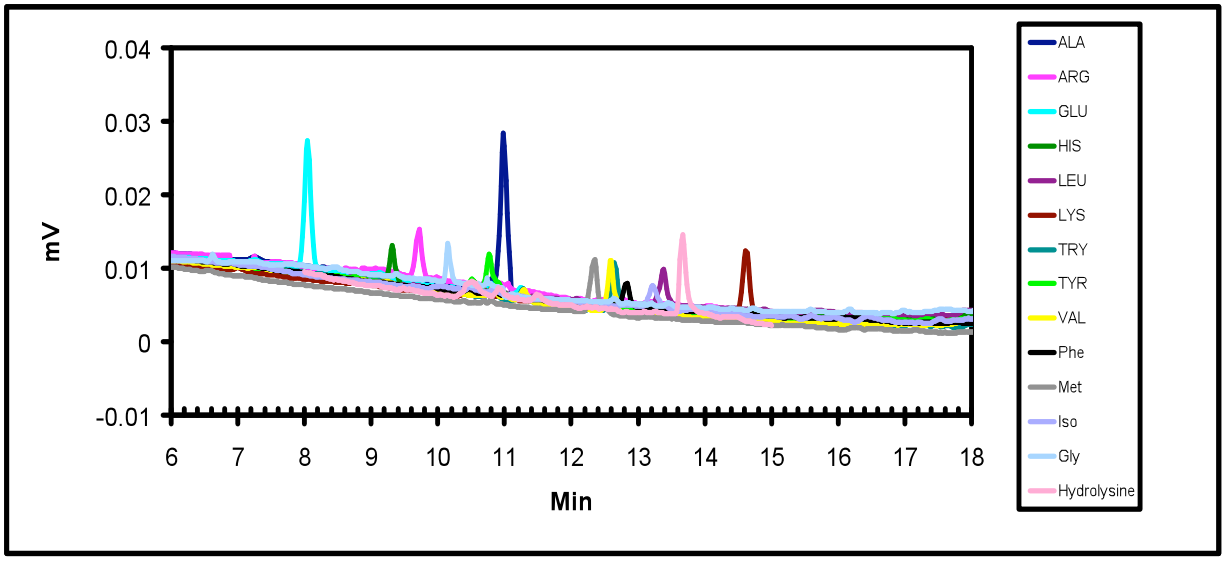

Figure 7.6: The chromatogram of some standard amino acids at the concentration of 1nM.

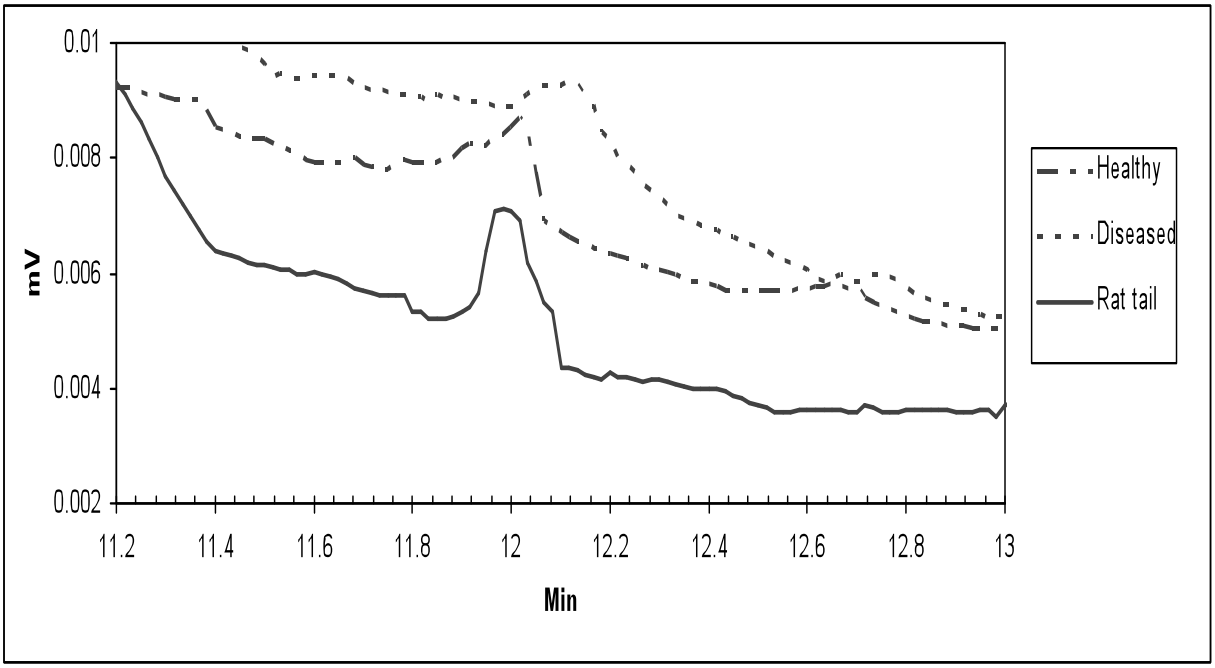

Figure 7.7: A chromatogram of mature pyridinoline cross-links of (from top to bottom) diseased leaflet, healthy leaflet and rat tail.

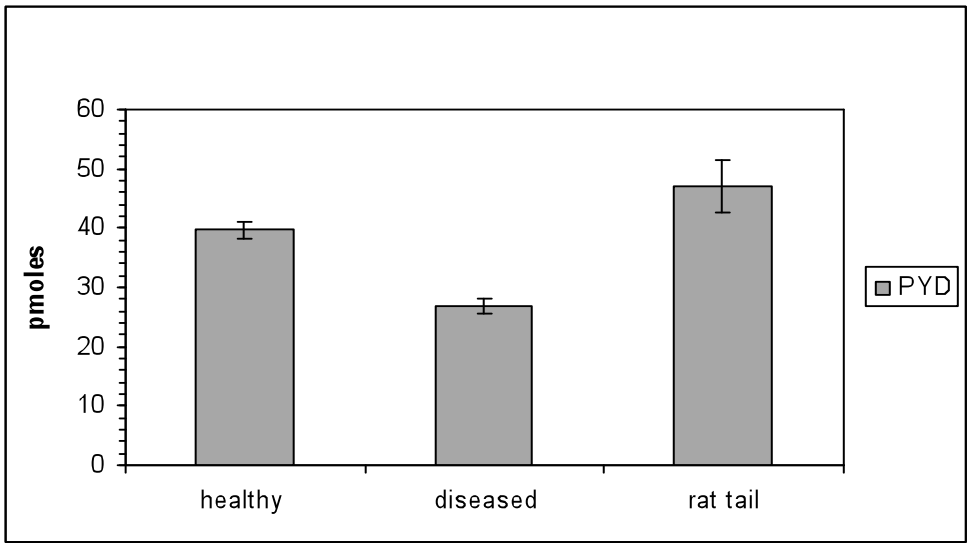

Figure 7.8: The amount of the pyridinoline cross-links in 20 µg of collagen sample. The error-bars are derived from standard deviation and for healthy, diseased and rat tail are 1.53, 1.16 and 4.37, respectively.

Discussion

The study of the reducible cross-links using the neutron diffraction has a very high sensitivity compared to other methods, such as chemical and chromatographic ones. However, it lacks the capacity to provide quantitative data about the cross-links. The study and quantification of collagen cross-links dates back to decades when Verzar (1964) reported a form of binding among collagen fibrils without knowing the exact nature of this binding. Reducible cross-links were then quantified and isolated by chemical reduction with radioactive sodium bromide (Baily and Lister, 1968) and Bailey and Shimokomaki (1971) compared the amount of reducible cross-links in different tissues of rat, bovine and human highlighting the issue of temporal age and physiological maturation of tissues. We now know that reducible cross-links are

intermediate compounds that are substituted with mature collagen cross-links as the tissue matures. Quantification of mature collagen cross-links is a good marker to assess the current status of collagen in a given tissue. They are almost trivalent (or sometimes tetravalent) with more than one amino acid side chain. Mature residues of the hydroxyallysine pathway (see Chapter one) are deoxypyridinoline and pyridinoline. Both compounds are naturally fluorescent (Saito *et al*., 1997) and are widely distributed in different tissues. However, deoxypyridinoline is found exclusively in bone and dentin, while pyridinoline is found in other tissues such as tendons, cartilage, and skin (Rosen, 1996). Pyridinoline can also found in the bone, where the ratio of pyridinoline to that of deoxypyridinoline is approximately 2:3. During collagen turn-over and remodelling, mature collagen cross-links are released into the blood circulation and excreted in the urine. Considering the high turn-over of bone in the healthy animal, almost all of these circulating mature cross-links are considered to originate from bone (Gerrits *et al*., 1995). Consequently, circulating mature cross-links can be used as a diagnostic or prognostic tool in various connective tissue disorders such as bone metastasis and fibromyalgia (Fontana and Delmas, 2000; Ribel-Madsen *et al.,* 2007). However, considering the total mass of the mitral valve leaflets, it is unlikely that the changes in the mitral valve leaflets would be reflected by changes in circulating mature cross-links, except when mitral valve alteration forms part of a generalised disease, such as Marfan syndrome.

As mentioned earlier these mature cross-links are naturally fluorescent and several chromatographic methods have been used for their detection, using a fluorescent detector. Saito *et al*. (1997) used cation-exchange column HPLC to measure the both

the reducible and mature cross-links in human articular cartilage, skin and the diaphysial femur. They applied the postcolumn derivatisation technique using *o*-phthalaldehyde to measure the reducible cross-links, as these cross-links are not naturally fluorescent. They quantified mature pyridinoline and deoxypyridinoline on the basis of their natural fluorescent characteristic. Reversed phase HPLC has also been used by Chen *et al.* (2000) to study pyridinoline and deoxypyridinoline in human yellow ligament. To our knowledge, there are no reports of the use of pre column reversed phase HPLC combined with a UV detector to detect pyridinoline and deoxypyridinoline. Derivatisation, using *o*-phthalaldehyde, was successfully applied and pyridinoline and deoxypyridinoline were detected in the standard solutions. The same procedure was used in the samples and, as the results show, in the leaflets and the rat tail tendon there was only one type of mature cross-links was detected, namely pyridinoline. This finding is in agreement with the fact that while there are two mature cross-links derived from the hydroxyallysine pathway, deoxypyridinoline is almost exclusive to bone connective tissues (Rosen, 1996).

Comparing the quantity of pyridinoline in the different groups clearly shows that rat tail has a considerably high amount of pyridinoline content than mitral valve leaflets. The difference may be explained by the collagen type. Rat tail tendon is almost exclusively made of type I collagen, which is necessary for the toughness and strength of the tail tendon. However, mitral leaflets in dogs might contain different types of the collagen molecules. This has been indeed shown in human mitral valves where normal human leaflets contain approximately 74% of type I, 24% of type III and 2% of type V. Even in diseased human valves, this changes to 67%, 31% and 2%

respectively (James *et al*., 1991). The current study has shown that there is a statistically significant decrease in the amount of pyridinoline in diseased valves compared to normal valves. This decrease may be related to a possible change in the ratio of collagen types in the normal and affected leaflets of dogs (see above). Therefore, the proportion of different collagen types in the dog mitral valve needs to be clarified with further studies. However, it is reasonable to argue that without alteration of the ratio of collagen types, in the dog valve the decrease in pyridinoline reflects a reduction in the synthesis of mature cross-links associated with disease.

A further explanation of this finding might be that, since, pyridinoline and other mature cross-links are the result of transformation of immature cross-links as the tissue matures, the neutron diffraction results in the current study reflect higher reducible immature cross-links. Therefore, one may explain the decrease in mature cross-links in the context of increased immature cross-links. It has also been shown during the remodelling of connective tissue in the granulation stage of wound healing in skin that there is an increase in the production of type III collagen (Haukipuro *et al.*, 1997). After deposition of the collagen strengthening of the tissue continues with the development of mature cross-links. This is also in agreement with other studies which showed that the high degree of collagen turn-over at this stage in skin corresponds with that found in embryonic tissues (Paul *et al*., 1997). So on the one hand, it seems that changing the proportions of the collagen type I and III in the disease state may be a part of a general process of the remodelling of collagen and on the other hand this increase in turn-over and remodelling gives rise to young collagen molecules with the bivalent or immature cross-links. A final consideration is, as the

underlying process of myxomatous degeneration continues there would be no time for complete maturation of the cross-links, as would otherwise happen in a normal tissue.

Chapter 8

Coherent anti-Stokes Raman scattering spectroscopy (CARS) study of canine mitral valve

History of spectroscopy

The science of spectroscopy started with Isaac Newton when he let the sunlight pass though a prism and produced a spectrum. In 1801, the dark lines in the solar spectrum were discovered by the English scientist William Wollaston. It was not until 1814 that Joseph Fraunhofer reproduced the Wollaston work and concluded that the dark lines were the result of the absorption of certain wavelengths. Then, in 1859 a German physicist called "Gusatv Kirchhoff" demonstrated that each pure substance causes a unique light spectrum.

Generally, there are 3 types of spectroscopy used today; emission, absorption and scattering spectroscopy. Absorption spectroscopy, such as infrared or ultraviolet spectroscopy, measures the wavelengths which a given matter absorbs. Fluorescent and laser spectroscopy measure the emitted light. Scattering spectroscopy measures the amount of light that a substance reflects at a given excitation wavelengths (Lambert *et al.*, 2006).

Raman spectroscopy

Raman spectroscopy, which is a type of scattering spectroscopy, takes its name from the Indian scientist Chandrasekhara Venkata Raman. In 1930, he and his colleagues found that, when a certain wavelength passed through a transparent chemical compound, there was a small fraction of beam emitted at a right-angle that possessed a different wavelength.

When an incident light hits a molecule it interacts with the electrons of the molecules causing existing covalent molecules to bend, stretch and rotate. Bonds in the molecule then become polarized, producing dipoles called induced dipole moments (P) which are directly related to the electrical field (E), produced by the incident light. The equation for this effect is:

$P = \chi E$ where χ is electric susceptibility constant (8.1)

During the interaction of a molecule with the incident light or electrical field the dipoles in the bonds oscillate at the same frequency of the incident light and emit wavelengths of almost the same frequency as the incoming beam when they are returning to the ground state. However, each and every bond in any molecule has its own resonant frequency, which is independent of the applied oscillation and excitation caused by the light beam. As molecules have different covalent bonds so they posses multiple and various resonant frequencies which are unique for each substance. These different patterns of resonant frequency are often plotted as intensity of the emitted beam against the energy or frequency of the vibration and are called Raman spectra.

When a molecule is hit by frequencies which equal their resonant frequencies, the dipoles resonate with greater amplitude, resulting in a significant absorption of the energy and the molecule releases a wavelength whose energy is less than the incoming beam. The molecule is then left in a lower energy state, in terms of vibrational energy, which is, however, still above the ground state. This phenomenon is called Stokes shift Raman. On the other hand, the opposite might also occur which

is called anti-Stokes shift Raman. A molecule which is already in a vibrational state releases a wavelength with a higher energy than the wavelength it absorbs (Figure 8.1). The ratio of the higher energy to the lower one can be calculated to give the Raman signal, which can then be compared with reference spectra (Cheng *et al*., 2002; Potma and Xie, 2004; Lambert *et al.*, 2006; Rodriguez *et al.*, 2006). Date was correct and the reference was added.

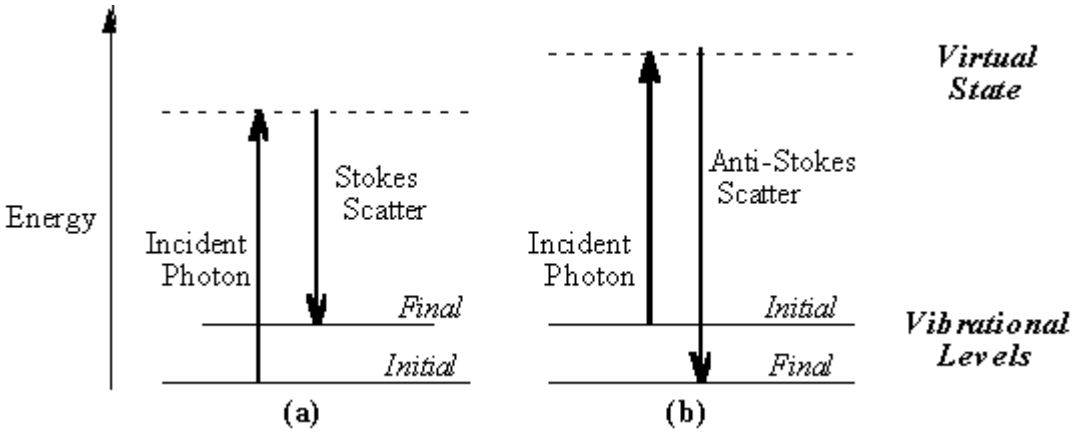

Figure 8.1: Stokes and anti-Stokes phenomena in a given molecule. In Stokes (a) the released photons are in a lower energy state and in anti-Stokes (b) the released photons are in higher energy state. Note that the new state of the energy is called virtual as the energy is immediately lost at this level through scattering.

CARS imaging

Introducing laser beams, with their ability of focusing high intensity beams on very small areas opened a new chapter in Raman spectroscopy. Before this, Raman spectroscopy had relied upon weak spontaneous, incoherent signals. Even with intense laser beams, biological samples were very difficult to measure. Coherent anti-Stokes Raman spectroscopy (CARS) was designed to deal with these problems. CARS is a method of acquiring Raman signals in which a molecule is stimulated until it achieves its vibrational state and then the same molecule is again stimulated to emit an anti-Stokes emission. The final emission (anti-Stokes) is achieved using two different laser frequencies. Higher frequency (pump) and lower frequency (Stokes) are combined together to form a modulated coherent sinusoidal wave with a high frequency beat ($\omega p + \omega s$) and a low frequency beat ($\omega p - \omega s$). When the lower frequency beat equals the vibrational frequency of the bond, the bonds begins to excite resonantly. In the second step, the already excited bond is hit by second higher frequency pump photons, resulting in the emission of an anti-Stokes photon that has a higher energy than the incoming photons. The equation for this anti-Stokes emission can be stated as follows:

$$\omega AS = 2\omega p - \omega s \qquad (8.2)$$

Where ωp is two combined beams and ωs is the wavelength of the Stokes beam and ωAS is the final anti-Stokes emission. Since there are 4 photons involved in the CARS process, namely 2 incoming photons, one Stokes and one anti-Stokes, this process is also called “four mixing process”. CARS imaging is a non-linear process

so the anti-Stokes photons travel in the same direction as the incident beam in a coherent way and are in phase with each other. This imaging approach provides some advantages for visualising biological samples, such as; offering chemical selectivity without the need for labelling; the near-infrared excitation beams scatter little and allow deeper penetration; due to the anti-Stokes effect, CARS signals have shorter wavelengths and higher energy making their detection feasible in the presence of the fluorescent background; coherent addition of the beam provides a very strong signal; non-linear pattern excitation intensities produces 3D-resolution; and, finally the non-invasive characteristic of approach presents an opportunity to even examine a live sample without any damage.

Aim

CARS imaging allows the identification of different types of chemical bonds. It also offers a unique chemical selectivity for compounds (see above). This experiment was designed to follow on in the investigating of collagen changes in MMVD in the previous chapters. Considering the structural changes in MMVD leaflets (Chapter 2 and 3) and changes in cross-links (Chapter 6 and 7), it was felt that not only could these changes be reflected in CARS images, but also the unique potential of CARS imaging would add new information to the understanding of MMVD.

Materials and methods

The set-up used in the current study is shown in Figure 8.2, which was similar to that of Evans *et al,* (2005). For CARS imaging the system was tuned in such a way that

the difference between the "pump" and the "Stokes" wavelengths equals about 2840 cm^{-1}, which corresponds to the symmetry of the CH_2 (bond) stretch vibration (Wang *et al.,* 2005). CARS imaging of CH_2 stretch has been intensively investigated in recent years in different tissues. It has been shown that it can be used to visualise endothelial cells, smooth muscles, axonal myelin, lipid bilayers, and fibrous protein structures such as elastin and collagen where CH_2 stretches are especially abundant around cross-link areas (Wang *et al.,* 2005; Wang *et al.,* 2008). The latter has recently been of a particular interest for identification of most tumour masses, where the surrounding tissues are abundant in collagen unlike the tumour itself (Cheng *et al.,* 2007).The CARS imaging facility at the University of Edinburgh has been established very recently and, due to time constraints and hardware problems with the instrument, it was only possible to run two samples obtained from a male beagle (5 years old) with MMVD grade I. They had been kept in -70°C and before experiment they were let to thaw in room tempreture. Each sample was collected from obviously diseased areas and measured 2 × 2 mm and was sandwiched between 2 cover-slips. The sample was scanned in 0.4 μm thick slices of an area 0.2 × 0.2 mm covering the entire depth of the leaflet. Images were taken with phosphate buffer saline (PBS) added to the sample to prevent drying artifacts.

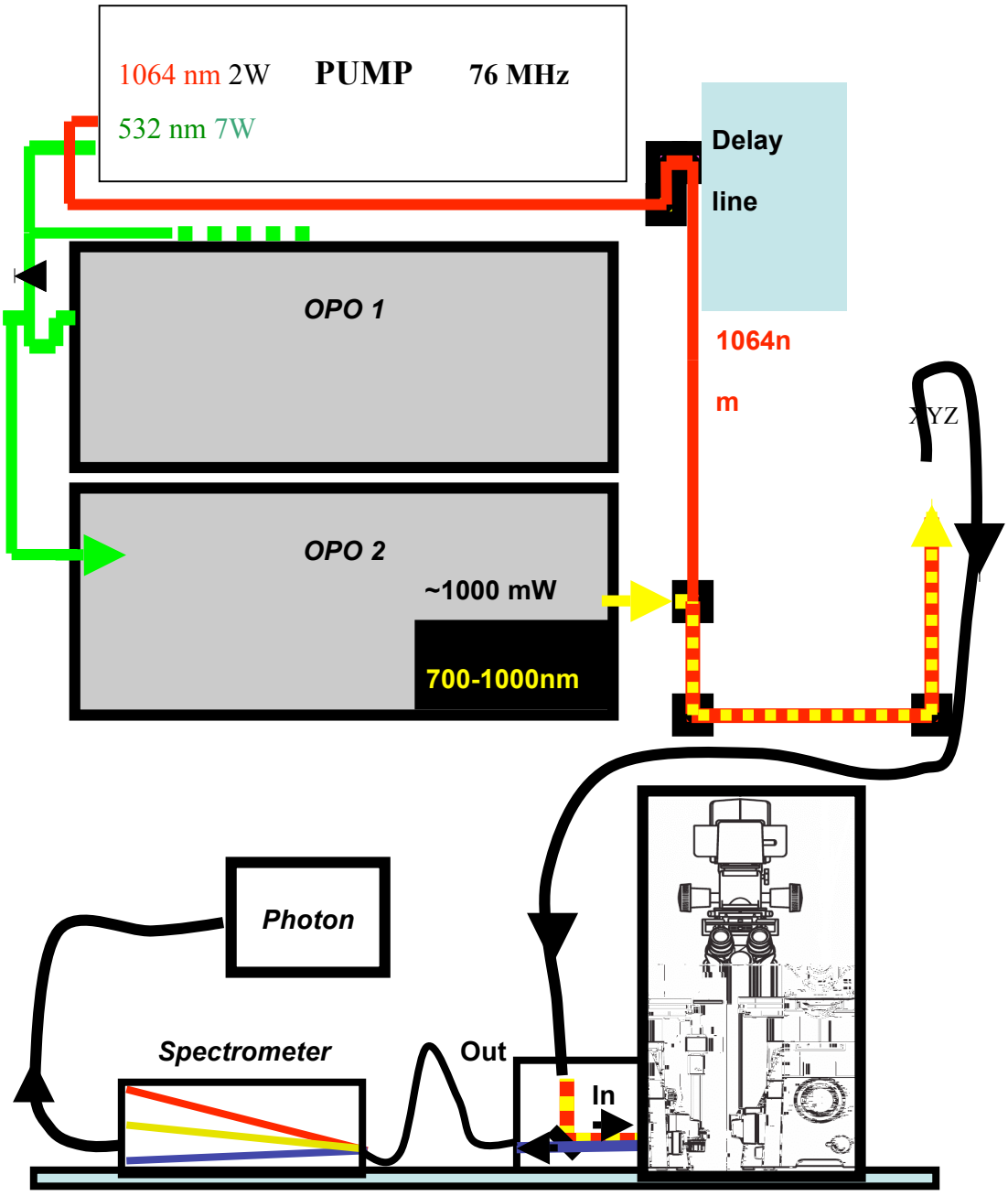

Figure 8:2: The setup for CARS imaging used in the experiment at the Institute of Materials and Processes at the University of Edinburgh. The system employs a Nd:YVO4 laser as "Stokes" (1064 nm), and a tunable optical parametric oscillator OPO (700 - 1000 nm) as

"pump" beam. Delay online or stage is responsible for the temporal overlap of the pump and Stokes pulses. The sample was staged on a confocal laser scanning microscope (Nikon BV 'C1', Amsterdam, Netherlands). Various wavelengths of custom-made long pass dichroic mirrors (Chroma, Rockingham, USA) are required within the scan unit, in order to separate the anti-Stokes (CARS signal) from the longer wavelength pump and Stokes (inputs).

Results and discussion

Figure 8.3 shows a series of CARS images obtained from grade I MMVD sample, based on CH_2 stretches. The extracellular matrix of the mitral leaflets, especially the fibrosa layer, is mainly composed of collagen. The network-like pattern of the image is mostly compatible with the collagen structure. These slices show how pattern and structure of the fibrils change in different depths of leaflets. Lipid droplet and lipid accumulation in the extracellular matrix can also give rise to very rich and strong CARS imaging, such as one can observe in the extracellular matrix of an atheroma (Le *et al.,* 2007). However, it is very unlikely that lipid accumulation can produce the network pattern observed in the MMVD samples and lipid accumulation has not been reported in MMVD.

Figure 8.3 (following pages): CARS images (from A-L) of CH_2 stretches of a diseased mitral leaflet. A series of 0.4 μm thick slices of an area 0.2 x 0.2 mm and 4.4 μm deep. Given the pattern of the image and considering that the main ingredient of extracellular matrix of the leaflet is collagen, it seems likely that collagen molecules are the main contributor to the image.

A 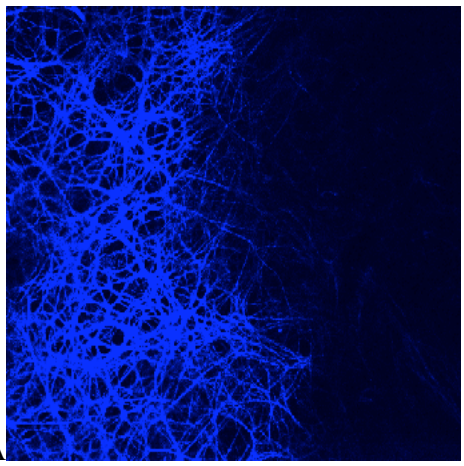

B 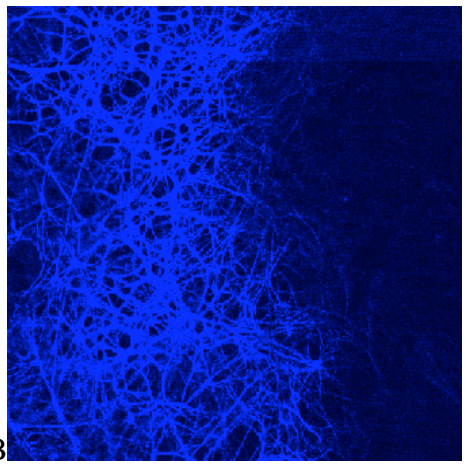

C 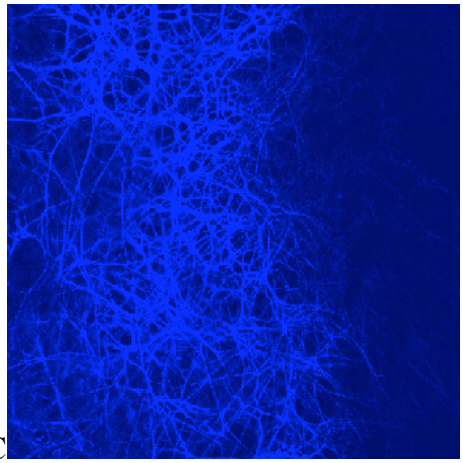

D 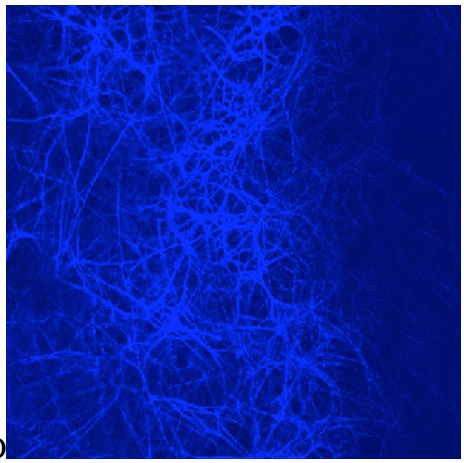

E 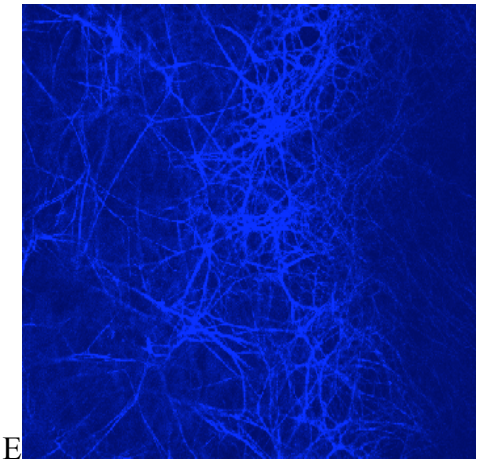

F 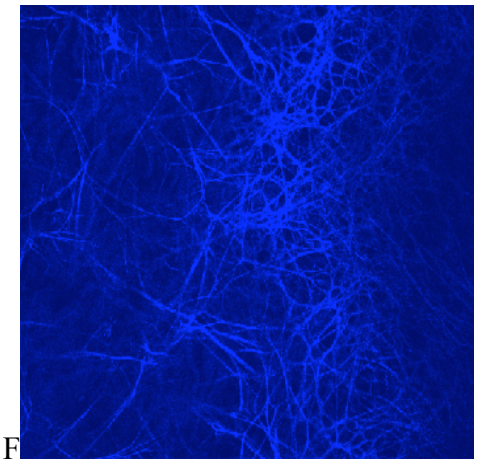

G 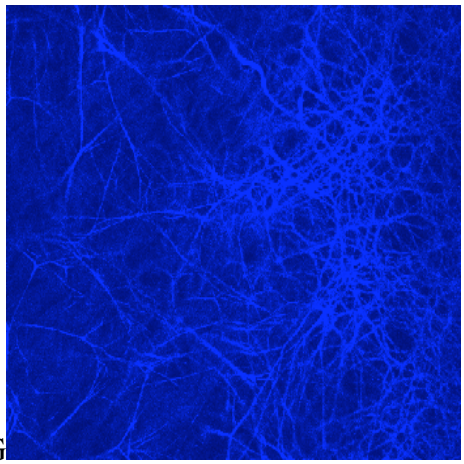

H 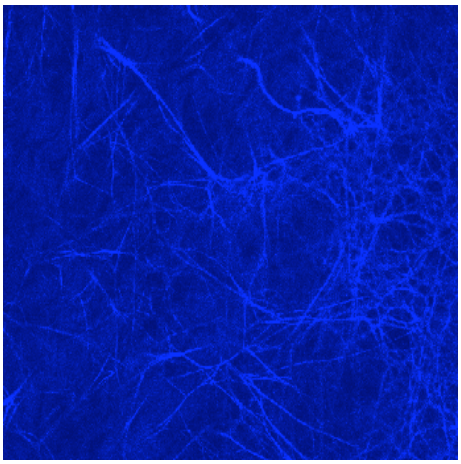

I 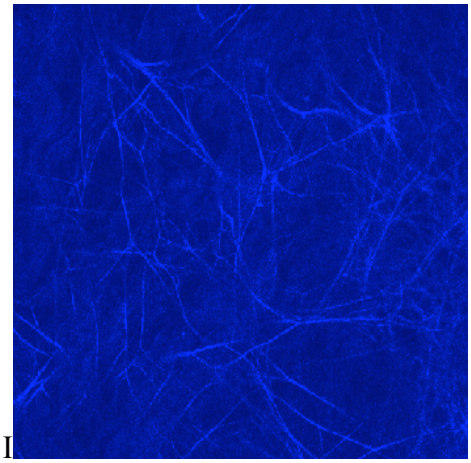

J 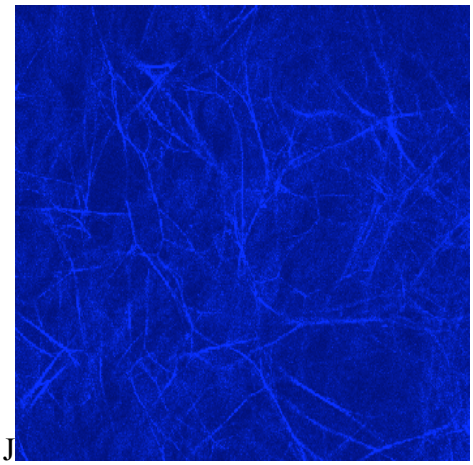

K 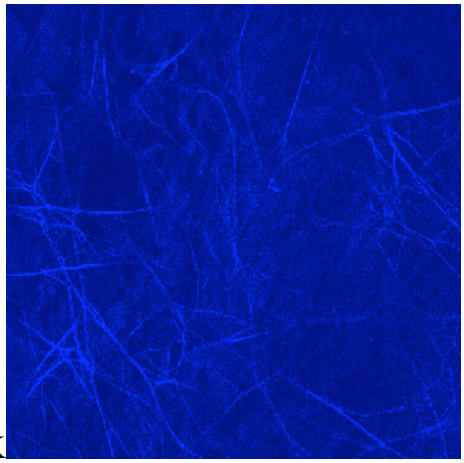

L 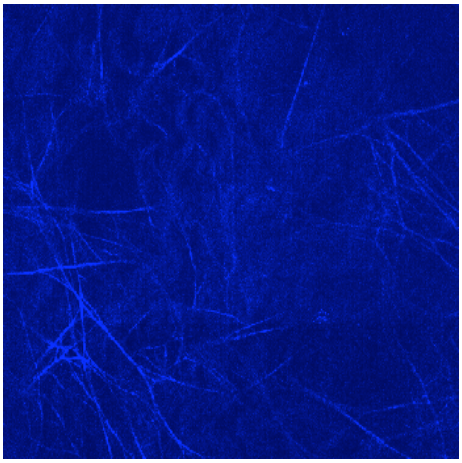

In the current CARS imaging, images were recorded from two affected areas (MMVD grade I) obtained from the same leaflet and due to the time and technical problems the running of more samples in order to draw a comparison between diseased and healthy leaflets was not possible.

It is possible to distinguish between collagen and elastin using the technique of second harmonic imaging (SHI). The unusual structure of collagen (noncentrosymmetric) and its high degree of crystallinity are able to convert the light to its second harmonic. To date, this is the strongest SH signal that has ever been obtained from a biological material (Williams *et al.*, 2005; Cox and Kable, 2006). Elastin can also be imaged by using two-photon excitation fluorescence (TPEF) (Cheng *et al.,* 2007). However, in CARS imaging, the best way to distinguish between collagen and elastin fibrils is based on their specific Raman spectra. Although the first experimental images of CARS were obtained in 1982 (Duncan *et al.,* 1982), measurement of the Raman spectrum of collagen dates back to the 70s (Frushour and Koenig, 1975). Attempts to obtain specific collagen Raman spectra (Figure 8.5) from mitral leaflets were unsuccessful. The Stokes beams had very low intensities at the frequencies that were suggested for collagen and this may explain my failure. This may be resolved by technical modification of the equipment, and this is currently being evaluated.

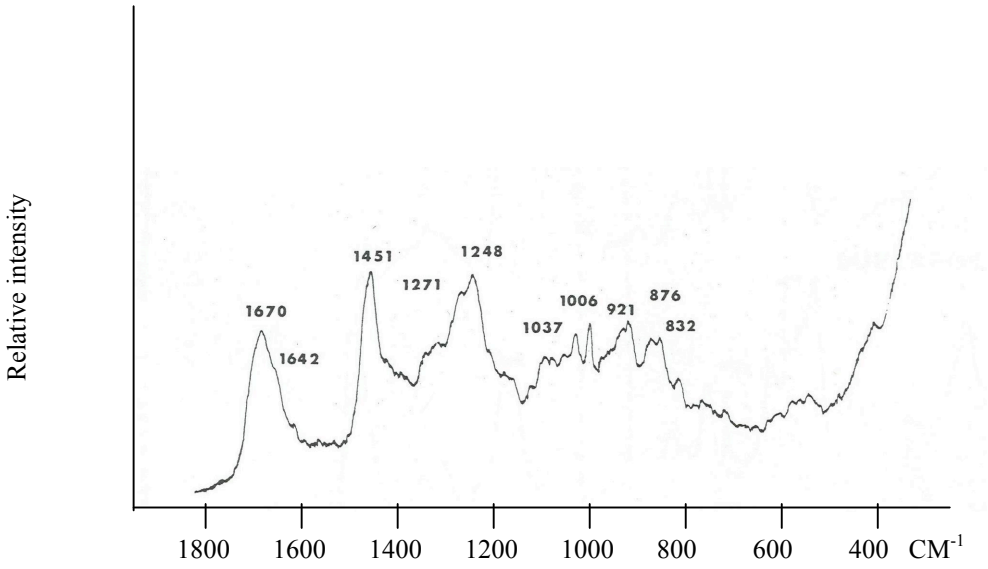

Figure 8.5: Raman spectrum of collagen (Achilles tendon of bovine) adapted from Frushour and Koenig (1975).

To conclude this section, it should be mentioned that, although imaging of CH_2 stretches has been carried out in different tissues, to the best of my knowledge, this was the first time that the technique has been applied, in a limited fashion, to the structure of heart valve leaflets. It demonstrates an interesting pattern of the fibril structure at different depths of the leaflets. Although further studies using a large number of both diseased and healthy leaflets are required to validate the current results, these changes in lay-out of the fibrils may shed more light into pathogenesis of the disease. It may also be useful in designing and engineering artificial valves.

CARS imaging offers several advantages for biology and medicine. CARS imaging is a non-destructive approach that can even be applied to living cells. CARS signals are much stronger than spontaneous Raman scattering. This makes it possible to acquire images in a time scale of less than one second, compared to confocal Raman images that may take several hours. By the use of specific vibrational frequencies of different bonds in a certain molecule, it uniquely provides a chemically-selective tool to differentiate between bio-materials and bio-molecules, without the need for labelling. As CARS depends upon the non-linear excitation intensity, it produces a signal only in the focal centre, giving rise to a 3 dimensional spatial resolution. Moreover, the use of the infrared lasers with long wavelength of excitation produces a deep penetrative beam which also reduces the amount of the scattered light in the tissue. As well as the considerable set-up costs for CARS instruments, another major disadvantage of CARS results from the non-resonant background. This interferes with weak Raman bands and reduces the sensitivity of the method (Rodriguez *et al*., 2006; Cheng *et al.,* 2007; Djaker *et al.,* 2007). All in all, it seems CARS imaging has

huge potential as a tool for biological and medical investigation.

Chapter 9

Conclusions

Conclusions

This study has markedly improved our understanding of the structural changes that occur at the molecular level in MMVD, and has demonstrated the applicability of various techniques to further understanding of the disease. Important findings of this study with respect to mild or moderate MMVD can be summarised as follows:

1. The orientation, the degree ofalignment and density of collagen fibrils are altered in diseased areas of the affected leaflets in MMVD;

2. A 10% depletion of collagen in the affected areas was demonstrated compared to the healthy regions;

3. The affected regions have 20% less fibrillar collagen;

4. The diseased regions have increased numbers of immature reducible cross-links in comparison to the healthy areas;

5. The diseased regions contain 25% fewer mature cross-links (pyridinoline) compared to the healthy zones;

Much is known about MMVD its natural history, diagnosis, clinical development, therapy and outcome. However, the exact pathophysiology of the disease still remains unclear. Work to date, in our laboratory and others, has identified ultrastructural changes, endothelial alteration and changes to the proteome in

diseased dog mitral valves, and many of those finding match those reported for mitral valve disease in humans. The matrix of leaflets and one of its major components (collagen fibrils) have central roles in the function of mitral valves. By selecting mild and moderate grades of MMVD, I was able to investigate the events mid-way through development of the condition, before it advances to end-stage and a completely dysfunctional and insufficient valve. The information revealed gives clues about the origin and progression of the disease.

Collagen molecules cannot be stretched and contracted to the same extent as elastin fibrils, so the orientation of collagen fibrils (Chapter 1) reveals how the mitral valve leaflet responds to mechanical load during the heart cycle. The x-ray experiments provided detailed maps of collagen fibrils in affected regions and differentiated between fibrillar and non-fibrillar collagen. They also provided strong confirmation that the changes in collagen fibrils only occurred in the free margins of the leaflets. The question of why free margins are more prone to injury than other regions remains to be answered. The DSC experiments gave important information about the thermal characteristics of collagen molecules, and showed that not just tertiary structure is important in determining the thermal characteristics of a molecule, but also the microenvironment in which the molecule lies. The DSC and x-ray data showed that there was 20% depletion of fibrillar collagen while hydroxyproline assay showed that there was only 10% depletion of collagen molecules.

Affected regions also had 25% fewer mature cross-links. Some of this reduction may result from depletion of mature collagen, while increased levels of non-fibrillous collagen may also contribute to this sequel. However, the neutron scattering

experiment found more reducible cross-links in these affected regions. This increase in reducible cross-links may be explained by increased production of new collagen in which the cross-links are yet to mature. Conversely, the higher level of non-fibrillous collagen may be explained either by disruption of fibrils, or by the production of collagen molecules that have not yet assembled into fibrils. Increased collagen synthesis in response to injury has been reported in human MVP (Cole *et al*., 1984) but has not yet been clearly demonstrated in the dog. Recent work by our group and others (Disatian *et al.,* 2008; Han *et al.,* 2008) has shown increased numbers of activated-myofibroblasts close to the valve surface and reduced numbers of inactive-myofibroblasts in the valve spongiosa of dogs with MMVD. The valvular interstitial cells in mitral valve leaflets have also been shown to undergo changes with age and environmental condition (they are even suspected to change under mechanical stress) (Schoen, 2008). MMVD has been closely linked with ageing in the dog. Considering the age-association changes in collagen such as the change in the nature of cross-links and alteration of the lysyl oxidase activity, the reported cellular changes might be associated with MMVD. The increase in reducible cross-links may be explained by increased collagen synthesis, which may also be related to the activity of lysyl oxidase. Numerous factors have been associated with MMVD, including aging, repeated stress, involvement of various cytokines, involvement of advance glycation end (AGEs), endothelial cell breakage followed by neovascularisation etc. However, it may be postulated that endothelial damage initiates a stromal interstitial transformation from quiescent fibroblasts to activated myofibroblasts. These cells migrate towards the site of endothelial damage and as a part of their activation increase production of proteolytic enzymes (MMPs) which destroys the mature

collagen present in the leaflet, while at the same time increase production of immature collagen. However, this collagen fails to mature and what should proceed as a reparative process turns into a dyscollagenesis with collagen loss and reduced mechanical strength of the remaining collagen. Coupled with this is an increase in GAG expression from the activated myofibroblasts which further compromises collagen organisation and maturation and itself reduces valve mechanical strength. This loss of mechanical integrity increases the chance of appositional trauma of the leaflet edges and results in further endothelial damage. The process continues in this fashion until the whole free edge of the leaflet is severely damaged. However, whether the procedure is exactly similar to that of repair and what triggers these events in the first place is still not known.

The DEI imaging demonstrated the potential of this technique for the studying of structural changes in extracellular matrix. MMVD starts with small macroscopic nodules resulted from disruption of matrix structure and as disease progresses this disruption become more marked (Chapter 1). In the current study, the DEI was able to highlight associated features of lesions and healthy areas and differentiating boundaries between them. The similarities found between MMVD and human breast cancer images were interesting, considering the pathological changes that occur in MMVD, such as destruction and production of collagen, activation and potential apoptosis of vascular interstitial cells.

The CARS imaging experiment demonstrated how effectively this approach can be applied to mitral valve leaflets. The observation of different patterns of collagen network at different depths gave an insight into the pathogenesis of the disease. The

specificity and selectivity of CARS that result from the unique Raman spectrum of each type of molecule can also be exploited to differentiate changes that are happening in MMVD.

To conclude, the present study bridges the knowledge gap and helps to provide better understanding about collagen changes in the pathogenesis of MMVD. The consequences of these collagen changes can be readily appreciated, in terms of significant mitral valve regurgitation and eventual left sided heart failure. Furthermore, as MMVD bears considerable similarities to human valvular disease (especially mitral valve prolapse) and given the importance of this disease in humans, the finding in this thesis can be equally taken into account in human studies as well. However, the current study was limited by some factors such as the qualitative state of the neutron diffraction study and low number of samples in the same study. These factors and others (see below) should be taken into account when interpreting the results of this thesis.

Future studies in this area could include investigation of collagen structure in severe forms of disease and in different breeds. This work can also be expanded to embrace specific age groups as a recent study by our lab (unpublished data) has shown that beagles as young as one year old were suffering from MMVD. Cytoskeletal proteins such as vimentin through multi-adhesive matrix proteins such as fibronectin interact with other matrix proteins such as collagen and elastin. Although cells are responsible for secreting and remodelling the matrix, but matrix also plays an important role in maturation, differentiation and migration of its cellular content. Thus, understanding of the function of multi-adhesive and cytoskeletal proteins and

their relation with collagen fibrils seems imperative. Moreover, identifying of exact composition of collagen in mitral valve leaflets can shed more light on the pathogenesis of the disease. Although type I and III are the major types, it has shown that in some tissues two quantitatively minor fibrillar collagen type V and type XI coassemble with type I collagen regulating the structure and properties of the fibres (Lodish *et al.,* 2008). In cartilage proteoglycans through collagen type IX are cross-linked to collagen type II and contribute to the mechanical properties of the matrix. Therefore, study of proteoglycans and their relation with matrix proteins can also be considered in future studies.

Finally advanced glycation end products (AGEs) are opening a new field of study and are currently receiving considerable attention. It has been shown that high level of pentosidine, one of the advanced glycation end products (AGE), can be considered as a risk factor in patients suffering from heart conditions (reference).Given their importance, more studies can be directed to elucidate AGEs and receptors of AGEs (RAGE) roles in MMVD. More recently an experiment has been recently designed by the author and funded by Small Project Grant scheme (University of Edinburgh) in order to investigate plasma concentration of carboxymethyllysine (CML), an AGE product, between young healthy, old healthy and cardiac patients".

Chapter 10

References

Aghamohammadzadeh, H., Newton, R.H. and Meek, K.M. 2004. X-ray scattering used to map the preferred collagen orientation in the human cornea and limbus. Structure. 12(2), 249-56.

Agozzino, L., Falco, A., de Vivo, F., de Vincentiis, C., de Luca, L., Esposito, S. and Cotrufo, M. 1992. Surgical pathology of the mitral valve: gross and histological study of 1288 surgically excised valves. Int. J. Cardiol. 37(1), 79-89.

Akeson, W.H., Amiel, D., Mechanic, G.L., Woo, S.L., Harwood, F.L. and Hamer, M.L. 1977. Collagen cross-linking alterations in joint contractures: changes in the reducible cross-links in periarticular connective tissue collagen after nine weeks of immobilization. Connect. Tissue Res. 5(1), 15-9.

Akhtar, S., Meek, K.M. and James, V. 1999. Ultrastructure abnormalities in proteoglycans, collagen fibrils, and elastic fibers in normal and myxomatous mitral valve chordae tendineae. Cardiovasc. Pathol. 8, 191-201.

Atanasova, M., Konova, E., Betova, T. and Baydanoff, S. 2008. Non-enzymatic glycation of human fibrillin-1. Gerontology. [Epub ahead of print] available at: http://content.karger.com [Accessed 24 October 2008].

Bächinger, H.P. and Davis, J.M. 1991. Sequence specific thermal stability of the collagen triple helix. Int. J. Biol. Macromol. 13(3), 152-6.

Bailey, A.J. and Lister, D. 1968. Thermally labile cross-links in native collagen. Nature 220, 280-281.

Bailey, A.J. and Shimokomaki, M.S. 1971. Age related changes in the reducible cross-links of collagen. FEBS Lett. 16(2), 86-88.

Banks, W.B. 1993. Applied Veterinary Histology. 3rd edition.s Mosby, St. Louise, pp 271-272.

Bann, J.G., Peyton, D.H. and Bächinger, H.P. 2000. Sweet is stable: glycosylation stabilizes collagen. FEBS Lett. 473(2), 237-40.

Barlow, J.B., Pocock, W.A., Marchand, P. and Denny, M. 1963. The significance of late systolic murmurs. Am. Heart J. 66, 443-452.

Barth, P.J., Koster, H. and Moosdorf, R., 2005. CD34+ fibrocytes in normal mitral valves and myxomatous mitral valve degeneration. Pathol. Res. Pract. 201, 301-304.

Bartolomeo, M.P., Maisano, F., 2006. Validation of a reversed-phase HPLC method for quantitative amino acid analysis. J. Biomol. Tech. 17(2), 131-7.

Bates, C.J. 1977. Proline and hydroxyproline excretion and vitamin C status in elderly human subjects. Clin. Sci. Mol. Med. 52(5), 535-43.

Beardow, A.W. and Buchanan, J.W. 1993. Chronic mitral valve disease in cavalier King Charlesspaniels: 95 cases (1987-1991). J. Am. Vet. Med. Assoc. 203, 1023-1029.

Benjamin, E.J. 2001. Mitral valve prolapse: past misconceptions and future research directions. Am. J. Med. 111, 726-728.

Berisio, R., Granata, V., Vitagliano, L. and Zagari, A. 2004. Imino acids and collagen triple helix stability: characterization of collagen-like polypeptides containing Hyp-Hyp-Gly sequence repeats. J. Am. Chem. Soc. 126(37), 11402-3.

Bienkowski, R.S., Baum, B.J. and Crystal, R.G. 1978. Fibroblasts degrade newly synthesised collagen within the cell before secretion. Nature. 276(5686), 413-6.

Birk, D.E. and Trelstad, R.L. 1984. Extracellular compartments in matrix morphogenesis: collagen fibril, bundle, and lamellar formation by corneal fibroblasts. J. Cell Biol. 99(6), 2024-33.

Black, A. French, A.T., Dukes-McEwan, J. and Corcoran, B.M., 2005. Ultrastructural morphologic evaluation of the phenotype of valvular interstitial cells in dogs with myxomatous degeneration of the mitral valve. Am. J. Vet. Res. 66(8), 1408-1414.

Bonfanti, L., Mironov, A.A. Jr., Martínez-Menárguez, J.A., Martella, O., Fusella, A., Baldassarre, M., Buccione, R., Geuze, H.J., Mironov, A.A. and Luini, A.1998. Procollagen traverses the Golgi stack without leaving the lumen of cisternae: evidence for cisternal maturation. Cell. 95(7), 993-1003.

Bornstein. P. 1974. The biosynthesis of collagen. Annu. Rev. Biochem. 43(0), 567-603.

Bradshaw, J.P. 1985. A study of the structure of biological macromolecules.Thesis (D Phil). The University of Oxford. Oxford.

Braunwald, E. 2001. Valvular Heart Disease. In: Braunwald, E, Fauci, A.S., Kasper, D.L., Hauser, S.L., Longo, D.L. and Jameson, J.L. (Eds), Harrison's Principles of Internal Medicine. McGraw-Hill, New York, pp 1348-1349.

Buchanan, J.W. 1977. Chronic valvular disease (endocardiosis) in dogs. Adv. Vet. Sci. Comp. Med. 21, 75-106.

Bullen, G. J. 1962. X-ray diffraction. In: Florkin, M. and Stotz, E. (Eds), Methods for the study of molecules. Comprehensive Biochemistry (series). 1(3), 33-51.

Cameron, G.J., Alberts, I.L., Laing, J.H. and Wess, T.J. 2000. Structure of type I and type III heterotypic collagen fibrils: an x-ray diffraction study. J. Struct. Biol. 137(1-2), 15-22.

Canty, E.G. and Kadler, K.E. 2005. Procollagen trafficking, processing and fibrillogenesis. J. Cell Sci. 118(Pt 7), 1341-53.

Canty, E.G., Lu, Y., Meadows, R.S., Shaw, M.K., Holmes, D.F. and Kadler, K.E. 2004. Coalignment of plasma membrane channels and protrusions (fibripositors) specifies the parallelism of tendon. J. Cell Biol. 165(4), 553-63.

Chapman, D., Thomlinson, W., Johnston, R.E., Washburn, D., Pisano, E., Gmur, N., Zhong, Z., Menk, R., Arfelli, F. and Sayers, D. 1997. Diffraction enhanced x-ray imaging. Phys. Med. Biol. 42, 2015-2025.

Chen, J.R., Takahashi, M., Kushidam, K., Suzuki, M., Suzuki, K., Horiuchi, K. and Nagano A. 2000. Direct detection of cross-links of collagen and elastin in the hydrolysates of human yellow ligament using single-column high performance liquid chromatography. Anal. Biochem. 278(2), 99-105.

Cheng, J.X., Jia, Y.K., Zheng, G. and Xie, X.S. 2002. Laser-scanning coherent anti-Stokes Raman scattering microscopy and applications to cell biology. Biophys. J. 83(1), 502-9.

Cheng, J.X., Jia, Y.K., Zheng, G. and Xie, X.S. 2006. Laser-scanning coherent anti-Stokes Raman scattering microscopy and applications to cell biology. Biophys. J. 83(1), 502-9.

Cheng, J.X., Wang, H., Te, T.L., Fu, Y., Huff, T.B. and Wang, H. 2007. Chasing lipids in health and diseases by CARS microscopy. CACS Communications, feature article. Fall issue, 13-18.

Chou, H.T., Hung, J.S., Chen, Y.T., Wu, J.Y. and Tsai, F.J. 2004. Association between COL3A1 collagen gene exon 31 polymorphism and risk of floppy mitral valve/mitral valve prolapse. Int. J. Cardiol. 95, 299-305.

Chou, H.T., Shi, Y.R., Hsu, Y. and Tsai, F.J. 2002. Lack of association between transforming growth factor-beta1 gene polymorphisms and mitral valve prolapse in Taiwan Chinese. J. Heart Valve Dis. 11(4), 478-84.

Cole, W.G., Chan, D., Hickey, A.J. and Wilcken, D.E. 1984. Collagen composition of normal and myxomatous human mitral heart valves. Biochem. J. 219, 451-460.

Cole, W.G., Chan, D., Hickey, A.J. and Wilcken, D.E. 1984. Collagen composition of normal and myxomatous human mitral heart valves. Biochem. J. 219(2), 451-60.

Collier, R.J., Stiening, C.M., Pollard, B.C., VanBaale, M.J., Baumgard, L.H., Gentry, P.C., Coussens, P.M., 2006. Use of gene expression microarrays for evaluating nvironmental stress tolerance at the cellular level in cattle. J. Anim. Sci. 84 Suppl: E1-13.

Colville, T. and Bassert, J.M. 2002. Clinical anatomy & physiology for veterinary technicians. Mosby, St. Louis.

Cox, G. and Kable, E. 2006. Second-harmonic imaging of collagen. Methods. Mol. Biol. 319, 15-35.

Cox, S.W., Eley, B.M., Kiili, M., Asikainen, A., Tervahartiala, T. and Sorsa, T. 2006. Collagen degradation by interleukin-1beta-stimulated gingival fibroblasts is accompanied by release and activation of multiple matrix metalloproteinases and cysteine proteinases. Oral Dis. 12(1), 34-40.

Criley, J.M., Lewis, K.B., Humphries, J.O. and Ross, R.S. 1966. Prolapse of the mitral valve: clinical and cine-angiocardiographic findings. Br. Heart J. 28, 488-496.

da Silva, E.P., Pedro, M.M., Varela, M.G., Cortez-Dias, N., Bicho, M.P., Madeira, H.C. and Lopes, M.G. 2007. Heart rate and blood pressure in mitral valve prolapse patients: divergent effects of long-term propranolol therapy and correlations with catecholamines. Anadolu. Kardiyol. Derg. Suppl 1:107-9.

Das, K.M. and Tashjian, R.J. 1965. Chronic mitral valve disease in the dog. Vet. Med. Small Anim. Clin. 60(12), 1209-16.

Davies, S.M., Epand, R.F., Bradshaw, J.P. and Epand, R.M. 1998. Modulation of lipid polymorphism by the feline leukaemia virus fusion peptide: implications for the fusion mechanism. Biochemistry. 37(16), 5720-9.

Degandt, A.A., Weber, P.A., Saber, H.A. and Duran, C.M. 2007. Mitral valve basal chordae: comparative anatomy and terminology. Ann. Thorac. Surg. 84(4), 1250-5.

Dellmann, H.D. and Eurell, J.A., 1998. Textbook of veterinary histology. Williams & Wilkins, Baltimore.

Desai K, Wu L.2007. Methylglyoxal and advanced glycation endproducts: new therapeutic horizons? Recent Patents Cardiovasc. Drug Discov. 2(2), 89-99.

Detweiler, D.K. and Patterson, D.F. 1965. The prevalence and types of cardiovascular disease in dogs. Ann. N. Y. Acad. Sci. 127(1), 481-516.

Diegelmann, R.F. 2001. Collagen metabolism. Wounds, 13,177-182.

Dilip, M. 2004. Principles and chemical applications of neutron scattering. Graduate Student Seminar Series. The University of Alabama.

Disatian, S., Ehrhart, E.J. 3rd, Zimmerman, S. and Orton, E.C. 2008. Interstitial cells from dogs with naturally occurring myxomatous mitral valve disease undergo phenotype transformation. J. Heart. Valve. Dis. 17(4), 402-11.

Djaker, N., Lenne, P., Marguet, D., Colonna, A., Hadjur, C. and Rigneault, H. 2007. Coherent anti-Stokes Raman scattering microscopy (CARS): Instrumentation and applications, Nuclear Instruments and Methods in Physics Research A. 571(1-2), 177-181.

Dobrzynski, L., Blinowski, K. 1994. In: Cooper, M. (Ed), Neutrons and solid state physics. Vol. 3, Ellis Horwood Series and number, New York, pp 8-16.

Droge, W. 2002. Free radicals in the physiological control of cell function. Physiol. Rev. 82, 47-95.

Duncan, M. D., Reintjes, J. and Manuccia, T. J. 1982. Scanning coherent anti-Stokes Raman microscope. Opt. Lett. 7(8), 350-352.

Erler, J.T., Bennewith, K.L., Nicolau, M., Dornhöfer, N., Kong, C., Le, Q.T., Chi, J.T., Jeffrey, S.S. and Giaccia, A.J. 2006. Lysyl oxidase is essential for hypoxia-induced metastasis. Nature. 440(7088), 1222-6.

Espino, D.M., Shepherd, D.E. and Buchan, K.G. 2007. Effect of mitral valve geometry on valve competence. Heart Vessels. 22(2), 109-15.

Evans, C.L., Potma, E.O., Puoris'haag, M., Cote, D., Lin, C.P. and Xie, X.S., 2005. Chemical imaging of tissue in vivo with video-rate coherent anti-Stokes Raman scattering microscopy. Proc. Natl. Acad. Sci. (PNAS), 102(46), 16807-12.

Eyre, D.R., Dickson, I.R. and Van Ness, K., 1988. Collagen cross-linking in human bone and articular cartilage. Age-related changes in the content of mature hydroxypyridinium residues, Biochem. J. 252, 495-500.

Filho, A.S., Maciel, B.C., Martín-Santos, R., Romano, M.M. and Crippa, J.A. 2008. Does the association between mitral valve prolapse and panic disorder really exist? Prim. Care Companion J. Clin. Psychiatry. 10(1), 38-47.

Fletcher, T. F. and Weber, A. F. 2004. Veterinary developmental anatomy. University of Minnesota. [Online] available at: vanat.cvm.umn.edu/vanat.pdf/EmbryoLectNotes.pdf [Accessed 22 August 2008].

Fontana, A. and Delmas, P.D. 2000. Markers of bone turnover in bone metastases. Cancer. 15, 88(12 Suppl), 2952-60.

Franks, A. 1996. The first hundred years In: Michette, A. and Pfauntsch, S. (Eds), X-rays: the first hundred years. John Wiley & Sons, Chichester, pp 1-19.

Freed, L.A., Levy, D., Levine, R.A., Larson, M.G., Evans, J.C., Fuller, D.L., Lehman, B. and Benjamin, E.J. 1999. Prevalence and clinical outcome of mitral-valve prolapse. N. Engl. J. Med. 341, 1-7.

Friedli, G. 1996. Interaction of deamidated soluble wheat protein (SWP) with other food proteins and metals. Thesis (PhD). The University of Surrey. Surrey.

Frushour, B.G., and Koenig, J.L. 1975. Raman scattering of collagen, gelatin, and elastin. Biopolymers. 14(2), 379-91.

Gacheru, S.N., Trackman, P.C., Shah, M.A., O'Gara, C.Y., Spacciapoli, P., Greenaway, F.T. and Kagan, H.M. 1990. Structural and catalytic properties of copper in lysyl oxidase. J. Biol. Chem. 265(31), 19022-7.

Garnero, P., Borel, O., Byrjalsen, I., Ferreras, M., Drake, F.H., McQueney, M.S., Foged, N.T., Delmas, P.D. and Delaissé, J.M. 1998. The collagenolytic activity of cathepsin K is unique among mammalian proteinases. J. Biol. Chem. 273(48), 32347-52.

Ge, G., Zhang, Y., Steiglitz, B.M. and Greenspan, D.S. 2006. Mammalian tolloid-like 1 binds procollagen C-proteinase enhancer protein 1 and differs from bone morphogenetic protein 1 in the functional roles of homologous protein domains. J. Biol. Chem. 281(16), 10786-98.

Gerrits, M.I., Thijssen, J.H. and van Rijn, H.J. 1995. Determination of pyridinoline and deoxypyridinoline in urine, with special attention to retaining their stability. Clin. Chem. 41(4), 571-4.

Gething, M.J. 1999. Role and regulation of the ER chaperone BiP. Semin. Cell Dev. Biol. 10(5), 465-72.

Grande, J.P., Melder, D.C. and Zinsmeister, A.R. 1997. Modulation of collagen gene expression by cytokines: stimulatory effect of transforming growth factor-beta1, with divergent effects of epidermal growth factor and tumor necrosis factor-alpha on collagen type I and collagen type IV. J. Lab. Clin. Med. 130(5), 476-86.

Grande-Allen, K.J., Borowski, A.G., Troughton, R.W., Houghtaling, P.L., Dipaola, N.R., Moravec, C.S., Vesely, I. and Griffin, B.P. 2005. Apparently normal mitral valves in patients with heart failure demonstrate biochemical and structural derangements. J. Am. Coll. Cardiol. 45, 54-61.

Grande-Allen, K.J., Calabro, A., Gupta, V., Wight, T.N., Hascall, V.C. and Vesely, I. 2004. Glycosaminoglycans and proteoglycans in normal mitral valve leaflets and chordae: association with regions of tensile and compressive loading. Glycobiology, 14, 621-633.

Grillo, M.A. and Colombatto, S. 2008. Advanced glycation end-products (AGEs): involvement in aging and in neurodegenerative diseases. Amino Acids. 35(1), 29-36.

Gronemann, S.T., Ribel-Madsen, S., Bartels, E.M., Danneskiold-Samsoe, B. and Bliddal H. 2004. Collagen and muscle pathology in fibromyalgia patients. Rheumatology, 43(1), 27-31.

Grynpas, M.D. Eyre, D.R. and Kirschner, D.A. 1980. Collagen type II differs from type I in native molecular packing. Biochim. Biophys. Acta. 626(2), 346-55.

Gupta, V., Barzilla, J.E., Mendez, J.S., Stephens, E.H., Lee, E.L., Collard, C.D., Laucirica, R., Weigel, P.H. and Grande-Allen KJ. 2008. Abundance and location of proteoglycans and hyaluronan within normal and myxomatous

mitral valves. Cardiovasc. Pathol. [Epub ahead of print] available at: http://www.sciencedirect.com [Accessed 24 October 2008].

Gustavson, K.H. 1955. The function of hydroxyproline in collagens. Nature.175 (4445), 70-4.

Hadian, M., Corcoran, B.M., Han, R.I., Grossmann, J.G. and Bradshaw, J.P. 2007. Collagen organization in canine myxomatous mitral valve disease: an x-ray diffraction study. Biophys. J. 93(7), 2472-6.

Hadley, J., Malik, N. and Meek, K. 2001. Collagen as a model system to investigate the use of aspirin as an inhibitor of protein glycation and cross-linking. 2001. Micron. 32(3), 307-15.

Häggström, J., Hamlin, R.L., Hansson, K. and Kvart C. 1996. Heart rate variability in relation to severity of mitral regurgitation in Cavalier King Charles spaniels. J. Small Anim Pract. 37(2), 69-75.

Häggstrom, J., Hansson, K., Kvart, C. and Swenson, L. 1992. Chronic valvular disease in the cavalier King Charles spaniel in Sweden. Vet. Rec. 131, 549-553.

Häggstrom, J., Kvart, C. and Pedersen, H.D. 2005. Acquired Vvalvular Hheart Ddisease. In: Ettinger, S.J. and Feldman, E.C. (Eds), Textbook of veterinary internal medicine: diseases of the dog and cat. Elsevier Saunders, St Louis, pp 1022-1039.

Hammer, D., Leier, C.V., Baba, N., Vasko, J.S., Wooley, C.F. and Pinnell, S.R. 1979. Altered collagen composition in a prolapsing mitral valve with ruptured chordae tendineae. Am. J. Med. 67(5), 863-6.

Han, R.I., Black, A., Culshaw, G.J., French, A.T., Else, R.W. and Corcoran, B.M. 2008. Distribution of myofibroblasts, smooth muscle-like cells, macrophages, and mast cells in mitral valve leaflets of dogs with myxomatous mitral valve disease. Am. J. Vet. Res. 69(6), 763-9.

Hansson, K. 2004. Diagnostic imaging of cardiopulmonary structures in normal dogs and dogs with mitral regurgitation. Thesis (PhD). Swedish University of Agricultural Sciences, Uppsala.

Harroun, T.A., Wignall, G.D. and Katsaras, J. 2006. Neutron scattering for biology. In: Fitter, J., Gutberlet, T. and Katsaras, J. (Eds), Neutron scattering in biology: techniques and applications. Springer, Berlin-Heidelberg, pp 1-15.

Harwood, F.L. and Amiel, D. 1992. Differential metabolic responses of periarticular ligaments and tendon to joint immobilization. J. Appl. Physiol. 72(5), 1687-91.

Hasselbalch, H. 1987. Urinary hydroxyproline excretion in the myelofibrosis-osteomyelosclerosis syndrome and related diseases. Eur. J. Haematol. 39(5), 447-51.

Haukipuro, K., Melkko, J., Risteli, L., Kairaluoma, M. and Risteli, J. 1991. Synthesis of type I collagen in healing wounds in humans. Ann. Surg. 213(1), 75-80.

Haus, J.M., Carrithers, J.A., Trappe, S.W. and Trappe, T.A. 2007. Collagen, cross-linking, and advanced glycation end products in aging human skeletal muscle. J. Appl. Physiol. 103(6), 2068-76.

Hayek, E. and Griffin, B., 2002. Mitral valve prolapse: Old beliefs yield to new knowledge. Cleve. Clin. J. Med. 69, 889-896.

Hayek, E., Gring, C.N. and Griffin, B.P., 2005. Mitral valve prolapse. Lancet. 365,507-518.

Hendershot, L.M., and Bulleid, N.J. 2000. Protein-specific chaperones: the role of hsp47 begins to gel. Curr. Biol. 2000 10(24), R912-5.

Ho, S.Y. 2002. Anatomy of the mitral valve. Heart. 88 Suppl. 4, iv5-10.

Höhne, G., Hemminger, W., Flammersheim, H.-J. 1996. Differential scanning calorimetry, an introduction for practitioners. Springer. Berlin-Heidelberg.

Holmes, D.F., Chapman, J.A., Prockop, D.J. and Kadler, K.E. 1992. Growing tips of type I collagen fibrils formed in vitro are near-paraboloidal in shape, implying a reciprocal relationship between accretion and diameter. Proc. Natl. Acad. Sci. 89(20), 9855-9.

Holzapfel, G.A. 2008. Collagen in arterial walls: biomechanical aspects. In: P. Fratzl (Ed.), Collagen, structure and mechanics. Springer-Verlag, Heidelberg, pp 285-324.

Horstmeyer, A., Licht, C., Scherr, G., Eckes, B. and Krieg, T., 2005. Signalling and regulation of collagen I synthesis by ET-1 and TGF-beta1. FEBS J. 272, 6297-6309.

Hou, W.S., Li, Z., Gordon, R.E., Chan, K., Klein, M.J., Levy, R., Keysser, M., Keyszer, G. and Bromme, D., 2001. Cathepsin K is a critical protease in synovial fibroblast-mediated collagen degradation. Am. J. Pathol. 159, 2167-2177.

Hu, C.A., Phang, J.M. and Valle, D. 2008. Proline metabolism in health and disease. Amino Acids. 35(4), 651-2.

Huerre, C., Junien, C., Weil, D., Chu, M.L., Morabito, M., Van Cong, N., Myers, J.C., Foubert, C., Gross, M.S., Prockop, D.J., Boué, A., Kaplan, J.C., de la Chapelle, A. and Ramirez, F. 1982. Proc. Natl. Acad. Sci. 79(21), 6627-30.

Humphrey, J.D. 2002. Cardiovascular solid mechanics: cells, tissues, and organs. Springer-Verlag, New York, pp 499-598.

Hurtig, M., Pearce, S., Warren, S., Kalra, M., Mirzaie, M. 2001. Arthroscopic mosaic arthroplasty in the equine third carpal bone. Vet. Surg. 30, 228-239.

Hyun, C., 2005. Mitral valve prolapse in cavalier King Charles spaniel: a review and case study. J. Vet. Sci. 6, 67-73.

Ihlberg, L., Haukipuro, K., Ristelim L., Oikarinen, A., Kairaluoma, M.I. and Risteli, J. 1993. Collagen synthesis in intact skin is suppressed during wound healing. Ann. Surg. 217(4), 397-403.

Ishida, Y., Kubota, H., Yamamoto, A., Kitamura, A., Bächinger, H.P. and Nagata, K. 2006. Type I collagen in Hsp47-null cells is aggregated in endoplasmic reticulum and deficient in N-propeptide processing and fibrillogenesis. Mol. Biol. Cell. 17(5), 2346-55.

James, V.J., McConnell, J.F. and Capel, M. 1991. The d-spacing of collagen from mitral heart valves changes with ageing, but not with collagen type III content. Biochim. Biophys. Acta. 1078(1), 19-22.

Jarrett, H.W., Cooksy, K.D., Ellis, B., Anderson, J.M., 1986. The separation of o-phthalaldehyde derivatives of amino acids by reversed-phase chromatography on octylsilica columns. Anal. Biochem. 153(1), 189-98.

Jones, B.N. 1986. Amino acid analysis by o-phthaldialdehyde precolumn derivatization and reverse-phase HPLC. In: Shively, J.E. (Ed), Methods of protein microcharacterization, a practical handbook. Humana Press, Clifton, NJ, pp 121-151.

Jonkaitiene, R., Benetis, R., Ablonskyte-Dudoniene, R. and Jurkevicius, R. 2005. Mitral valve prolapse: diagnosis, treatment and natural course. Medicina (Kaunas) 41, 325-334.

Jouan, J., Tapia, M., Cook, R.C., ansac, E., and Acar, C., 2004. Ischemic mitral valve prolapse: mechanisms and implications for valve repair. European Journal of Cardio-thoracic Surgery 26, 1112-1117.

Kadler, K.E., Holmes, D.F., Trotter, J.A. and Chapman, J.A. 1996. Collagen fibril formation. 316 (Pt 1), 1-11.

Kagan, H.M. 1986. Characterization and regulation of lysyl oxidase. In: Mecham, R.P. (Eed) Biology of extracellular matrix. Academic Press, Orlando, pp 321-389.

Kagan, H.M. and Li, W. 2003. Lysyl oxidase: properties, specificity, and biological roles inside and outside of the cell. J. Cell Biochem. 88(4), 660-72.

Kealey, D. and Haines, P.J. 2002. Analytical chemistry. BIOS Scientific Publishers Ltd., Oxford, pp 119-165.

Keene, D.R., San Antonio, J.D., Mayne, R., McQuillan, D.J., Sarris, G., Santoro, S.A. and Iozzo, R.V. 2000. Decorin binds near the C terminus of type I collagen. J. Biol. Chem. 275(29), 21801-4.

Khatib, A.M., Siegfried, G., Messai, H., Moldovan, F. and Mitrovic, D.R. 2002. Mechanism of inhibition of endothelin-1-stimulated proteoglycan and collagen synthesis in rat articular chondrocytes. Cytokine. 17, 254-261.

Kitlinski, M., Stepniewski, M., Nessler, J., Konduracka, E., Solarska, K., Piwowarska, W. and Erhardt, L. 2004. Is magnesium deficit in lymphocytes a part of the mitral valve prolapse syndrome? Magnes. Res. 17, 39-45.

Kittleson, M.D. 1998. Myxomatous atrioventricular valvular degeneration. In: Kittleson, M.D. and Kienle, R.D. (Eds), Small animal cardiovascular medicine. Mosby, St. Louise, pp 297-318.

Kivirikko, K.I. and Myllylä, R. 1984. Biosynthesis of collagens. In: Piez, K.A. and Reddi, A.H. (Eds), Extracellular matrix biochemistry. Elsevier, New York, pp 83-118.

Koide, T. and Nagata, K. 2005. Collagen biosynthesis. In: Brinckmann, J., Notbohm, H., Muller, P.K. (Eds), Collagen: primer in structure, processing and assembly (Topics in Current Chemistry). Springer-Verlag, Berlin Heidelberg, pp 86-110.

Kurg, T., Stinson, R.H. and Millman, B.M. 1982. X-ray diffraction from striated muscles and nerves in normal and dystrophic mice. Muscle Nerve. 5(3), 238-46.

Lambert, P.J., Whitman, A.G., Dyson, O.F. and Akula, S.M., 2006. Raman spectroscopy: the gateway into tomorrow's virology. Virol. J. 3,51.

Lapiere, C.M., Lenaers, A. and Kohn, L.D. 1971. Procollagen peptidase: an enzyme excising the coordination peptides of procollagen. Proc. Natl. Acad. Sci. 68(12), 3054-8.

Laurent, G.J. 1987. Dynamic state of collagen: pathways of collagen degradation in vivo and their possible role in regulation of collagen mass. Am. J. Physiol. 252(1 Pt 1), C1-9.

Laye, P.G. 2002. Differential thermal analysis and differential scanning calorimetry. In: Haines, P.J. (Ed), Principles of thermal analysis and calorimetry. Royal Society of Chemistry (Great Britain), Cambridge, pp 55-65.

Le, T.T., Langohr, I.M., Locker, M.J., Sturek,M. and Cheng, J.X. 2007. Label-free molecular imaging of atherosclerotic lesions using multimodal nonlinear optical microscopy. J. Biomed. Opt. 12(5), 054007-1--054007-10.

Lewis, R. 1997. Medical applications of synchrotron radiation x-rays. Phys. Med. Biol. 42, 1213-1243.

Lewis, R.A., Hall, C.J., Hufton, A.P., Evans, S., Menk, R.H., Arfelli, F., Rigon, L., Tromba, G., Dance, D.R., Ellis, I.O., Evans, A., Jacobs, E., Pinder, S.E. and Rogers, K.D. 2003. X-ray refraction effects: application to the imaging of biological tissues. Br. J. Radiol. 76, 301-308.

Lewis, R.A., Rogers, K.D., Hallm C.J., Towns-Andrews, E., Slawson, S., Evans, A., Pinder, S.E., Ellis, I.O., Boggis, C.R., Hufton, A.P. and Dance, D.R. 2000. Breast cancer diagnosis using scattered x-rays. J. Synchrotron Radiat. 7(Pt 5), 348-52.

Li, J., Zhong, Z., Lidtke, R., Kuettner, K.E., Peterfy, C., Aliyeva, E. and Muehleman, C., 2003. Radiography of soft tissue of the foot and ankle with diffraction enhanced imaging. J. Anat. 202, 463-470.

Lin, C.X., Rhaleb, N.E., Yang, X.P., Liao, T.D., D'Ambrosio, M.A. and Carretero, O.A. 2008. Prevention of aortic fibrosis by N-acetyl-seryl-aspartyl-

lysyl-proline in angiotensin II-induced hypertension. Am. J. Physiol. Heart Circ. Physiol. 295(3), H1253-H1261.

Lin, Y.L., Brama, P.A., Kiers, G.H., DeGroot, J. and van Weeren, P.R., 2005. Functional adaptation through changes in regional biochemical characteristics during maturation of equine superficial digital flexor tendons. Am. J. Vet. Res. 66, 1623-1629.

Lodish, H., Berk, A., Kaiser, C.A., Krieger, M., Scott, M.P., Bretscher, A., Ploegh, H. and Matsudaira, P. 2008. Molecular cell biology. 6th edition. W.H, Freeman and Company, New York, pp 820-830.

Lucero, H.A., and Kagan, H.M., 2006. Lysyl oxidase: an oxidative enzyme and effector of cell function. Cell. Mol. Life. Sci. 63(19-20), 2304-16.

Macnab, A., Jenkins, N.P., Ewington, I., Bridgewater, B.J., Hooper, T.L., Greenhalgh, D.L., Patrick, M.R. and Ray, S.G. 2004. A method for the morphological analysis of the regurgitant mitral valve using three dimensional echocardiography. Heart 90, 771-776.

Mäki, J., 2002. Lysyl oxidases, cloning and characterization of the fourth and the fifth human lysyl oxidase isoenzymes and the consequences of a targeted inactivation of the first described lysyl oxidase isoenzyme in mice. Thesis (PhD), University of Oulu, Oulu.

Malhotra, V. and Mayor, S. 2006. Cell biology: the Golgi grows up. Nature. 441(7096), 939-40.

Mauviel, A., Heino, J., Kähäri, V.M., Hartmann, D.J., Loyau, G., Pujol, J.P. and Vuorio, E. 1991. Comparative effects of interleukin-1 and tumour

necrosis factor-alpha on collagen production and corresponding procollagen mRNA levels in human dermal fibroblasts. J. Invest. Dermatol. 96(2), 243-9.

Meek, K.M. and Quantock, A.J. 2001. The use of x-ray scattering techniques to determine corneal ultrastructure. Prog. Retin. Eye Res. 20(1), 95-137.

Menk, R.H., Rigon, L. and Arfelli, F. 2005. Diffraction-enhanced x-ray medical imaging at the Elettra synchrotron light source. Nucl. Instrum. Meth. A. 548(1-2), 213-220.

Michette, A. 1993. X-rays and their properties. In: Michette, A. and Buckley, C.J. (Eds), X-ray science and technology. Institute of Physics Publishing, Bristol, pp 1-47.

Miles, C.A. 1993. Kinetics of collagen denaturation in mammalian lens capsules studied by differential scanning calorimetry. Int. J. Biol. Macromol. 15(5), 265-71.

Miles, C.A. and Ghelashvili, M. 1999. Polymer-in-a-box mechanism for the thermal stabilization of collagen molecules in fibres. Biophys. J. 76(6), 3243-52.

Miles, C.A., Burjanadze, T.V. and Bailey, A.J. 1995. The kinetics of the thermal denaturation of collagen in unrestrained rat tail tendon determined by differential scanning calorimetry. J. Mol. Biol. 245(4), 437-46.

Miles, C.A., Wardale, R.J., Birch, H.L. and Bailey, A.J. 1994. Differential scanning calorimetric studies of superficial digital flexor tendon degeneration in the horse. Equine Vet. J. 26(4), 291-6.

Millard, C.J. 2007. Structural and functional characterisation of the collagen binding domain of fibronectin. Thesis (PhD), The University of Oxford. Oxford.

Miller, A., Bradshaw, J., Jones, E.Y., Fraser, R.D., MacRae, T.P. and Suzuki, E. 1985. The structure of collagen. Ciba Found. Symp. 114, 65-79.

Miller, A., Orgel, J.P. and Wess, T.J. 1999. X-ray studies on biological fibres. Fibre Diffraction Review. 8, 27-31.

Mishra, R., Emancipator, S.N., Kern, T.S. Simonson, M.S. 2006. Association between endothelin-1 and collagen deposition in db/db diabetic mouse kidneys. Biochem. Biophys. Res. Commun. 339, 65-70.

Monnier, V.M. 1989. Toward a Maillard reaction theory of aging. Prog. Clin. Biol. Res. 304, 1-22.

Monnier, V.M., Sell, D.R., Dai, Z., Nemet, I., Collard, F. and Zhang, J. 2008. The role of the amadori product in the complications of diabetes. Ann. N. Y. Acad. Sci. 1126, 81-8.

Mow, T. and Pedersen, H.D. 1999. Increased endothelin-receptor density in myxomatous canine mitral valve leaflets. J. Cardiovasc. Pharmacol. 34, 254-260.

Muehleman, C., Majumdar, S., Issever, A.S., Arfelli, F., Menk, R.H., Rigon, L., Heitner, G., Reime, B., Metge, J., Wagner, A., Kuettner, K.E. and Mollenhauer, J. 2004. X-ray detection of structural orientation in human articular cartilage. Osteoarthritis Cartilage 12, 97-105.

Munro, I. 1996. Synchrotron radiation. In: Michette, A. and Pfauntsch, S. (Eds), X-rays, the first hundred years. John Wiley & Sons, Chichester, pp 131-154.

Murray, R.K., Granner, D.K., Mayes, P.A., and Rodwell, V.W. 2000. Harper's Biochemistry. McGraw-Hill Companies, New York.

Myers, P.R. and Tanner, M.A. 1998. Vascular endothelial cell regulation of extracellular matrix collagen: role of nitric oxide. Arterioscler. Thromb. Vasc. Biol. 18,717-722.

Myllylä, R., Anttinen, H. and Kivirikko, K.I. 1979. Metal activation of galactosylhydroxylysyl glucosyltransferase, an intracellular enzyme of collagen biosynthesis. Eur. J. Biochem. 101(1), 261-9.

Nagata, K. 2003. HSP47 as a collagen-specific molecular chaperone: function and expression in normal mouse development. Semin. Cell Dev. Biol. 14(5), 275-82.

Nelson, D.L. and Cox, M.M. 2005. Lehninger principles of biochemistry. W.H. Freeman and Company, New York.

Nelson, S.A. 2008. X-ray crystallography. [Online] available at: http://www.tulane.edu/~sanelson/eens211/x-ray.htm [Accessed 30 October 2008].

Nicula, R. 2002. Introduction to differential scanning calorimetry, practical course. Physics Dept., Rostock University. Rostock.

Niu, Y., Xie, T., Ge. K., Lin. Y. and Lu, S. 2008. Effects of extracellular matrix glycosylation on proliferation and apoptosis of human dermal fibroblasts via the receptor for advanced glycosylated end products. 30(4):344-51.

Noden, D.M. and de Lahunta, A., 1985. Cardiovascular system II: heart. In: Stamathis, G. (Ed), The embryology of domestic animals Williams & Wilkins, Baltimore, pp 231-245.

Nuytinck, L., Tükel, T., Kayserili, H., Apak, M.Y. and De Paepe, A. 2000. Glycine to tryptophan substitution in type I collagen in a patient with OI type III: a unique collagen mutation. J Med. Genet. 37(5), 371-5.

O'Leary, R., Rerek, M. and Wood, E.J. 2004. Fucoidan modulates the effect of transforming growth factor (TGF)-beta1 on fibroblast proliferation and wound repopulation in in-vitro models of dermal wound repair. Biol. Pharm. Bull. 27(2), 266-70.

Olsen, L.H, Fredholm, M. and Pedersen, H.D. 1999. Epidemiology and inheritance of mitral valve prolapse in dachshunds. J. Vet. Intern. Med. 13(5), 448-56.

Olsen, L.H., Martinussen, T. and Pedersen, H.D. 2003a. Early echocardiographic predictors of myxomatous mitral valve disease in dachshunds. Vet. Rec. 152, 293-297.

Olsen, L.H., Mortensen, K., Martinussen, T., Larsson, L.I., Baandrup, U. and Pedersen, H.D. 2003b. Increased NADPH-Diaphorase activity in canine myxomatous mitral valve leaflets. J. Comp. Path. 129, 120-130.

Paul, R.G., Tarlton, J.F., Purslow, P.P., Sims, T.J., Watkins, P., Marshall, F., Ferguson, M.J. and Bailey, A.J. 1977. Biomechanical and biochemical study

of a standardized wound healing model. Int. J. Biochem. Cell Biol. 29(1), 211-20.

Pedersen, H.D. 2000. Diagnosing canine myxomatous mitral valve disease. Waltham Focus. 10, 3-9.

Pedersen, H.D. and Häggstrom, J. 2000. Mitral valve prolapse in the dog: a model of mitral valve prolapse in man. Cardiovasc. Res. 47, 234-243.

Pedersen, H.D., Koch, J., Poulsen, K., Jensen, A.L. and Flagstad, A. 1995. Activation of the renin-angiotensin system in dogs with asymptomatic and mildly symptomatic mitral valvular insufficiency. J. Vet. Intern. Med. 9, 328-331.

Pedersen, H.D., Lorentzen, K.A. and Kristensen, B.O. 1999. Echocardiographic mitral valve prolapse in cavalier King Charles spaniels: epidemiology and prognostic significance for regurgitation. Vet. Rec. 144(12), 315-20.

Pedersen, H.D., Olsen, L.H., Mow, T. and Christensen, N.J. 1998. Neuroendocrine changes in dachshunds with mitral valve prolapse examined under different study conditions. Res. Vet. Sci. 66,11-17.

Pfeiffer, B.J., Franklin, C.L., Hsieh, F.H., Bank, R.A. and Phillips, C.L. 2005. Alpha 2(I) collagen deficient oim mice have altered biomechanical integrity, collagen content, and collagen cross-linking of their thoracic aorta. Matrix. Biol. 24, 451-458.

Phang, J.M., Hu, C.A. and Valle, D. 2001. Disorders of proline and hydroxyproline metabolism. In: Scriver, C.R., Beaudet, A.L., Sly, W.S. and

Valle. D. (Eds), Metabolic and molecular basis of inherited disease. McGraw-Hill, New York, pp 1821-1838.

Pisano, E.D., Johnston, R.E., Chapman, D., Geradts, J., Iacocca, M.V., Livasy, C.A., Washburn, D.B., Sayers, D.E., Zhong, Z., Kiss, M.Z. and Thomlinson, W.C. 2000. Human breast cancer specimens: diffraction-enhanced imaging with histologic correlation--improved conspicuity of lesion detail compared with digital radiography. Radiology. 214(3), 895-901.

Ploetz, C., Zycband, E.I. and Birk, D.E. 1991. Collagen fibril assembly and deposition in the developing dermis: segmental deposition in extracellular compartments. J. Struct. Biol. 106(1), 73-81.

Pocock, W.A. and Barlow, J.B. 1970. Postexercise arrhythmias in the billowing posterior mitral leaflet syndrome. Am. Heart J. 80,740-745.

Potma, E.O. and Xie, X.S. 2004. CARS microscopy for biology and medicine. Optics and Photonics News 15, 40-45.

Prockop, D.J., Sieron, A.L. and Li, S.W. 1989. Procollagen N-proteinase and procollagen C-proteinase. Two unusual metalloproteinases that are essential for procollagen processing probably have important roles in development and cell signaling. Matrix Biol. 16(7), 399-408.

Pschirrer, E.R., Ramin, S.M. and Gilstrap, L.C. 2002. Mitral valve prolapse. Prim. Care Update Ob/Gyns. 9,169-173.

Rabkin, E., Aikawa, M., Stone, J.R., Fukumoto, Y., Libby, P. and Schoen, F.J. 2001. Activated interstitial myofibroblasts express catabolic enzymes and mediate matrix remodelling in myxomatous heart valves. Circulation. 104, 2525-2532.

Raggi, P., Callister, T.Q., Lippolis, N.J. and Russo, D.J. 2000. Is mitral valve prolapse due to cardiac entrapment in the chest cavity? A CT view. Chest. 117(3), 636-42.

Ramachandran, V.S., Paroli, R.M., Beaudoin, J.J. and Delgado, A. H. 2003. Handbook of thermal analysis of construction materials. William Andrew Inc. New York, pp 1-34.

Raspanti, M., Viola, M., Forlino, A., Tenni, R., Gruppi, C. and Tira, M.E. 2008. Glycosaminoglycans show a specific periodic interaction with type I collagen fibrils. J. Struct. Biol. 164(1), 134-9.

Reddy, V.P. and Beyaz, A. 2006. Inhibitors of the Maillard reaction and AGE breakers as therapeutics for multiple diseases. Drug Discov. Today. 11(13-14), 646-54.

Reiser, K.M. 1998. Nonenzymatic glycation of collagen in aging and diabetes. Proc. Soc. Exp. Biol. Med. 218(1), 23-37.

Ribel-Madsen, S., Christgau, S., Gronemann, S.T., Bartels, E.M., Danneskiold-Samsøe, B. and Bliddal, H. 2007. Urinary markers of altered collagen metabolism in fibromyalgia patients. Scand. J. Rheumatol. 36(6), 470-7.

Rishikof, D.C., Ricupero, D.A., Liu, H. and Goldstein, R.H. 2004. Phenylbutyrate decreases type I collagen production in human lung fibroblasts. J. Cell Biochem. 91(4), 740-8.

Robins, S.P. and Bailey, A.J., 1977. The chemistry of the collagen cross-links. Biochem. J. 163, 339-346.

Rodriguez, L.G., Lockett, S.J. and Holtom, G.R. 2006. Coherent anti-Stokes Raman microscopy: A biological review. Cytometry A 69(8), 779-791.

Rosen, C.J. 1996. Biochemical markers of bone turnover. In: Rosen, C.J. (Ed), Osteoporosis: diagnostic and therapeutic principles. Humana Press, Totowa, pp 130-133.

Rünger, T.M., Quintanilla-Dieck, M.J. and Bhawan, J. 2006. Role of cathepsin K in the turnover of the dermal extracellular matrix during scar formation. J. Invest. Dermatol. 127(2), 293-7.

Saito, M., Marumo, K., Fujii, K. and Ishioka, N. 1997. Single-column high-performance liquid chromatographic-fluorescence detection of immature, mature, and senescent cross-links of collagen. Anal. Biochem. 253(1), 26-32.

Salsas-Escat, R. And Stultz, C.M. 2007. The molecular mechanics of collagen degradation: implication for human disease. Exp. Mech. [Online] available at: http://www.springerlink.com [Accessed 20 September 2008].

Saltzman, L.E., Moss, J., Berg, R.A., Hom, B. and Crystal, R.G. 1982. Modulation of collagen production by fibroblasts. Effects of chronic exposure to agonists that increase intracellular cyclic AMP. Biochem. J. 204(1), 25-30.

Schmidt, D., Muggli, R. and Zülli, F. 2002. Collagen glycation and sking aging. [Online] available at: http://www.mibellebiochemistry.com/pdfs/Collagen_glycation_and_skin_aging_-_CT_2002.pdf [Accessed 10 October 2008].

Schoen, F.J. 1999. The heart. In: Cotran, R.S., Kumar, V. and Collins, T. (Eds), Robbins pathologic basis of disease. W.B. Saunders, Philadelphia, pp 568-570.

Schoen, F.J. 2005. Cardiac valves and valvular pathology: update on function, disease, repair, and replacement. Cardiovascular Pathology 14,189-194.

Schoen, F.J. 2008. Evolving concepts of cardiac valve dynamics: the continuum of development, functional structure, pathobiology, and tissue engineering. Circulation. 118(18), 1864-80.

Schoen, F.J. and Levy, R.J. 2005. Calcification of tissue heart valve substitutes: Progress toward understanding and prevention. Ann. Thorac. Surg. 79, 1072-1080.

Scordo, K.A. 2005. Mitral valve prolapse syndrome health concerns, symptoms, and treatments. Western Journal of Nursing Research. 27, 390-405.

Scott, J.E. 1991. Proteoglycan: collagen interactions and corneal ultrastructure. Biochem. Soc. Trans. 19(4), 877-81.

Scott, J.E. and Orford, C.R., 1981. Dermatan sulphate-rich proteoglycan associates with rat tail-tendon collagen at the d band in the gap region. Biochem. J. 197, 213-216.

Sellaro, T. L., 2003. Effects of collagen orientation on the medium-term fatigue response of heart valve biomaterials. Thesis (MSc). School of Engineering, University of Pittsburgh, Pittsburgh.

Shiraki, M., Kuroda, T., Tanaka, S., Saito, M., Fukunaga, M. and Nakamura, T. 2008. Nonenzymatic collagen cross-links induced by glycoxidation (pentosidine) predicts vertebral fractures. J. Bone. Miner. Metab. 26(1), 93-100.

Singh, R., Barden, A., Mori, T. and Beilin L. 2001. Advanced glycation end-products: a review. Diabetologia. 44(2), 129-46.

Sionkowska, A. Thermal denaturation of UV-irradiated wet rat tail tendon collagen. 2005. Int. J. Biol. Macromol. 35(3-4), 145-9.

Smith-Mungo LI, Kagan HM. 1998. Lysyl oxidase: properties, regulation and multiple functions in biology. Matrix Biol. 16(7), 387-98.

Sodek J. 1976. A new approach to assessing collagen turnover by using a micro-assay. A highly efficient and rapid turnover of collagen in rat periodontal tissues. Biochem. 160(2), 243-6.

Stefanadis, C. and Toutouzas, P. 2000. Mitral valve prolapse: the merchant of Venice or much ado about nothing? Eur. Heart J. 21, 255-258.

Stricklett, P.K., Hughes, A.K. and Kohan, D.E., 2005. Endothelin-1 stimulates NO production and inhibits cAMP accumulation in rat inner medullary collecting duct through independent pathways. Am. J. Physiol. Renal Physiol. 290(6), F1315-9.

Stubbs, G., 1999. Developments in fiber diffraction. Curr. Opin. Struct. Biol. 9, 615-619.

Szauter, K.M., Cao, T., Boyd, C.D. and Csiszar, K. 2005. Lysyl oxidase in development, aging and pathologies of the skin. Pathologie Biologie. 53(7), 448-56.

Szombathy, T., Janoskuti, L., Szalai, C., Csaszar, A., Miklosi, M., Meszaros, Z., Kempler, P., Laszlo, Z., Fenyvesim T., and Romics, L. 2000. Angiotensin

II type 1 receptor gene polymorphism and mitral valve prolapse syndrome. Am. Heart J. 139, 101-105.

Takahashi, K., Tatsunami, R. and Tampo, Y. 2008. Methylglyoxal-induced apoptosis of endothelial cells. Yakugaku Zasshi. [Online] 128(10):1443-8. Abstract only. Available at: http://www.ncbi.nlm.nih.gov/pubmed [Accessed 12 October 2008].

Tallaj, J., Wei, C.C., Hankes, G.H., Holland, M., Rynders, P., Dillon, A.R., Ardell, J.L., Armour, J.A., Lucchesi, P.A., and Dell'Italia, L.J. 2003. Beta1-adrenergic receptor blockade attenuates angiotensin II-mediated catecholamine release into the cardiac interstitium in mitral regurgitation. Circulation, 108, 225-230.

Tamura, K., Fukuda, Y., Ishizaki, M., Masuda, Y., Yamanaka, N. and Ferrans, V.J. 1995. Abnormalities in elastic fibers and other connective-tissue components of floppy mitral valve. Am. Heart J. 129, 1149-1158.

Trebacz, H. and Wójtowicz, K. 2005. Thermal stabilization of collagen molecules in bone tissue. Int. J. Biol. Macromol. 37(5), 257-62.

Urios, P., Grigorova-Borsos, A.M. and Sternberg, M. 2007. Aspirin inhibits the formation of pentosidine, a cross-linking advanced glycation end product, in collagen. Diabetes Res. Clin. Pract. 77(2), 337-40.

Van Vleet, J.F. and Ferrans, V.J. 2001. Cardiovascular system. In: McGavin, M.D., Carlton, W.W. and Zachary, J.F. (Eds), Thomson's special veterinary pathology. Mosby, Missouri, pp 211-213.

Verzar, F. 1964. Aging of the collagen fiber. Int. Rev. Connect. Tissue Res. 2, 234-300.

Wang, H., Fu, Y., Zickmund, P., Shi, R. and Cheng, J.X. 2005. Coherent anti-Stokes Raman scattering imaging of axonal myelin in live spinal tissues. Biophys. J. 89(1), 581-91.

Wang, H., Le, T.T. and Cheng, J.X. 2008. Label-free imaging of arterial cells and extracellular matrix using a multimodal CARS microscope. Opt. Commu. 281(7), 1813-1822.

Watson, F. 1996. X-ray diffraction. In: Michette, A. and Pfauntsch, S. (Eds), X-rays, the first hundred years. John Wiley & Sons, Chichester, pp 101-129.

Wautier, J.L. and Schmidt, A.M. 2004. Protein glycation: a firm link to endothelial cell dysfunction. Circ. Res. 95(3), 233-8.

Weber, I.T., Harrison, R.W. and Iozzo, R.V. 1996. Model structure of decorin and implications for collagen fibrillogenesis. J. Biol. Chem. 271(50), 31767-70.

Weis, S.M., Emery, J.L., Becker, K.D., McBride, D.J. Jr., Omens, J,H,, and McCulloch, A.D. 2000. Myocardial mechanics and collagen structure in the osteogenesis imperfecta murine (oim). Circ. Res. 87(8), 663-9.

Wess, T.J., Miller, A. and Bradshaw, J.P. 1990. Cross-linkage sites in type I collagen fibrils studied by neutron diffraction. J. Mol. Biol. 213, 1-5.

Wess, T.J., Wess, L. and Miller, A. 1996. The chemical reactivity and structure of collagen studied by neutron diffraction. Basic Life Sci. 64, 369-83.

Wess, T.J., Wess, L., Miller, A., Lindsay, R.M. and Baird, J.D. 1993. The in vivo glycation of diabetic tendon collagen studied by neutron diffraction. J. Mol. Biol. 230, 1297-1303.

Weyman, A.E. and Scherrer-Crosbie, M. 2004. Marfan syndrome and mitral valve prolapse. J. Clin. Invest. 114, 1543-1546.

Whitney, J.C. 1974. Observations on the effect of age on the severity of heart valve lesions in the dog. J. Small Anim. Pract. 15(8), 511-22.

Whittaker, P., Boughner, D.R., Perkins, D.G. and Canham, P.B. 1987. Quantitative structural analysis of collagen in chordae tendineae and its relation to floppy mitral valves and proteoglycan infiltration. Br. Heart J. 75, 264-269.

Wilkinson-Berka, J.L., Kelly, D.J., Koerner, S.M., Jaworski, K., Davis, B., Thallas, V. and Cooper, M.E. 2002. ALT-946 and aminoguanidine, inhibitors of advanced glycation, improve severe nephropathy in the diabetic transgenic (mREN-2)27 rat. Diabetes. 51(11), 3283-9.

Willett, T.L., Labow, R.S. and Lee, J.M. 2008. Mechanical overload decreases the thermal stability of collagen in an in vitro tensile overload tendon model. J. Orthop. Res. 26(12), 1605-10.

Williams, R.M., Zipfel, W.R. and Webb, W.W. 2005. Interpreting second-harmonic generation images of collagen I fibrils. Biophys. J. 88(2), 1377-86.

Williams, T.H. and Jew, J.Y. 2004. Is the mitral valve passive flap theory overstated? An active valve is hypothesized. Med. Hypotheses, 62, 605-11.

Zdrojewski, T.R., Wyrzykowski, B. and Krupa-Wojciechowska, B. 1995. Renin-aldosterone regulation during upright posture in young men with mitral valve prolapse syndrome. J. Heart Valve Dis. 4, 236-241.

Appendix

Publications arising from this thesis during course of my PhD

2472 Biophysical Journal Volume 93 October 2007 2472–2476

Collagen Organization in Canine Myxomatous Mitral Valve Disease: An X-Ray Diffraction Study

Mojtaba Hadian,* Brendan M. Corcoran,† Richard I. Han,† J. Günter Grossmann,‡ and Jeremy P. Bradshaw*
*Veterinary Biomedical Sciences, Royal (Dick) School of Veterinary Studies, University of Edinburgh, Summerhall, Edinburgh EH9 1QH, United Kingdom; †Hospital for Small Animals, Veterinary Clinical Sciences, Easter Bush Veterinary Centre, University of Edinburgh, Roslin Midlothian EH25 9RG, United Kingdom; ‡Science and Technology Facilities Council Daresbury Laboratory, Daresbury Science and Innovation Campus, Warrington WA4 4AD, United Kingdom

ABSTRACT Collagen fibrils, a major component of mitral valve leaflets, play an important role in defining shape and providing mechanical strength and flexibility. Histopathological studies show that collagen fibrils undergo dramatic changes in the course of myxomatous mitral valve disease in both dogs and humans. However, little is known about the detailed organization of collagen in this disease. This study was designed to analyze and compare collagen fibril organization in healthy and lesional areas of myxomatous mitral valves of dogs, using synchrotron small-angle x-ray diffraction. The orientation, density, and alignment of collagen fibrils were mapped across six different valves. The findings reveal a preferred collagen alignment in the main body of the leaflets between two commissures. Qualitative and quantitative analysis of the data showed significant differences between affected and lesion-free areas in terms of collagen content, fibril alignment, and total tissue volume. Regression analysis of the amount of collagen compared to the total tissue content at each point revealed a significant relationship between these two parameters in lesion-free but not in affected areas. This is the first time this technique has been used to map collagen fibrils in cardiac tissue; the findings have important applications to human cardiology.

INTRODUCTION

The mitral or left atrioventricular valve of the heart lies between the left atrium and the left ventricle and prevents backflow to the left atrium during ventricular systole. The mitral valve has two leaflets, namely the mural and the aortic (Fig. 1). Normally the leaflets are thin, translucent, and soft, although during disease processes a set of different pathological and morphological changes may occur. Tendinous cords attach the leaflets to two closely arranged groups of papillary muscles. Myxomatous mitral valve disease (MMVD) is the most common acquired cardiac disease of dogs. It is a disease of significant veterinary importance and also of emerging comparative interest. It is usually known as mitral valve prolapse in humans. The condition is typified by the loss of mechanical integrity of the valve leaflets, failure of proper coaptation of the leaflet edges during ventricular systole, mitral valve regurgitation, and, in a significant proportion of affected dogs, left-sided congestive heart failure (1–3).

The etiopathogenesis of acquired MMVD is poorly understood in both dogs and humans, and there is little information about alteration of collagen in canine MMVD, in particular regarding changes in the spatial distribution of collagen fibrils in the valves. Thus, greater knowledge of collagen structure is a necessary step in the course of understanding the disease processes. Moreover, tissue engineering and bioartificial valves are rapidly burgeoning areas that would benefit from detailed information about heart valve structure. The purpose of this study was to determine the changes in collagen fibril organization between diseased and healthy areas of valve leaflets using the technique of small-angle x-ray diffraction. X-ray diffraction has the advantage over electron microscopy that the tissue is maintained during the x-ray exposure so that prior chemical processing of the tissue is eliminated. Furthermore, unlike electron microscopy, which examines a very localized volume of tissue, x-rays pass through the entire the sample thickness, and the results thus represent averages throughout the tissue.

MATERIAL AND METHODS

Mitral valve leaflets were collected from five confirmed affected dogs and one healthy control. All tissue samples were frozen within 10 min of collection. In addition to the control sample, because diseased and normal areas coexist in one leaflet, each valve could also be used as its own control.

X-ray diffraction measurements

Collagen molecules lie almost parallel to the fibril axis and diffract x-rays from the 670 Å repeating pattern of gap and overlap regions. The intensity of diffraction is related to the amount of collagen, and the alignment of the diffraction pattern reflects the alignment of the fibers. Therefore, diffraction patterns can be used to probe the alignment of the collagen fibrils that produced that diffraction. The technique can also be used to determine total tissue content (collagenous and noncollagenous) by quantitative analysis of total x-ray scattering at any point (4–6).

X-ray diffraction measurements were performed with synchrotron radiation (Experimental Station 2.1, Synchrotron Radiation Source, The Council for the Central Laboratory of the Research Councils (CCLRC), Daresbury, UK) using a method developed from that of Aghamohammadzadeh and co-workers (4). Briefly, specimens were mounted in a specially designed

Submitted April 3, 2007, and accepted for publication May 30, 2007.

Address reprint requests to Mojtaba Hadian, Veterinary Biomedical Sciences, Royal (Dick) School of Veterinary Studies, University of Edinburgh, Summerhall, Edinburgh EH9 1QH, UK. Tel.: 44-131-650-6142; Fax: 44-131-650-6511; E-mail: m.hadian@ed.ac.uk.

Editor: Marcia Newcomer.

0006-3495/07/10/2472/05 $2.00

doi: 10.1529/biophysj.107.107847

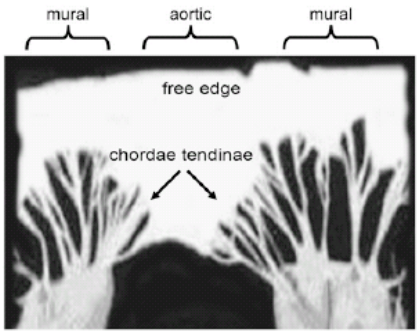

FIGURE 1 A normal canine mitral valve spread open by cutting through the mural leaflet.

sample cell and attached to a movable sample stage. The stage was programmed to translate in a raster of 1-mm steps, horizontally and vertically, while a finely focused (0.1 mm vertical × 1 mm horizontal) beam of 1.54 Å wavelength x-rays recorded the fiber diffraction pattern for 45 s at each point. Each sample was typically measured at 300 points, in a grid of 20 × 15 pixels. A multiwire two-dimensional area detector, placed 4 m from the sample, collected the diffraction data. The collection of diffraction data and movement of the sample relative to the beam were coordinated by a computer running a Python (www.python.org) script file. Calibration measurements included the detector response, in which the efficiency of each pixel was determined by a long exposure to a randomly decaying radioactive source, and detector calibration, which used the well-characterized diffraction pattern of wet rat tail collagen.

Data analysis

The diffraction pattern of a fibrous material, such as collagen, contains information in the meridional plane, describing structure along the axis of the fiber, and in the equatorial plane, describing lateral structure. For this study, Bragg reflections of the meridional diffraction pattern were recorded and analyzed to provide information about the collagen content and the degree and prevailing angle of alignment of the fibrils. The level of background scattering was also determined to give an indication of the amount of noncollagen tissue. Data analysis was performed using the program FiberFix (Collaborative Computational Project for Fiber Diffraction and Solution Scattering, CCP13). A ring was defined, centered on the middle of the diffraction pattern and wide enough to encompass the third, fourth, and fifth orders of meridional diffraction (Fig. 2). This region was chosen because it was sufficiently clear of any x-ray scattering from the backstop but included strongly diffracting Bragg peaks. The third and fifth orders of diffraction are characteristically very bright for type I collagen and have excellent signal/noise ratios, thereby simplifying the tasks of background subtraction and peak shape analysis. PeakFit (Version 4, AISN Software) was used to fit Gaussian peaks to the annular distribution of scattering intensity (Fig. 3). The Gaussians were then analyzed in terms of peak area (total diffracted intensity of the selected area of the diffraction pattern, related to the amount of collagen), peak center (angle of preferred fibril orientation), peak width (degree of fibril alignment), and mean background level (related to the amount of nonordered material). These values were then plotted to produce maps of each parameter across each valve leaflet.

Statistical analysis

The numerical diffraction values of total issue density, collagen fibril density, and degree of collagen alignment were analyzed separately for each leaflet using a two-sample *t*-test to compare affected and lesion-free areas. Significant differences were taken at $p < 0.05$. Analysis of regression was carried out to determine whether there was any relationship between amount of collagen and total tissue density in diseased and lesion-free areas.

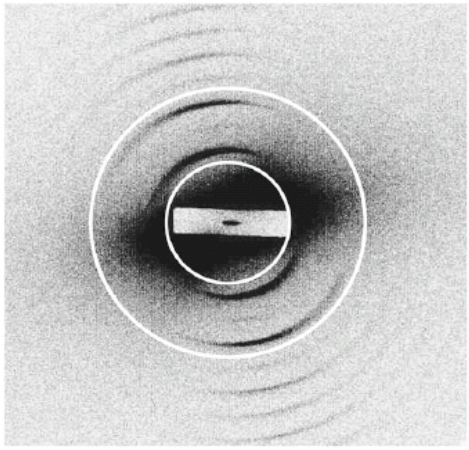

FIGURE 2 A representative x-ray diffraction pattern from canine mitral valve collagen. The pattern is dominated by a series of meridional Bragg reflections, arising from constructive diffraction of x-rays by the regularly repeating 670 Å axial structure of collagen fibrils within the sample. X-ray diffraction measurements were performed using synchrotron radiation (Experimental Station 2.1, Synchrotron Radiation Source, CCLRC, Daresbury, UK). The superimposed circles define a ring encompassing the third, fourth, and fifth Bragg peaks of meridional diffraction. Circular integration of diffracted intensity in this region was used to provide quantitative information on the amount of collagen fibrils and their orientation.

RESULTS

A typical small-angle x-ray diffraction pattern from a dog mitral valve leaflet is shown in Fig. 2. The x-ray beam passed

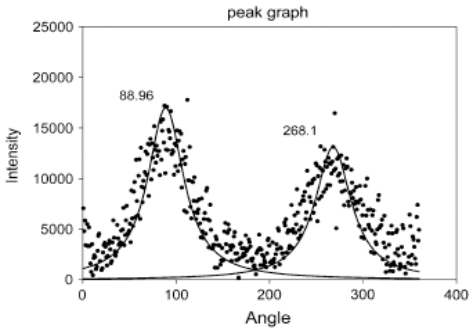

FIGURE 3 The annular distribution of diffracted intensity from canine mitral valve collagen. The data result from circular integration as described in the text and Fig. 2. Horizontal axis, angle; vertical axis, intensity (arbitrary units). Also shown is a pair of fitted Gaussian distributions centered at 88.96° and 268.1°.

through the sample perpendicular to the plane of the leaflet. Because collagen fibrils can occur in all possible orientations within this plane, the diffraction pattern may appear as a series of concentric circles. The anisotropic distribution (Fig. 3) of intensity in this example reveals a preferred angle of orientation of the fibrils.

Estimation of total tissue

Highly ordered material, such as collagen, produces a well-defined diffraction pattern, which overlays an anisotropic background of x-ray scattering by any disordered material that the x-ray beam strikes. A sensitive measure of the amount of tissue (collagenous and noncollagenous) at any one point on the leaflet is provided by the quantitative analysis of this noncoherent scattering of x-rays. Absorption of the x-ray beam by the sample can also be estimated by comparing the current measured at ion chambers before and behind the sample. A regression analysis of the two methods for one of our samples showed that they are closely related (>95% significance), thereby validating our approach. Total tissue density differed significantly ($p < 0.05$) between affected and lesion-free areas. The contour maps of the diseased samples (an example is given in Fig. 4 *A*) also revealed a considerable variation in total tissue content distribution among diseased and unaffected areas that was not consistent with a specific pattern.

Collagen fibril orientation

Fig. 4 *B* illustrates a map of collagen fibril orientation across a single leaflet. In the visibly normal areas of the midzone of the leaflets, the collagen fibrils run parallel to the free edge, meaning they take up a transverse course between two commissures. However, when they approach the edge of leaflets close to the annulus, they become oriented more vertically, such that they are orthogonal to the adjacent areas. In diseased areas, which are mostly located on the free margins of the

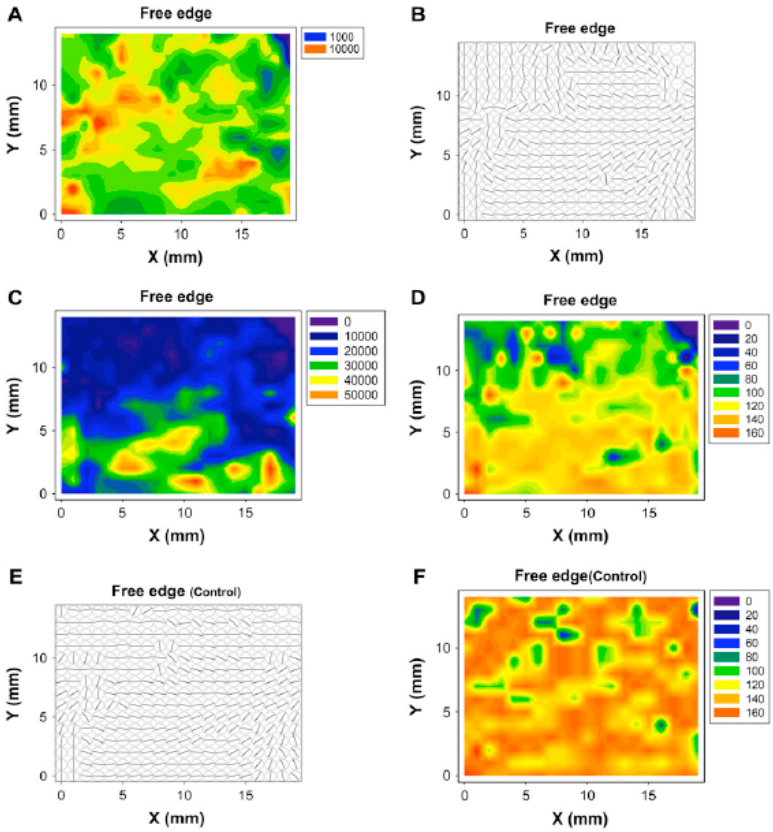

FIGURE 4 Contour maps showing an area of 20 × 15 mm of a single canine mitral valve leaflet. (*A*) Total (noncollagenous) tissue density, determined from the background (incoherent) x-ray scattering in a ring centered on the middle of the diffraction pattern and enclosing the third, fourth, and fifth meridional Bragg peaks. The background was measured in a region of reciprocal space that contained no diffraction features from collagen fibrils. Preferred orientation of collagen fibrils in diseased (*B*) and apparently healthy (*E*) mitral valve leaflets, determined by fitting Gaussian distributions to the Bragg peaks and determining the angular position of the peak center. The major difference between normal and diseased valves is in the free margins of the leaflets, where the disordered collagen fibrils of the diseased valve contrast starkly with the well-aligned fibrils of normal tissue. Collagen fibril density (*C*), determined from the total area under the Bragg peaks (total diffracted intensity). Degree of alignment of collagen fibrils in diseased (*D*) and apparently healthy (*F*) valve leaflets, determined from the width of the fitted Gaussian distributions. For ease of comparison with the other plots, the data are expressed as $180° - W$, where W is the full width at half height (in degrees) of the Gaussian distribution. Note that free edges of the leaflets are the locations where lesions are usually found. The healthy valve (*F*) displays a remarkable degree of alignment across the entire leaflet.

leaflets, the orientations of fibrils are haphazard. This contrasts with healthy regions and healthy valve (Fig. 4 *E*), where the direction of fibrils is more or less continuous with the fibrils in neighboring chordae tendineae and there is an ordered pattern of collagen fibrils across the valve.

Collagen fibril density

Fig. 4 *C* is a representative plot of collagen fibril density, determined on the basis of the strength of collagen diffraction at each point. These plots were derived from two different fibril populations: those with a preferred orientation and those without. This plot therefore shows the total diffraction irrespective of fibril orientation and so represents directly the relative amount of collagen fibers in the path of the x-ray beam. In all samples, the total diffraction, and therefore the amount of collagen, significantly increased ($p < 0.05$) from the diseased free edge of the leaflet to the unaffected base of the valves.

Degree of collagen alignment

Plots were drawn to map the degree of preferred alignment of the collagen fibrils. All the diseased leaflets showed nonuniform distribution of collagen alignment, with clear differences in the degree of preferential alignment between the diseased and healthy areas. These differences were consistent in all samples, and, as illustrated by Fig. 4 *D*, it was clear that the maximally aligned collagen is located toward the lesion-free periphery of the leaflets ($p < 0.05$). A comparison of these affected regions with the same areas in apparently healthy leaflets (Fig. 4 *F*) is a clear indication of the effect the disease has on collagen fibril alignment.

DISCUSSION

We have shown that small-angle x-ray diffraction may be used to study the different characteristics of the axially projected structure of collagen fibrils in myxomatous mitral valve. We have applied this technique to determine the various attributes of collagen fibrils in the diseased canine mitral valves and here present detailed maps of collagen fibril orientation, collagen density, the degree of alignment of the fibrils, and the relative amount of tissue density. This allows us to understand better the spatial arrangements of collagen within diseased valves. Any changes that affect the quality, quantity, or organization of collagen could lead to the mechanical failure and dysfunction of mitral valves.

The identification of collagen fibril orientation is one of the most striking findings of this study and shows that the mass of preferentially aligned collagen runs differently in different regions. In the main lesion-free body of the leaflets, collagen has a transverse course between the commissures. Near the free edge, it is almost a continuation of the collagen fibrils in the chordae tendineae. Because fiber orientation is the most effective way to optimize strength without increasing weight, fiber direction tends to reflect the prevalent tensile forces acting on a tissue (7). Therefore, knowledge of pattern of fibril alignment would have important implications for mechanical, bioprosthetic, and tissue-engineered valves and may inform the design of mitral valve substitutes. In contrast, diseased areas showed no distinct preferred orientation, and the collagen fibrils were disorganized with a haphazard and irregular arrangement. This confirmed what was previously suspected from histopathological and transmission electron microscopy studies (8).

In other tissue types dynamic changes in collagen alignment can occur in response to continuous mechanical force, but the short time frame of valve leaflet movement is unlikely to allow collagen fibrils to rearrange in response to changes in force alone. In MMVD, which is an age-related disease, the alignment of fibrils declines, whereas in aged specimens of other tissues, collagen tends to have the best-defined patterns, which indicates a greater degree of regularity from increased cross-linking of the collagen molecules (9). This suggests that the collagen changes that occur with MMVD are not simply an aging process.

The quantity of collagen was also greatly reduced in the affected areas compared to nonaffected areas. Because the tensile strength of collagen fibrils is directly proportional to the mass of the fibrils, it can be assumed that the affected areas will be less capable of resisting the load and strain imposed by ventricular systole. The free edge of normal leaflets is the thickest part of the leaflet (10), and in healthy valves, collagen content is related to tissue thickness. The plots of baseline scattering in this study showed notable variation across the leaflets, which did not correspond to diseased areas. Regression analysis of the amount of collagen compared to the total tissue content at each pixel ($p \leq 0.01$, $n = 120$ points) revealed that there was significant relationship between these two parameters in lesion-free areas. However, this relationship did not hold true in affected areas, where depletion of collagen is not reflected in a parallel decline in total tissue content. One possible explanation is that MMVD involves increased production and deposition of glycosaminoglycans (GAGs). The different types of GAGs have diverse properties for absorbance and for destructive and constructive interference (1), and although some of them could produce a clear and ordered diffraction pattern, others would only contribute to tissue density. It is also believed that GAGs in the right proportions do play a role to maintain collagen fibrils in specific spatial order. Thus, the increasing amount of the GAGs would not only disturb that spatial order but, by reducing the physical space, might also encourage the process of collagen depletion. Furthermore, determining the exact types of concerned GAGs as another step forward in understating of the disease is suggested. An additional confounding factor is that the type of collagen present in connective tissues is linked to the type and quantity of related GAGs. Type III collagen tends to

be associated with more GAGs, although there are conflicting reports on the changes in Type III collagen content in human myxomatous mitral valve disease (9,11), and the exact makeup of collagen types in canine MMVD still needs to be determined.

This work was supported by the CCLRC, the Cavalier King Charles Spaniel Club, and the Kennel Club. Mojtaba Hadian is sponsored by Iran Ministry of Science. The authors would like to thank Kalotina (Tina) Geraki for her technical support.

REFERENCES

1. Kittleson, M. D. 1998. Myxomatous atrioventricular valvular degeneration. *In* Small Animal Cardiovascular Medicine. M. D. Kittleson and R. D. Kienle, editors. Mosby, St. Louis. 297–318.
2. Pedersen, H. D., and J. Haggstrom. 2000. Mitral valve prolapse in the dog: a model of mitral valve prolapse in man. *Cardiovasc. Res.* 47: 234–243.
3. Van Vleet, J. F., and V. J. Ferrans. 2001. Cardiovascular system. *In* Thomson's Special Veterinary Pathology. M. D. McGavin, W. W. Carlton, and J. F. Zachary, editors. Mosby, St. Louis. 211–213.
4. Aghamohammadzadeh, H., R. H. Newton, and K. M. Meek. 2004. X-ray scattering used to map the preferred collagen orientation in the human cornea and limbus. *Structure.* 12:249–256.
5. Meek, K., and A. J. Quantock. 2001. The use of x-ray scattering techniques to determine corneal ultrastructure. *Prog. Retin. Eye Res.* 20: 95–137.
6. Miller, A., J. P. Bradshaw, E. Y. Jones, R. D. Fraser, T. P. MacRae, and E. Suzuki. 1985. The structure of collagen. *Ciba Found. Symp.* 114:65–79.
7. Sellaro, T. L. 2003. Effects of collagen orientation on the medium-term fatigue response of heart valve biomaterials. Dissertation. School of Engineering, University of Pittsburgh, Pittsburgh.
8. Tamura, K., Y. Fukuda, M. Ishizaki, Y. Masuda, N. Yamanaka, and V. J. Ferrans. 1995. Abnormalities in elastic fibers and other connective-tissue components of floppy mitral valve. *Am. Heart J.* 129:1149–1158.
9. James, V. J., J. F. McConnell, and M. Capel. 1991. The d-spacing of collagen from mitral heart valves changes with ageing, but not with collagen type III content. *Biochim. Biophys. Acta.* 1078:13–22.
10. Ho, S. Y. 2002. Anatomy of the mitral valve. *Heart.* 88:iv5–iv10.
11. Hammer, D., C. V. Leier, N. Baba, J. S. Vasko, C. F. Wooley, and S. R. Pinnell. 1979. Altered collagen composition in a prolapsing mitral valve with ruptured chordae tendineae. *Am. J. Med.* 67:863–866.

Papers presented in congresses

1. **Hadian, M.**, Corcoran, B., Bradshaw, J.P., Grossmann, J.G., Tromba, G. and Menk, R.H. *Synchrotron anatomy, the use of x-rays to map tissue structure in myxomatous mitral valve disease in dogs.* The Biophysical Society Annual Meeting, February 18-22, 2006, Salt Lake City, USA.

2. **Hadian, M.,** Corcoran. B. and Bradshaw, J.P. *A differential scanning calorimetry study of collagen phase transition in myxomatous mitral valves.* The Biophysical Society Annual Meeting, March 3-7, 2007, Baltimore, USA.